1-1-2017

Clinical Applications Of Advanced Rotational Radiation Therapy

Adrian Nalichowski
Wayne State University,

CLINICAL APPLICATIONS OF ADVANCED ROTATIONAL RADIATION THERAPY

by

ADRIAN NALICHOWSKI

DISSERTATION

Submitted to the Graduate School

of Wayne State University,

Detroit, Michigan

in partial fulfillment of the requirements

for the degree of

DOCTOR OF PHILOSOPHY

2017

MAJOR: MEDICAL PHYSICS

Approved By:

_____

Advisor Date

_____

_____

_____

_____

DEDICATION

I dedicate my dissertation to my wife Ruth and our kids Leah and Zane for their endless love, support, and constant sacrifice during this journey.

I also dedicate it to my parents for their love and never ending encouragement.

ACKNOWLEDGEMENTS

I would like to thank my advisor, Dr. Jay Burmeister, for his guidance, support and encouragement. I'm grateful for his advice and always being available for long discussions and brainstorming sessions. I would like to thank the rest of my dissertation committee, Dr. Indrin Chetty, Dr. Dan Ionascu, Dr. Joseph Rakowski, and Dr. Michael Snyder for their constructive criticism, new ideas and directions for my research.

I would also like to thank all those who helped me or contributed to my research: Dr. Tewfik Bichay, Todd Bossenberger, Don Eagle, Dr. Ron Fisher, Julie Fredrick, John Gallo, Dr. Michael Joiner, Dr. Isaac Kaufman, Ezequiel Ramirez, Alan Mayville, Dr. Mark Smith, Dr. Tim Solberg, and Dr. Yulong Yan.

This research has been sponsored in part by Accuray Inc.

PREFACE

Note to the reader:

Chapters 2-6 of this dissertation were originally written individually for publication in peer reviewed scientific journals, and while much has been added to tie the chapters together as a single cohesive document, they were originally intended as stand-alone manuscripts. At the time of submission, Chapters 2, 3 and 5 have been accepted for publication while Chapter 4 is currently in the second round of the review process in the journal *Medical Dosimetry* and the manuscript from Chapter 6 is intended to be submitted to the International Journal of Radiation Oncology Biology and Physics.

Chapter 2 was originally published in Medical Physics (2013) under the title "Dosimetric comparison of helical tomotherapy treatment plans for total marrow irradiation created using GPU and CPU dose calculation engines." Chapter 3 was originally published in Medical Dosimetry (2016) under the title "Dosimetric evaluation of total marrow irradiation using 2 different planning systems." Chapter 5 was originally published in the Journal of Applied Clinical Medical Physics (2017) under the title "Single fraction radiosurgery/stereotactic body radiation therapy (SBRT) for spine metastasis: A dosimetric comparison of multiple delivery platforms".

TABLE OF CONTENTS

LIST OF TABLES

LIST OF FIGURES

LIST OF ABBREVIATIONS

3DCRT……..……3 Dimensional Conformal Radiation Therapy

2D……..…….2 Dimensional

AAA ……..……..Analytical Anisotropic Algorithm

AP …….. Anterior-Posterior

BMT ……..……..Bone Marrow Transplant

CCCS…… Collapsed-Cone Convolution/Superposition

CK …….. CyberKnife

CPU ……..…… Central Processing Unit

CT …… Computed Tomography

Cy ……...……..Cyclophosphamide

D”xx” ……..……Dose to xx% of Volume

DCS ……..……..Dose Control Servo

DVH ……..……. Dose Volume Histogram

FFF ……...…… Flattening Filter Free

FW ……. Field Width

GB ……. Gigabyte

GPU ……...…….Graphic Processing Unit

GVHD ……..……. Graft vs. Host Disease

HDMLC ……..…….High Definition Multi Leaf Collimator

HT ……..Helical Tomotherapy

HVL……..……..Half Value Layer

IMAT……..Intensity Modulated Arc Therapy

IMRT ……. Intensity Modulated Radiation Therapy

IP ……..……. Interstitial Pneumonitis

LPC……Lethal Pulmonary Complication

LQ ……..…….. Linear Quadratic

MC…….……Monte Carlo

MF ……..…….. Modulation Factor

MLC ……..……Multi Leaf Collimator

MRI ……..……. Magnetic Resonance Imagine

MU ……..…… Monitor Units

MVA……..……. Multivariate Analysis

NVBB ……..…….. NonVoxel-based Broad-Beam

OAR ……....Organ at Risk

OR……..……Odds Ratio

PA ……Posterior-Anterior

PGI ……..…… Paddick dose Gradient Index

PTV……..……Planning Target Volume

QA ……..……Quality Assurance

RTOG……..……. Radiation Therapy Oncology Group

SBRT ……..……. Stereotactic Body Radiation Therapy

SRS ……..Stereotactic Radiosurgery

TB ……TrueBeam

TBI ……Total Body Irradiation

TMI ……..…… Total Marrow Irradiation

TPS ……..…….Treatment Planning System

V”xx” …….……Volume Receiving “xx” dose

VMAT ……..…….Volumetric Modulated Arc Therapy

VoLO …….……..Voxel-Less Optimization

VP-16 …….. Etoposide

CHAPTER 1 "OVERVIEW"

1. Introduction

Cancer is the second most common cause of death in the United States, surpassed only by heart disease, and accounts for nearly 1 of every 4 deaths. In 2016 there were approximately 1.7 million new cancer cases diagnosed and about 600 thousand deaths from this disease in the United States alone[1]. Treatment options depend on type, location and stage of the cancer and may involve radiation therapy, chemotherapy, surgery, hormonal therapy and/or targeted therapy. With about half of all cancer patient receiving radiation therapy, it plays an important role in the treatment of cancer and can be used with a curative intent or as a palliative treatment to alleviate pain or symptoms. Due to a combination of improvements in early diagnosis and treatment techniques, the 5 year relative survival has been steadily increasing over the last few decades. However, there is still much room for improvement in both survival and patient quality of life, and potential future improvements from radiation therapy will depend on our ability to better apply and to improve our technology and treatment techniques. This thesis investigates the potential improvements possible for a subset of these radiation therapy treatment techniques.

1.1 Radiation Therapy

Shortly after the discovery of radioactivity by Maria Skłodowska Curie, and its ability to kill cancer cells, the first patient was treated with external beam radiation therapy. The applications of radiation to the treatment of tumors have evolved tremendously ever since. Some of the technical innovations include the use of ^{60}Co

for teletherapy, followed by the much more complex electron linear accelerator in the pursuit of higher energy beams for the ability to treat deep seated tumors. Advances in computer technology in the 1970's and the invention of computed tomography (CT), made it possible to image the patient and map the tumor and surrounding healthy tissue in 3 dimensions (3D). At the same time, improvements in beam collimation led to the introduction of 3D conformal radiation therapy (3DCRT). With the detailed knowledge of the shape and position of the tumor, it was now possible to conform the spatial distribution of the prescription dose to the 3D target volume, while minimizing the dose to the surrounding healthy organs. The delivery of 3DCRT is typically accomplished with a set of radiation beams positioned at fixed gantry angles, which are shaped using a beams eye view of the target volume. The intensity of the radiation beams is usually uniform across the field or may be altered by simple fluence modifying devices such as wedges or compensators. Subsequently, the introduction of the multi-leaf collimator (MLC),[2] largely replacing cast blocks for beam shaping, and advancements in dose calculation algorithms, led to the introduction of intensity modulated radiation therapy (IMRT).

1.1.1 IMRT Delivery Techniques

Intensity modulated radiation therapy is based on the use of optimized non uniform radiation beam intensities to deliver highly conformal and uniform dose to the target volume while minimizing dose to adjacent normal tissue. Historically, the beam fluence modulation was achieved by compensators, which varied in thickness across the plane perpendicular to the central axis. The limitations of compensators

included limited dynamic range of fluence modulation as well as time consuming and laborious fabrication of these patient specific devices.

The first clinical MLC system was the MIMiC collimator which was mounted on a conventional linear accelerator as a tertiary collimator. The beam was collimated to a narrow (~ 2cm) slice and the gantry was rotated about the patient in an arc mode. The binary leaves were temporally modulated to vary the beam intensity as a function of gantry angle. Typical treatment consisted of delivering several adjacent axial slices. Due to the serial nature of this delivery, extreme accuracy of couch positioning was incredibly important. Couch positioning errors of as little as 1 mm could cause dose errors as high as 20% in the overlap region.[3-4] This approach was initially called tomotherapy which literally means slice therapy, but subsequently renamed serial tomotherapy.

The “Tomotherapy” device proposed by Mackie et al.[5-6] used a similar binary collimator but delivers helical tomotherapy. The Tomotherapy machine consists of 6MV linear accelerator mounted on a ring gantry that rotates around the patient while the patient is translated through the bore at constant speed effectively creating a helical path of radiation delivery. The beam is collimated by 64 binary leaves with a width of 6.25 mm projected at isocenter, forming a maximum field size in the lateral direction of 40 cm. The leaves are pneumatically driven to either open or closed position through 51 “projections” (approximately 7 degrees) of the gantry rotation and beam modulation is achieved by varying the time that each leaf is open during a projection. For the inferior-superior direction, a movable set of tungsten jaws collimates the width of the fan beam slice to nominal values of 1, 2.5 and 5 cm

wide. More recent models of Tomotherapy machines provide dynamic jaw movement, which allows the jaws to move to any position between 0 and 5cm and move during the treatment. Details of this functionality have been described previously by Chen et al.[7]

Another common technique to produce intensity modulated beam is by the use of the conventional MLC. This type of MLC has a set of leaves on each side of the field creating opposing leaf pairs. The design and shape of the leaves may vary from machine to machine, but the principal functions are the same. Each pair of opposing leaves is moved across the field under computer control, with the radiation beam on, to produce desired beam modulation. This type of delivery is termed dynamic or sliding window. Alternatively, beam modulation can be accomplished by a series of multiple field segments, called subfields, created by the MLC. The beam is turned off during the leaf motion between the individual subfields. This method is known as step-and-shoot or segmental IMRT delivery. Another conventional MLC IMRT approach, called intensity modulated arc therapy (IMAT), was described by Yu et al.[8-10] Beam modulation in this approach is achieved by multiple irregular fields shaped by the MLC during gantry rotation. This method required several overlapping arcs to attain desired dose distribution. Otto et al.[11] proposed a novel aperture-based algorithm to achieve efficient dose delivery in singe dynamically modulated arc as opposed to multiple superimposed arcs as in IMAT to achieve similar dose distribution with reduced treatment time. This technique has been termed Volumetric Modulated Arc Therapy (VMAT). VMAT delivery employs continuously variable MLC field shape, fluence rate and gantry speed.

Finally, an intensity modulated dose distribution can be created by the delivery of multiple individual beamlets. This method was described by Webb[12-13] and is commonly employed using a small x-band linear accelerator mounted on an industrial robot. The beamlet sizes are dependent on the collimation system and can range from 5 to 60 mm in diameter and can be circular or 12-sided polygon. This type of robotic delivery using a small accelerator allows beamlets to be aimed at the tumor from any orientation giving this IMRT delivery method more flexibility than any of those previously discussed.

1.1.2 IMRT Optimization

All the IMRT delivery techniques described above have in common the ability to deliver non-uniform fluence patterns which add up to desired conformal dose distributions. Regardless of the of delivery technique, the optimization of such fluence patterns requires significant computational power and is performed using a computerized treatment planning system (TPS). The TPS must be able to create a plan which meets the goals of the clinician and these goals are commonly conveyed to the treatment planning system as goals or constraints which the TPS attempts to meet through a process called inverse treatment planning. Historically, planning for 3DCRT was performed in forward planning manner, where beam shape is defined by the planner, the dose is calculated and the resulting plan is then evaluated for target dose coverage and organs at risk (OAR) dose limits. Improvements to the plan are then performed by changing the geometry of the beam and/or adding beam modifiers and new dose distribution is calculated. The process continues until a satisfactory plan is generated. In inverse treatment planning, the planner specifies

the desired outcome and asks the TPS figure out how to achieve that goal. The clinical objectives are commonly specified mathematically in the form of a cost function. The optimization algorithm iteratively adjusts the intensities of all available beamlets to minimize the cost function in an attempt to satisfy the constraints set by the planner. Most IMRT optimization systems use dose-volume based criteria and commonly use the cost function to minimize the variance between the computed dose and the desired dose for each target volume and Organ at Risk (OAR). A typical cost function is the sum of the variances for each target and OAR multiplied by penalty or weighting factor based on the assigned importance of that structure.

During IMRT optimization, the dose distribution from each iteration is evaluated and used to calculate the cost function before the next iteration can be initiated. Typical treatment plan requires hundreds (for gradient method) to tens of thousands (for stochastic method) of iterations to achieve an acceptable results, therefore the speed of dose calculation algorithm is extremely important. Besides the speed, the algorithm must also be able to accurately calculate dose in regions of complex tissue heterogeneities delivered by conformal beams consisting or small beamlets forming steep dose gradients.

1.1.3 Dose Calculation

Correction based dose calculation algorithms[14-15] do not account for electron contamination, transmission through the jaws and MLC, scatter outside the field, finite source size and extrafocal radiation generated by the primary collimator. These algorithms also lack accuracy in heterogeneous media and are unsuitable for use in IMRT dose calculations. More recent, commercially available dose calculation

algorithms that address some of the limitations of the correction based algorithms can be divided into two categories: model based and Monte Carlo (MC) based. These dose calculation methods are not perfect and still exhibit some limitations in accuracy and/or calculation speed, however they have been routinely used in IMRT treatment planning. In order to improve calculation speed without compromising accuracy, several attempts have been made to modify the existing calculation models while leveraging advancements in computing power. In 2011, Chen et al. presented a novel algorithm for computing collapsed-cone convolution/superposition (CCCS) dose on modern graphic processing unit (GPU).[16] Results from validation and clinical application of this algorithm are presented in chapter 2 of this dissertation.

1.1.4 Prescription Dose and Fractionation

The mechanical accuracy of external beam therapy machines has improved dramatically and sub-millimeter targeting is now achievable. This presents new challenges as well as new opportunities. For example, the opportunity to see the tumor immediately prior to treatment and treat it with high conformity is accompanied by the risk of missing the target due to patient or tumor motion. Once these challenges are addressed, delivering highly conformal dose to the target volume will result in lower doses to the surrounding healthy organs and lower toxicities. Subsequently, the prescription dose, which is usually limited by the OAR toxicities can be escalated and potentially offer higher tumor control probability.

Increasing prescription doses is also possible through fractionation. Healthy, normal tissues and OAR are considered late-reacting tissue cells and have higher

propensity for repair than do tumor cells. By fractionating the prescription dose and allowing sufficient time between the fractions for sublethal cell damage repair, the healthy tissues will have a higher surviving fraction than the tumor. Historically, the most common fractionation scheme was in 1.8 Gy – 2.0 Gy fractions delivered once a day. The daily separation between the fractions made it not only convenient, but also allowed sufficient time for cell damage repair. The fraction size of 1.8 - 2.0 Gy was derived from cell survival curves displaying greatest separation between tumor and late-reacting normal tissue cells.

Not all tumors and healthy tissues have the same cell repair characteristics. The fractionation sensitivity parameter, α/β, ranges for tumors and healthy tissues from 5 Gy to 20 Gy and from 1 Gy to 4 Gy, respectively. Due to the vast range of these values, different fractionation schemes have been proposed and studied. Some healthy tissues have very low α/β values and conventional fractional doses may not provide optimal therapeutic benefit, thus a hyperfractionated scheme may be warranted. In this scheme, low doses of 1.0 Gy to 1.5 Gy are delivered twice or even three times a day for a total dose that is higher than in conventional fractionation regimen. The situation is the opposite for tumors with low α/β ratios, in which case hypofractionation may be desirable. Patients treated with this fractionation regimen receive lower prescription dose delivered in a smaller number of large fractions typically separated by 2 or more days. All the fractionation schemes depend on the accurate knowledge of the α/β ratios, and their efficacy can only be confirmed by clinical trials.

1.2 Statement of the Problem

With the advancements in IMRT dose calculation algorithms and treatment delivery methods it is now possible to apply this new technology to challenging clinical cases such as total marrow irradiation (TMI) and stereotactic radiosurgery (SRS). The conditioning regimen for bone marrow transplantation (BMT) has historically included irradiation of the bone marrow, and total body irradiation (TBI) has been employed because the technology was not mature enough to allow treatment of the bone marrow only. TBI treatments have traditionally been delivered at extended distances due to radiation field limitations, and dose calculations were done very simplistically as most commercial planning systems are not designed to handle such calculations at extended distances. The introduction of Tomotherapy machine has overcome some of these limitations. The capability of treating up to a 160cm target in the longitudinal direction eliminates the need for treatment at an extended distance and/or field matching as it would be required when using conventional C-arm linacs. With IMRT, it is possible to target the marrow and spare OARs with what is now known as Total Marrow Irradiation (TMI). As would be expected the very large structures and dose calculation volumes for TMI result in significantly larger optimization and dose calculation times for the treatment planning system. This limitation has now been addressed with the introduction of a novel Graphics Processing Unit (GPU)-based dose calculation and optimization algorithm. The first stage of this work was to evaluate the accuracy and efficacy of Tomotherapy's GPU-based TPS system for the treatment of TMI (Chapter 2) and further compare the plan quality and planning efficiency with plans created using the

Varian Eclipse TPS (Varian Medical Systems Inc, Palo Alto, CA) using VMAT (Chapter 3).

The process of treatment planning for TMI cases is not without significant challenges. Due to the extremely large target volume, the optimization parameters routinely used for other clinical sites are not optimal for TMI plans. Some of the parameters cannot be used to their full extent due to either machine limitations or treatment plans resulting in excessive beam-on times. To address these challenges, a comprehensive planning guide for TMI treatments was developed (Chapter 4).

Before the introduction of dynamic jaws, all the Tomotherapy plans resulted in excessive dose spillage in the superior and inferior direction outside the target volume. This issue was especially concerning for small targets and targets abutting critical structures located superiorly or inferiorly to the target. In order to lessen this effect, smaller filed sizes were typically used, which resulted in improved plans, but at the expense of longer beam-on time. Dynamic jaws were designed to limit the dose spillage and improve the beam-on time without sacrificing plan quality. The goal for this part of the study was to determine whether there are significant differences in planning and delivery capabilities of Tomotherapy as compared to other delivery platforms within the context of RTOG 0631 radiosurgery/SBRT trial (Chapter 5).

Currently there is no consensus on the optimal fractionation and conditioning regimen for BMT treatments. Published results from clinical trials show vast differences in treatment methods. These differences include the use of different chemotherapy agents, some of which have a synergistic effect with radiation.

Differences in the TBI component alone include differences in the prescription doses, number of fractions used, frequency of radiation delivery, dose rates, and amount and method of lung shielding. The final goal of this research was to evaluate historical published data and, through the use of current radiobiological data and modeling, propose new fractionation schemes for TBI/TMI treatments that may be expected to be clinically and/or logistically superior to current schemes (Chapter 6).

CHAPTER 2 "GPU AND CPU BASED DOSE CALCULATION ALGORITHMS"

2.1 Introduction

Bone marrow transplantation (BMT) is commonly accompanied with radiotherapy in the form of total body irradiation (TBI). The TBI serves as a conditioning regimen and helps with immunosuppression in patients undergoing hematopoietic cell transplantation[17]. Previous randomized trials have shown excellent outcome using TBI as a conditioning regimen[18-20]. Higher TBI doses of 15.75Gy have also been shown to reduce post-transplant relapse rates in patients with chronic and acute myeloid leukemia[21-22]. However, higher doses did not improve overall survival due to increased incidence of Graft vs. Host Disease (GVHD) and excessive toxicity to organs at risk (OAR) such as lung and liver at these dose levels.

With the advancement of intensity modulated radiation therapy (IMRT) it is now possible to deliver a more targeted form of total body irradiation termed total marrow irradiation (TMI). Several institutions have published feasibility studies using fixed angle IMRT[23], Volumetric Modulated Arc Therapy (VMAT)[24-27] and Helical Tomotherapy (HT)[28-31] techniques. The objective of the different approaches is to deliver the prescription dose to the target volume and spare normal organs. All three IMRT methods were able to deliver the prescription dose while reducing doses to OARs by ~30% to 80%[23-31].

Each delivery technique has some disadvantages. Fixed angle IMRT and VMAT techniques require multiple isocenters to cover the entire treatment volume. Each isocenter may require 7-9 static fields or 2-3 arcs for IMRT and VMAT

respectively to achieve adequate coverage and OAR sparing. The patient has to be repositioned for each isocenter which may compromise intended dose distribution in the area of field overlap. Helical delivery is well suited for treatment of longitudinally large fields since field matching in critical areas is eliminated. The additional time required for patient repositioning on C-arm linac based systems adds to total treatment time, although the beam on time for VMAT is much shorter as compared to HT[27]. A common weakness for all three planning techniques is the optimization and dose computation time. Han at al.[27] reported planning times of about 5 hours for eight arc VMAT plans using an Eclipse v8.6 (Varian Medical Systems Inc, Palo Alto, CA) planning station using 8 Intel Xeon CPUs at 2.5Ghz with 4 GB of memory. The planning time from our TMI study on the TomoTherapy (Accuray Inc, Sunnyvale, CA) Hi-Art v4.2 CPU station was about 10 hours utilizing 14 nodes of quad core Intel Xeon CPUs at 2.8 GHz with 2GB of memory.

Recently, Lu[32] has developed a non-voxel-based broad-beam (NVBB) framework for optimization and dose calculation. This system has been incorporated in the TomoTherapy planning system utilizing a single workstation with one graphical processing unit (GPU) card. In this study, we compared TMI treatment plans between CPU and GPU systems in terms of plan quality and total calculation and optimization time.

2.2 Methods and Materials

In this study we used an anthropomorphic Rando (The Phantom Laboratory, Salem, NY) phantom to create TMI treatment plans with CPU and GPU based dose calculation engines. The computed tomography (CT) images of the phantom were

acquired on a large bore Somatom Sensation CT simulator (Siemens, Malvern, PA) with 60 cm field of view. A CT scan was acquired with 5mm slice thickness of the entire phantom which does not include upper extremities and ends inferiorly in the mid-femur region. Since the phantom does not have arms, two acrylic cylinders filled with water were placed on each side of the phantom to mimic the patient's arms. In a clinical setting, TMI patients are treated with intensity modulated beams from the top of the skull to mid femur and the rest of the lower extremities are treated on a conventional linear accelerator with abutting anterior-posterior (AP) and posterior-anterior (PA) beams. Treating the entire patient on the Tomotherapy unit is prohibitive due to the limitation of the machine's longitudinal couch movement. In order to complete the treatment on the tomotherapy unit, a second treatment plan would have to be created with the patient simulated in the feet-first position. Additional planning, QA, setup and relatively long beam-on-time would be required for a site that may not benefit from intensity modulation as there are no critical organs at risk in the lower extremities. Utilizing an AP/PA technique, dose delivery and calculation is greatly simplified, and the patient is set up such that the superior border of the lower extremity fields matches the inferior border of the Tomotherapy treatment. The CT data was exported to Eclipse (Varian Medical System Inc., Palo Alto, CA) treatment planning system for contouring.

Three different planning target volumes (PTVs) were created. Delineations of the PTVs were based on experience from centers currently treating total marrow with intensity modulation[28,30,33]. PTV1 consisted of all skeletal bone. Since the area of interest here is the marrow, contouring the bone provides the necessary margins

for setup uncertainty. PTV2 included the skeletal bone with additional 5 mm margins. PTV3 included all skeletal bone with 5 mm margins only on femurs and ribs. Also, the mandible was excluded from the PTV3 to limit dose to the oral cavity. The locations of normal organs were approximated by overlaying the images of the Rando phantom with a template image set. While several organs at risk were contoured, only the following five major organs were used in optimization and plan evaluation: lungs, liver, kidneys, heart and brain. The CT sets along with contours were then exported to the TomoTherapy Hi-Art v4.2 treatment planning system for CPU planning and a research treatment planning workstation for GPU planning.

There were five different treatment plans created. The plans differed from each other not only by the PTV volume chosen for optimization, but also by different optimization parameters and machine settings. Among the machine parameters varied in the planning process were longitudinal field width, pitch and modulation factor. The user has three options of field width selection: 1 cm, 2.5 cm and 5 cm. Since the contoured volumes are very large in the longitudinal extent, only 2.5 cm and 5 cm field widths were evaluated. The pitch is defined as the fraction of the field width that the treatment couch moves in the longitudinal direction during one gantry rotation. The pitch was selected to minimize the thread effect[34] and provide a good compromise between plan quality and treatment duration. The initial modulation factor was chosen to be either 2 or 2.5 which represent typical values used clinically. The modulation factor is defined as the ratio of the maximal open time of any MLC leaf to the average leaf opening time for all non-zero leaf opening times. Table 1 lists the key parameters for each of the five plans.

Plan #	Field Width	Pitch	Mod. Factor	Actual Mod. Factor (CPU, GPU)	PTV* Set
1	2.5	0.43	2	(1.761, 1.699)	PTV1
2	5	0.287	2	(1.735, 1.691)	PTV2
3	5	0.287	2	(1.728, 1.677)	PTV1
4	5	0.287	2.5	(2.139, 2.076)	PTV2
5	5	0.287	2.5	(2.176, 2.121)	PTV3

Table 1. Summary of plan parameters. *PTV1 - skeletal bone only, PTV2 - 5 mm expansion, PTV3 - 5 mm expansion on Ribs and Femurs only

The prescriptions for all plans were set to 12 Gy and “normal” calculation grid was used for dose calculation. The plans were generated to ensure that 95% of the PTV received the prescription dose. Several variations of optimization parameters were used to create the plans. The parameters were set at the beginning of the optimization and were not adjusted during the optimization process, which consisted of 100 iterations. This process eliminated user dependency of optimization outcome. All five plans were optimized and calculated with the same parameters on the CPU based planning station and the new GPU based research station. The new GPU system utilizes the TomoHD v136 treatment planning station running on a single workstation with quad core Intel i7 CPU at 3.07 GHz and NVIDIA GTX470 graphic card. The details of the GPU based dose calculation algorithm were published recently by Lu at al.[32] and Chen at al.[16].

The plans were evaluated based on D50 and D80 (dose to 50% and 80% of the OAR volume, respectively). The percentage of target coverage by the prescription dose is considered a hard constraint in the planning system; therefore all PTVs received 12 Gy to 95% of their volumes. The PTVs were then assessed based on V13.2 (volume of PTV receiving at least 13.2 Gy (110% of the

prescription)). A gamma (Γ) analysis[35] was performed to compare axial planes transecting the OARs calculated by each dose engine. The two dimensional dose distributions were extracted from the plans and exported to RIT software for gamma analysis (RIT, Colorado Springs, CO). The dose planes were exported via the Eclipse (Varian Medical Systems, Palo Alto, CA) planning system where the matrices were resampled by linear interpolation to 0.5mm resolution. The gamma analysis represents the percentage of pixels that agreed within 3% dose difference and/or 3mm distance to agreement. Finally, the planning process for the two dose engines was evaluated by comparing optimization and dose calculation time as well as changes in beam-on time duration between the two systems.

2.3 Results

The differences in the OAR doses from CPU based plans and corresponding GPU based plans were calculated as a percentage of the prescription dose and are summarized in Table 2. Since all the plans used different machine settings and optimization parameters the results are presented by evaluating each plan individually. All D80 and D50 parameters vary by less than 3% of the prescription dose with an average difference of 0.8%. The differences in V13.2 for the PTVs were under 3.5% with an average of 1.9% for the five plans. The average dose values for all the CPU and GPU plans for D50 and D80 are as follows: Lung 7.6Gy and 6.2Gy, Liver 5.5Gy and 4.6Gy, Kidneys 5.2Gy and 4.6Gy, Heart 5.0Gy and 4.4Gy, Brain 7.2Gy and 3.6 Gy. The average PTV volume receiving 13.2Gy between all the plans was 2.6%. The Γ(3%, 3mm)<1 analysis results are presented

in Table 3. All of the dose planes satisfied the 90% criterion with an average agreement of 97%.

	PTV	Lungs		Liver		Average Kidneys		Heart		Brain	
Plan	V13.2 (%)	D50	D80	D50	D80	D50	D80	D50	D80	D50	D80
1	-0.98	-1.8%	1.3%	0.1%	3.4%	0.5%	0.4%	1.6%	2.9%	-0.4%	1.5%
2	-3.17	-1.4%	-0.9%	0.0%	1.3%	0.1%	0.5%	1.9%	2.3%	-0.1%	0.7%
3	-0.99	-1.0%	-0.9%	-0.3%	1.8%	-0.2%	0.1%	2.2%	2.8%	-0.1%	0.9%
4	-3.43	-2.2%	-1.7%	-0.1%	1.3%	0.1%	0.5%	0.6%	0.5%	-0.1%	0.7%
5	-0.98	-1.5%	0.1%	0.7%	2.4%	0.2%	0.2%	2.7%	2.3%	-0.3%	1.1%

Table 2. Difference in dose relative to 12 Gy. Formula: (GPU-CPU)*100/12Gy.

Plan	Voxels satisfying Gamma Γ(3%, 3mm)<1 GPU vs CPU (%)				
#	Lungs	Liver	Kidneys	Heart	Brain
1	95.1%	93.7%	99.2%	92.3%	96.4%
2	98.5%	97.4%	99.1%	97.1%	95.4%
3	98.8%	99.1%	99.6%	97.5%	98.8%
4	91.7%	97.4%	97.6%	97.1%	98.6%
5	96.1%	92.1%	99.9%	95.5%	99.9%

Table 3. Gamma Γ(3%, 3mm)<1 analysis results.

The total optimization and dose calculation times are shown in Table 4. Total times include beamlet calculation, optimization of 100 iterations, full dose calculation and final dose calculation for the CPU system. The GPU system does not require pre-calculation of the beamlets, therefore total time includes optimization of 100 iterations, full dose and final dose calculations. The average time for the CPU based system was 579 minutes compared to 26.8 minutes for the GPU system. This represents greater than a twentyfold reduction in treatment planning time. There was no difference in calculated delivery times between the two systems. Beam-on time varied based on field width and pitch and ranged between 15min and 28min.

		Optimization/dose calculation time (min)					
		CPU			GPU		
Plan	Beamlet	Optimization	Final dose	Total time	Optimization	Final dose	Total time
1	468	105	12	585	26.0	0.5	26.5
2	453	120	9	582	27.3	0.6	27.9
3	448	126	11	585	27.0	0.5	27.5
4	471	111	9	591	27.4	0.6	28.0
5	457	83	12	552	23.5	0.5	24.0
			Average	579		Average	26.8

Table 4. Optimization/dose calculation time.

2.4 Discussion

In this study we investigated the plan quality and planning time characteristics of dose calculation using the new TomoTherapy GPU based dose calculation system and its application in total marrow irradiation. A recent publication[36] has validated the new GPU system for use with smaller target volumes with excellent results, however similar studies have not previously been performed for very large target volumes. There were very small differences in the quality of plans calculated with the GPU based system as compared to CPU based system. These differences could be attributed to the gradient descent nature of the optimization algorithms and fixed number of iterations that may stop the process at a slightly different solution each time. Gradient descent techniques are relatively fast, but are susceptible to getting stuck in local minima. Although optimization parameters such as the pitch, field size, PTV and OAR constraints, numbers of iterations, etc. entered by the planner were identical for plans calculated in both CPU and GPU based planning systems, the algorithms are fundamentally different. The CPU system uses voxel-based beamlet-superposition optimization framework whereas GPU system uses non-voxel-based broad-beam framework, where the objective function and derivative

are evaluated on continuous view point. This eliminated time consuming pre-calculation and storage of beamlets. The details of the algorithms were described by Lu.[32] In addition to the differences in the optimization algorithm, the new GPU system uses a novel collapsed cone convolution/superposition CCCS algorithm presented by Chen at al.[16] which uses tabulated and exponential kernels and takes full advantage of the parallel nature of the GPU. This algorithm uses CCCS for accurate dose calculation for one every ten iterations followed by Fluence-Map Convolution Broad Beam (FCBB) calculation for the remaining iterations. The FCBB calculates approximates 3D dose by 2D fluence map convolution with 1D ray tracing, resulting in orders of magnitude faster calculation than CCCS alone. The algorithm uses beam's eye view coordinate system and is also capable of direct treatment parameter optimization. These differences in the optimization and calculation algorithms are most likely the cause for differences in the treatment plan quality given the same optimization parameters.

This treatment site is likely to benefit the most from the use of the GPU dose engine since the average computational time is over 9 hours with the current cluster-based CPU system. In centers with only one CPU system, the time consuming planning of TMI cases can significantly inhibit other clinical work on that system. The introduction of GPU architecture in the TomoTherapy planning system will make the transition from conventional TBI to TMI treatments more feasible by preserving valuable clinical computational resources and providing more flexibility for QA and patient start times. The tremendous increase in planning speed provided by GPU

planning would also be extremely useful for potential future implementation of adaptive radiotherapy involving on-line replanning.

This study did not investigate the differences in delivery accuracy of the two systems as the GPU system was dedicated only for research and transferring GPU plans to our clinical Tomotherapy unit was not possible. Our prior work on commissioning TMI using the CPU based system resulted in delivery accuracy similar to all other clinical cases treated on Tomotherapy. Our QA criteria are +/-3% for two absolute point dose measurements with small volume ion chambers and $\Gamma(3\%, 3mm)<1$ for >90% of points in a film plane dose distribution.

Other groups[23-27] have studied the use of IMRT and VMAT for TMI. Dosimetrically, all of these intensity modulated methods are comparable and offer significant improvement in normal organ sparing over traditional TBI treatments. All intensity modulated approaches for treatment of total marrow have some limitations. With the larger apertures available from a C-arm linac system, the prescription dose can be delivered using VMAT in about half the time[27] it takes HT to deliver the same dose to a region covered by a single VMAT arc. However, this advantage is lost when comparing total treatment time and not just beam-on time since the linac based treatments require several treatment plans to cover the entire target volume. The patient has to be repositioned for each isocenter, thus prolonging the total treatment delivery time. Other groups[27] have reported limitations on the number of total arc degrees when using Volumetric Modulated Arc Therapy (VMAT) for large target volumes. The limitation on total arc degrees will affect the plan quality as only one arc can be used in a particular section of the PTV in order to cover the entire

treatment volume. In clinical practice, for other treatment sites, we typically use at least two full arcs to achieve good plan quality. As mentioned in the methods and materials section, the portion of the PTV below the mid femurs is treated without intensity modulation and simple AP-PA treatment is usually sufficient. Our Tomotherapy system does not have the capability to treat static beams. Our two options are to transfer the patient to a C-Arm linac for the remainder of treatment or reposition the patient to feet-first setup and continue the treatment on Tomotherapy. Both options add time and uncertainty to the treatment. The former option requires scheduling and transferring the patient to two machines. The latter option adds significantly to beam-on time.

2.5 Conclusions

We have presented dosimetric and computational results of the GPU based TomoTherapy planning system for Total Marrow Irradiation and compared them to similar results using the traditional CPU system. The agreement of dose distributions calculated with these two systems using the same targets and optimization parameters is excellent. The GPU dose calculation engine overcomes the significant time constraint limitations that have been associated with creating treatment plans for large target volumes, as it can calculate the plans in fraction of time of the traditional CPU system without degradation in plan quality.

CHAPTER 3. "DOSIMETRIC EVALUATION OF TOTAL MARROW IRRADIATION USING TWO DIFFERENT PLANNING SYSTEMS".

3.1 Introduction

Total Marrow Irradiation (TMI) is an advanced version of an existing radiation therapy treatment method called Total Body Irradiation (TBI). TBI is a radiation treatment and conditioning regimen used prior to a bone marrow transplant (BMT).[37-39] Results from previously published randomized trials have demonstrated excellent outcome from the use of TBI before hematopoietic cell transplants.[18-20] Dose escalation has proven to reduce post-transplant relapse rates with chronic and acute myeloid leukemia,[21,22] however, due to excessive toxicity to OARs, the overall survival did not improve.

Due to the field size limitations on a standard C-arm linear accelerator at standard treatment distances, TBI treatments are often delivered at extended distanced with (anterior-posterior) AP/PA or bilateral techniques. These techniques traditionally deliver a relatively uniform prescription dose to the entire patient including all organs at risk (OARs). The exception to this is that for higher doses and multi-fraction schedules, lung blocks are often used to reduce dose to the lungs. Lungs are the critical organs at risk, with pneumonitis being a major cause of complications after TBI treatments. One key study by Volpe, et al.[40] established a threshold mean dose of about 9.4 Gy to the lungs from TBI treatment, beyond which a significant increase in post BMT mortality exists.

With the advancement of intensity modulated radiation therapy (IMRT) it is now possible to deliver a therapeutic radiation dose to bone marrow while

significantly reducing the dose to all healthy organs for patients undergoing hematopoietic cell transplantation.[17,23,25-27,31] However, the attempt to conform the dose distribution to the marrow only results in a relatively complicated planning process which is quite dependent upon the particular TPS and delivery method used. In this study we report quality and efficiency of TMI plans created on two different treatment planning systems for two different delivery modalities using the same phantom and structure set.

3.2 Methods and Materials

3.2.1 Phantom and contouring

The patient used for this study was the Rando phantom (The Phantom Laboratory, Salem, NY), which represents the full human body, except for the extremities. This anthropomorphic phantom has a human skeleton embedded in material that mimics soft tissue. There are also air cavities and low density materials in the lungs to approximate the heterogeneities of a human body. The Rando phantom was placed in an immobilization device and simulated in the same manner as a TMI patient, including a CT scan of the entire length of the phantom with 5mm slice thickness. As is common in TMI,[27] the PTV extended from the most superior part of the skull to mid-femur. Since there are no critical OARs caudal to mid-femur, the lower extremities are treated without IMRT using abutting AP/PA fields.

The CT image set was transferred to the Eclipse (Varian Medical Systems Inc, Palo Alto, CA) TPS for contouring. All bony structures surrounding marrow were included in the CTV, with the exception of the mandible, which is not a part of marrow forming skeleton. For the ribs and femurs the PTV was created with 5mm margin. There

was no margin used for all the other bones because CTV is the bone but the target is the marrow. The OARs considered in this study and contoured on the CT image included brain, heart, lungs, liver, kidneys, and small bowel. Since these structures do not exist in the phantom, they were contoured based on an atlas to approximate the size, shape and location of the organs in the Rando phantom.

3.2.2 Modality and plan objectives

The Eclipse TPS was used to create a TMI plan using VMAT (Rapid Arc) delivery on a Varian iX treatment unit. The CT data set and contours were also exported to the VoLO TPS and used to create a helical tomotherapy treatment plan on a TomoTherapy Hi-Art treatment unit. The two planning systems use different optimization schemes and different objective function definitions, which makes it difficult to set the same planning objectives. Also, the dose delivery methods are quite different. In RapidArc mode, Varian uses volumetric arcs modulated by MLCs and stationary couch, whereas TomoTherapy uses helical delivery with binary MLCs and continuously moving couch. The objectives for both treatment planning systems were to deliver 1200cGy in 8 fractions to 95% of the PTV and minimize mean dose and D_{10} to OARs. Experienced planners created the treatment plans using planning parameters that are commonly used in our clinic as described below.

3.2.3 TomoTherapy Planning

Tomotherapy delivery for long treatment fields such as TMI is easier than for conventional C-arm linacs since there is no field matching. The couch movement through the bore during delivery allows the entire treatment to be delivered in one session as opposed to the multiple sets of fields required for treatment using

conventional linacs. As a result, the Tomotherapy planning in this study was much more straightforward than that for Eclipse.

Many plans were optimized during this study to evaluate the effects of variations in field width, pitch, and planning modulation factor (MF) necessary to yield a good plan. Each of these three parameters had only 2 values, and represented the most commonly used parameter in our clinic. Field width was either 5 cm or 2.5 cm. Pitch was either 0.287 or 0.430. Modulation factor was either 2.0 or 2.5. The final plan used for this study had parameters of 5cm field width, pitch of 0.287 and modulation factor or 2.5.

3.2.4 Eclipse Planning

The Eclipse portion of the study used Varian Eclipse version 8.9 and was planned for a Varian iX linac with Millennium 120 Multi-Leaf Collimator (MLC). This MLC system has 1 cm leaves in the outer portion of the field and 0.5 cm leaves in the inner 20 cm of the field. The optimizer in Eclipse was the Progressive Resolution Optimizer (PRO) version 2, which allowed a total beam angle across all arcs in one plan of 1500 degrees (just over 4 full arcs).

Initial plans primarily focused on optimizing the full PTV with either three or four full 360° RapidArc arcs. Each beam had its own isocenter, and the beams were arranged to overlap each other on the superior/inferior edges. Although some three-arc plans were successfully completed, the three overlapping arcs were found to be insufficient to provide good homogeneity within the PTV. Unfortunately, when 4 full arcs were used, the software reached the limit of 1500 degrees per plan and with the

very large PTV size; the computational power needs exceeded what was available in our workstation.

Due to these existing software and hardware limitations, the single large PTV was divided into four separate PTV's of roughly equal size. PTV1 covered the head and neck, PTV2 covered most of the thoracic region, PTV3 covered from about the top of the liver to mid-abdomen, and PTV4 covered from about mid-abdomen to about mid-femur. With the single PTV broken into four sub-PTV's, it was then possible to optimize to each PTV individually, thus avoiding the intensive calculations necessary to optimize the entire body all at once.

Two arcs were used for each sub-PTV with initial isocenter placement in the middle of each volume along a longitudinal line that would avoid lateral and vertical patient positioning shifts when going from one isocenter to the next. This approach used two arcs targeting each sub-PTV, with one rotating counter-clockwise, and the other rotating clockwise. This double arc set-up produced better plan quality than using only a single arc. Optimization was typically done first on the PTV2 plan in the thorax. The dose was calculated and the plan saved. Next, PTV1 was optimized using the dose from PTV2 as a "base dose" (an Eclipse term). The base dose is the final calculated dose distribution from the PTV2 plan which is brought into the PTV1 optimization and is "seen" by the optimizer as existing dose. Thus the optimizer only needs to place dose where no dose already exists, yielding a smooth junction between PTV's. The process continued like this, optimizing with previous dose distribution and then calculating the dose for the new PTV. PTV2 was usually first, followed by PTV1, then PTV3 and finally PTV4. The result of these plans was a

single plan with eight total beams consisting of four pairs of co-isocentric RapidArc beams.

Several collimator rotation angles were tested. With the maximum field size of 40cm in the longitudinal direction and 16cm in the lateral direction (with collimator at 0°), the degree of collimator rotation had significant implications on PTV coverage singe the distance between the isocenters was larger than the maximum 16cm field width. The arc overlap is necessary to create smooth dose transition between the sub-PTVs. With the collimator at 0° there was ample overlap between the beams but this geometry failed to provide "tangential" beamlets, which are critical in getting dose to structures such as the ribs without overdosing the underlying OARs, such as the lungs. An analysis of this "rib problem" is shown below in figure 1. Increasing the collimator to 45° provided sufficient overlap region to give smooth dose distribution between the sub-PTVs, and fairly good but not excellent PTV coverage due to some parts of the PTV missing that “tangential” beam. Finally, rotating the collimator to 90° provided excellent lateral coverage but the fields as designed were not long enough to overlap with each other as shown in figure 2a. To remedy the overlap regions, a carriage shift between the co-isocentric arcs was implemented to allow the entire PTV coverage. A schematic of this beam setup is shown in figure 2c.

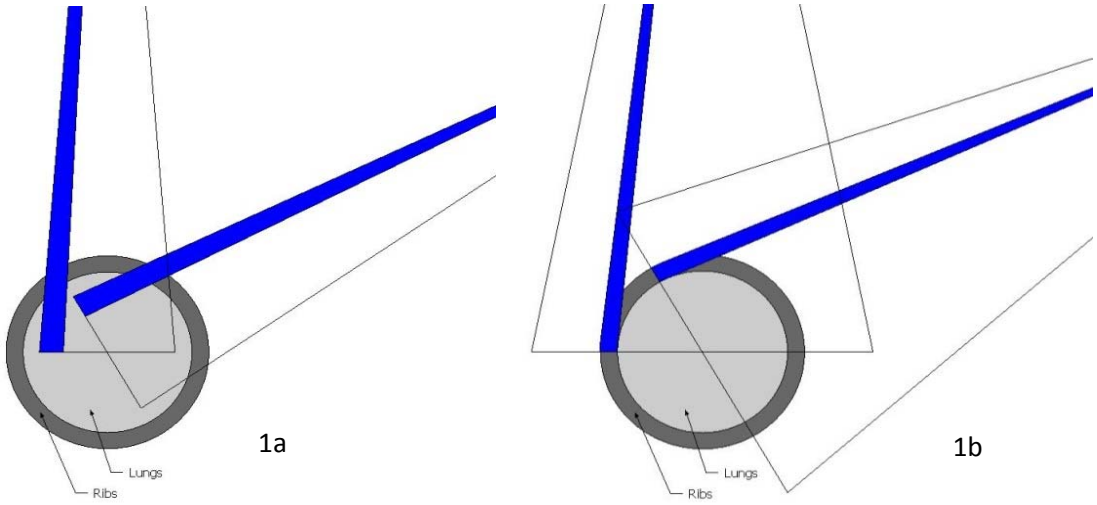

Figure 1. A schematic of the "rib problem". Both images show a RapidArc beam at two different gantry angles. Although zero collimator rotation (1a) appears to have good coverage, it is too narrow to allow any "tangential" beamlets to the ribs. Any dose to the ribs must also pass through the lungs. Image (1b) is an example of 90° collimator angle, showing how the much wider beam provides excellent access to tangential beamlets through the ribs, which avoid the lungs.

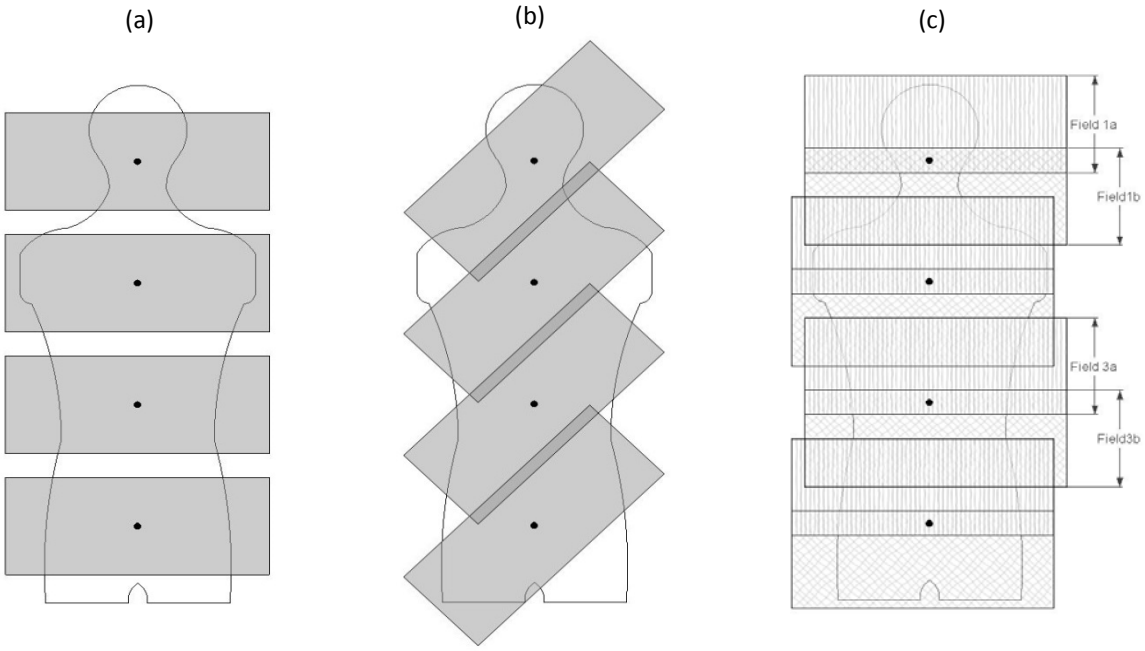

Figure 2. Eight arcs shown in three configurations. a) with a collimator rotation of 90°, showing lack of overlap with adjacent fields, b) with a collimator rotation of 45°, showing both good coverage and good overlap. (Note that the white areas of the body are fully covered as the arcs rotate around the body.) c) with a 90° collimator, but with the beams moved asymmetrically (fields are shown offset left and right for clarity).

3.3 Results

Both Eclipse and VoLO plans were normalized to deliver 1200 cGy to 95% of the PTV, and evaluated for mean, maximum and D_{10} PTV doses as well as mean dose and D_{10} to OARs.

3.3.1 PTV Analysis

The TomoTherapy plan resulted in superior coverage of the PTV, with a very steep DVH curve, increasing only about 100 cGy from the D95 level to the D10 level (figure 3). The Eclipse plan compared favorably with the Tomo plan, but was slightly "hotter", increasing about 156 cGy from D95 to D10. The max doses (table 5) differ by 76cGy between the two plans, with 1465 and 1541 cGy for TomoTherapy and Eclipse, respectively.

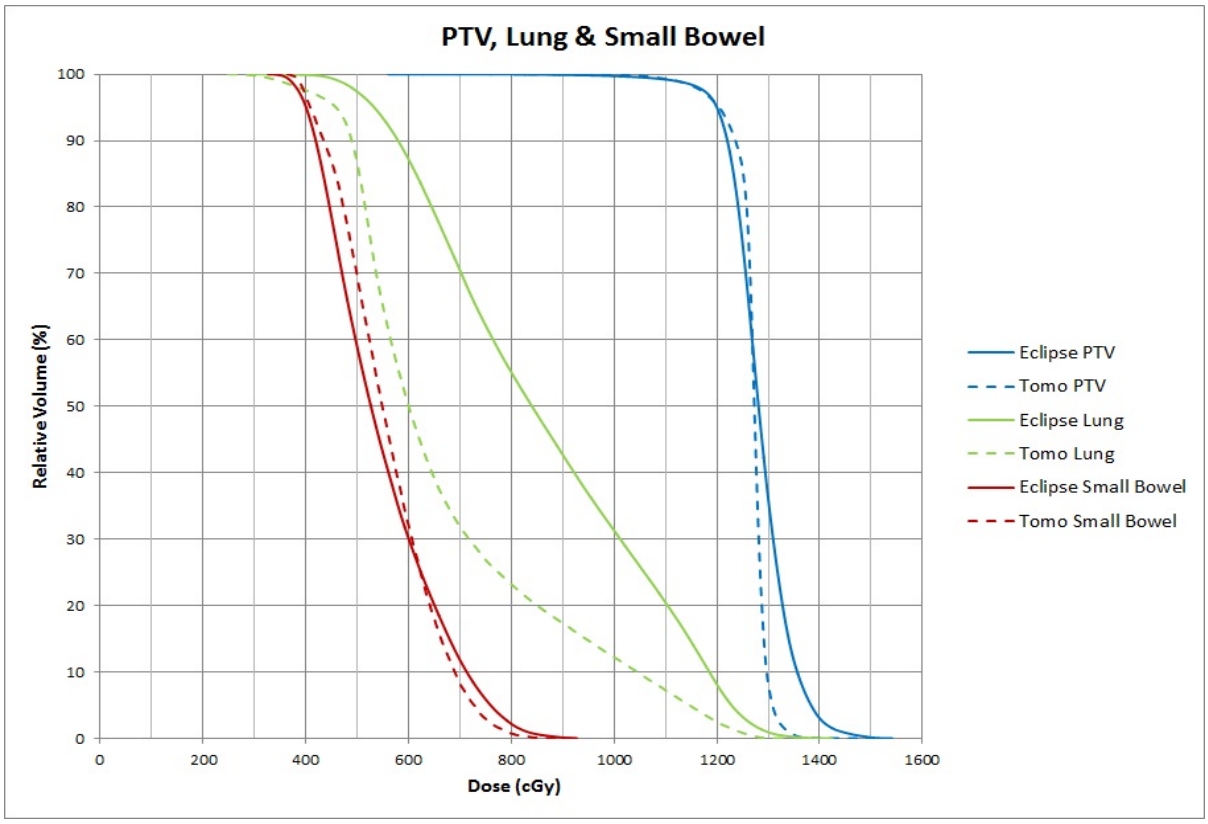

Figure 3. Doses to PTV, Lung and Small Bowel.

	D95	Mean Dose	D10	Max Dose
TomoTherapy	1200	1268	1297	1465
Eclipse	1200	1284	1356	1541

Table 5. Dose to PTV, in cGy.

3.3.2 OAR Sparing

The results of the critical OAR sparing for the two planning systems are presented in figures 3 to 5. The mean dose and maximum doses of all OARs considered are shown in table 6. The mean dose and D_{10} to every OAR was between 3% to 52% lower for the TomoTherapy plan, with the exception of the small bowel, where the Eclipse plan was slightly better.

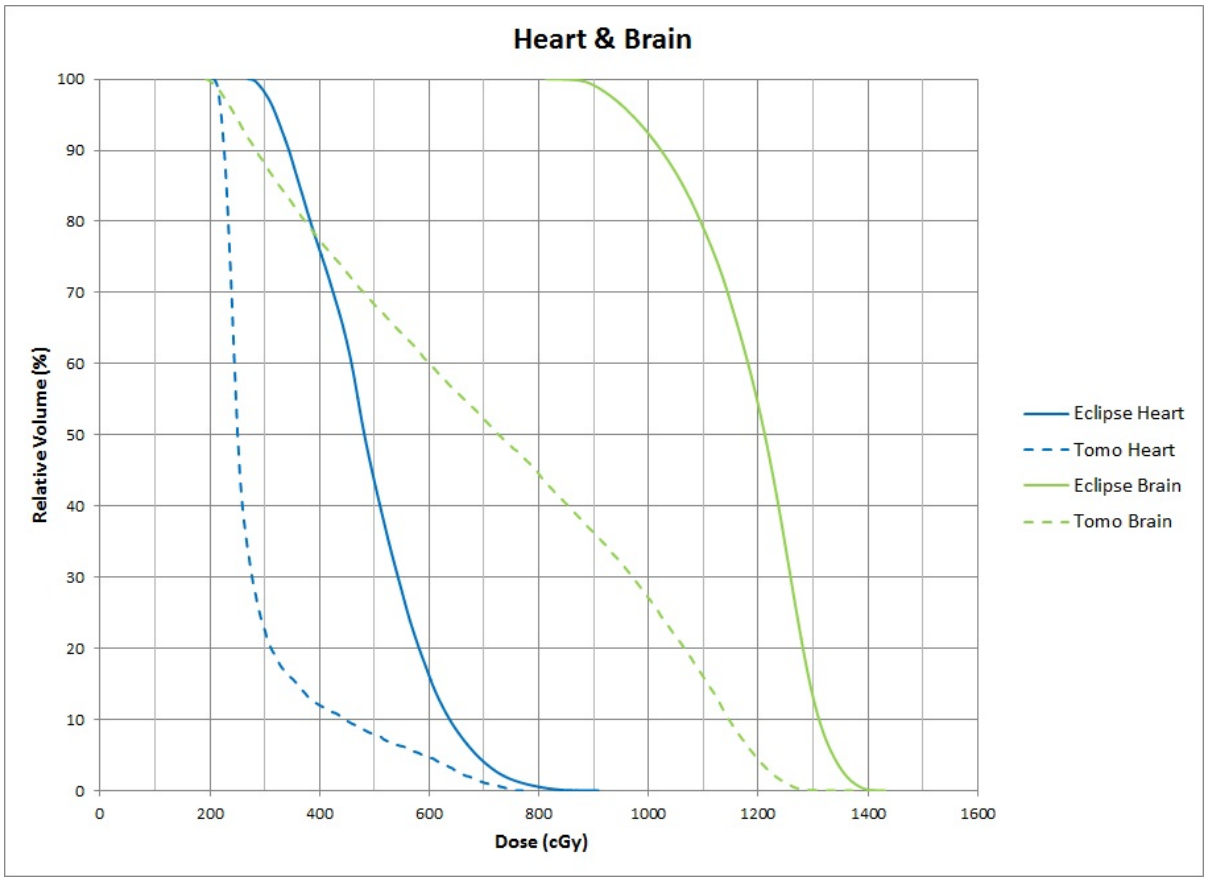

Figure 4. Heart and Brain DVHs.

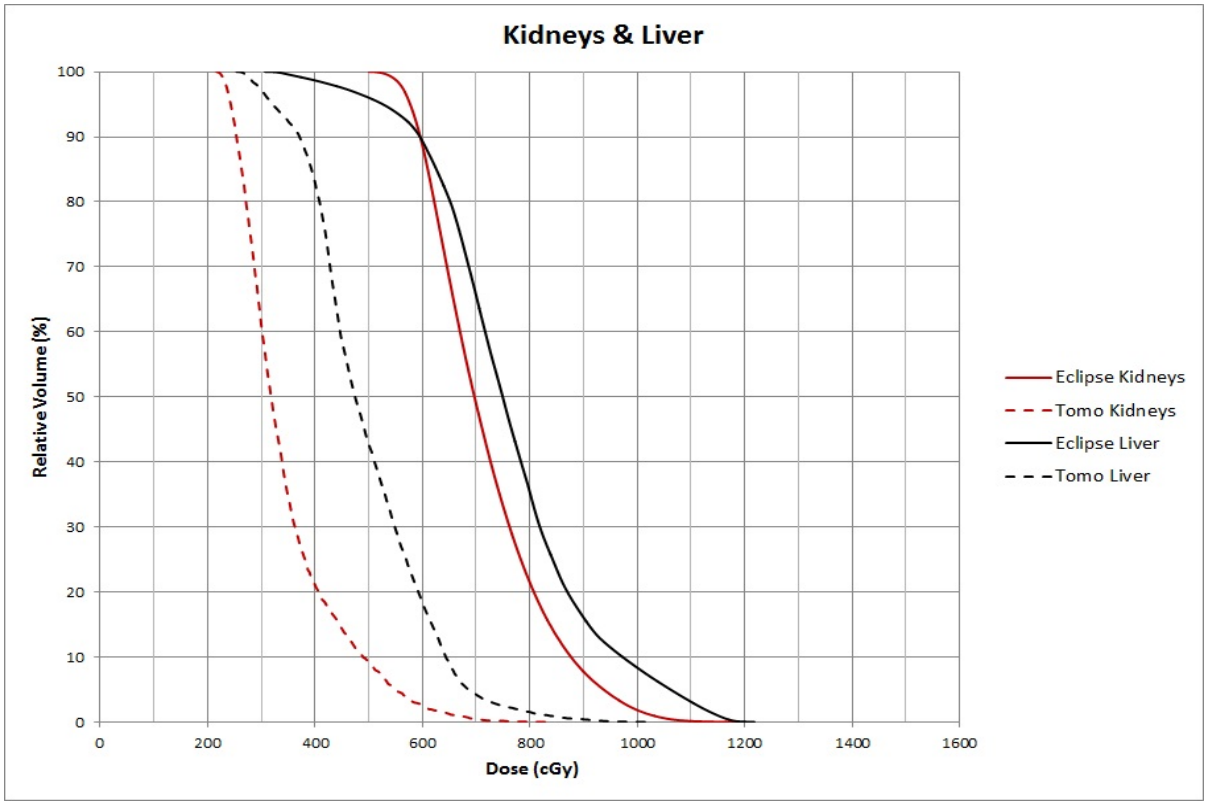

Figure 5. Kidney and Liver DHVs.

Due to its important role in post-BMT toxicity, the primary OARs considered in this study were the lungs. The right and left lungs were considered as a single structure for dose analysis. The mean dose to total lung in the TomoTherapy plan was 677 cGy, compared to 864 cGy for Eclipse. It is worth noting that both the TomoTherapy and Eclipse plans are below the ~9.4 Gy mean lung dose threshold discussed in the Volpe et al.[40] paper.

	Lung		Brain		Heart		Liver		Small Bowel		Kidneys	
	Mean	**D10**	**Mean**	**D10**	**Mean**	**D10**	**Mean**	**D10**	**Mean**	**D10**	**Mean**	**D10**
Tomo	677	1045	723	1146	294	446	496	643	558	690	345	492
Eclipse	864	1185	1188	1311	489	637	762	973	548	713	720	877
Difference	22%	12%	39%	13%	40%	30%	35%	34%	-2%	3%	52%	44%

Table 6. OAR doses in cGy. Difference shown as (Eclipse-Tomo)/Eclipse.

3.3.3 Treatment Planning Time

Although the time required to create a TMI plan would vary considerably based on both the skill of the planner and the speed of the computer used, an attempt was made in this study to track time spent on various tasks. These results are given as information for those planning to implement or study TMI in order to give a broad idea of times that may be required.

This process of optimization and dose calculation is from the conclusion of beam placement, prescription selection and selection of all optimization parameters to the conclusion of all dose calculation steps. Only software optimization and dose calculations times were therefore evaluated. Other tasks that are user dependent are not included in the results. The times are reported for the final plans created by each system.

Final computation time for Tomotherapy which consisted of optimization time and final dose calculation time was 0.9 hours. The optimization time took the majority of the computational time. The optimizer was run until there was no further visual improvement of the DVH with additional iterations. The objective functions were chosen by trial and error to achieve a plan with lowest PTV hot spots and lowest OAR doses.

The Eclipse final plan consisted of four separate plans. Each sub-plan was optimized several times to minimize hot-spots in the overlap regions. The final computation times, including optimization and dose calculation for the four plans was 3.8 hours.

3.3.4 Beam-On Time

In a simplified case, beam-on time would only be dependent on machine output (dose rate) and fraction size (dose). Beam-on time increases with dose and it is inversely proportional to the dose rate. In the Varian system the dose rate is variable and during beam delivery the dose rate is adjusted based on MLC and gantry position (in RapidArc mode). The more modulated (complex) the plan the lower the dose rate due to maximum MLC leaves speed limitations. In our study the dose rate varied between 200-300 MU/min, effectively delivering each arc in approximately 76 seconds for the total of 608 seconds. The dose rate of Tomotherapy is fixed at approximately 860 MU/min. Beam-on time in Tomotherapy is dependent on gantry speed, field size and the pitch. Despite higher dose rate, TomoTherapy's maximum field size is limited to 5cm in the longitudinal direction as opposed to up to 40cm for Varian, and due to the helical delivery mode with pitch of 0.287 the beam-on time was much longer at 1148 seconds. Older Tomotherapy systems were reported[52] to have problems with dose rate constancy which would affect final dose delivered to the patient. Our unit is equipped with a Dose Control Servo (DCS) system which keeps the output rate steady at 860 MU/min.

3.4 Discussion

The TomoTherapy TPS was able to achieve the best PTV coverage and superior sparing of most OARs. The helical nature of TomoTherapy delivery along with 40cm lateral field size allows the beam to enter from any angle and cover the entire PTV in the lateral direction. With pitch of 0.287, every voxel of the PTV "sees" the entry beam over 3 times. In a conventional C-arm gantry linac, the same voxel

will only “see” the entry beam once per arc. Tomo plans therefore result in more homogeneous dose distribution in the PTV and lower doses to the OARs due larger solution space available to the optimizer.

The differences in the plan quality are presented here for one case only and are meant to show general differences between the modalities and their respective treatment planning systems. Individual results of the OARs will be strongly dependent on optimization parameters chosen, their weights and priorities. Individual planning skillset as well as clinical practice will also influence final planning results. Even if it was possible to set the same optimization objectives between the two modalities, the plan differences would still exist due to different calculation algorithms. Eclipse TPS uses analytical anisotropic algorithm (AAA) and Tomotherapy utilizes collapsed cone convolution superposition (CCCS) algorithm for dose calculations. The AAA is pencil beam like superposition algorithm that uses only analytical functions for calculations. It makes assumptions that the dose at any given point is the sum of contributions of a depth dependent and a lateral part. In heterogeneous tissue the beamlet attenuation and lateral energy kernel are scaled based on “equivalent path”. The CCCS is volume based algorithm where primary energy is convolved with polyenergetic kernel that describes the energy spread of secondary particles and accounts for the lateral transport of energy. In heterogeneous media, the kernels are scaled using mass stopping power ratio and mass attenuation coefficient ratio. Both algorithms have been extensively studied and compared to the “gold standard” of Monte Carlo (MC) algorithm. Generally, the

CCCS algorithm show less deviation from MC as compared to AAA especially in heterogeneous tissue.[110]

Planning a TMI case in the TomoTherapy software followed routine planning processes regardless of the length of the target volume. However, the planning process in Eclipse required matching multiple arcs using multiple isocenters and was a cumbersome process. The sheer size of the PTV required several arcs to achieve an acceptable plan but the number of total arc degrees between all arcs in a plan is limited to 1500 degrees. The necessity of splitting the PTV in to smaller sub-PTVs was laborious and complicated as some of the organs overlapped two sub-PTVs, making the choice of optimization parameters for these structures difficult. The complexity of multiple isocenter plans in Eclipse also affects the treatment delivery. Although the beam-on time for Eclipse plan for Varian IX linac was just over half of that of TomoTherapy, the overall treatment time difference will be significantly smaller since for every isocenter, the therapists have to enter the room and reposition the patient.

It would be very difficult to accurately estimate the total time required to plan a TMI case on each planning system. Total time is dependent on the experience of the planner and the number of trials to achieve acceptable plan. Tracking total time therefore would be user dependent and very subjective. However, the tasks of optimization and dose calculation times can be objectively evaluated. The much longer time necessary for Eclipse to optimize and calculate the plans was partly due to the different optimization and dose calculation algorithms as well as the need to repeat the process for each sub-PTV. TomoTherapy takes advantage of the parallel

nature of the GPU system as described by Lu at al.[32] which can process data up to 20 times faster than comparable CPU based systems.[42] Dose delivery validation for TMI plans has been previously reported by Hui et al.[31] and Corvo et al.[43] therefore validation measurements have not been performed in this study.

3.5 Conclusions

The results of this study have demonstrated that the new TomoTherapy VoLO planning station was able to create better TMI treatment plans in terms of PTV coverage and OAR sparing. In addition, the simplicity of planning process as compared to multiple plans on Eclipse makes TomoTherapy the better choice for planning TMI treatments. Another advantage of the VoLO system used in this study was the ability to optimize and calculate the TMI plan about four times faster than Eclipse. With advancements in the software and continuous improvements in computational speed, the planning times may not be a factor in the future.

CHAPTER 4 "TOTAL MARROW IRRADIATION: A COMPREHENSIVE APPROACH TO TREATMENT PLANNING FOR HELICAL TOMOTHERAPY"

4.1 Introduction

Total body irradiation (TBI) plays an important role as an immunosuppression agent in patients undergoing bone marrow transplantation (BMT).[17] Traditionally the dose is delivered using standard radiotherapy equipment such as linear accelerator or Co-60 teletherapy machines. Due to the radiation field size limitations of these devices in treating the entire bone marrow, the patients are often treated at extended distances taking advantage of the divergent nature of the beam. Patients are positioned to be treated either bilaterally or anterior-posteriorly.[37-39] Two opposed beams deliver the prescription dose specified at the mid-depth with a goal of dose uniformity of ±10%. If the patient thickness varies significantly, additional blocks are used to keep the dose uniformity within 10%. If the beam is delivered uniformly to the entire body, as is conventionally performed, every organ at risk receives approximately the prescription dose. With higher doses it is common to use lung blocks to reduce the dose to the lungs and decrease the risk of pneumonitis. Radiation pneumonitis is the most critical morbidity, and a mean dose of 9.4 Gy to the lungs results in a significant increase in post-BMT mortality.[40] Although higher doses reduce post-transplant relapse, the excessive toxicity in organs at risk reduces the overall survival with the traditional two field delivery methods.[21,22]

With the use of intensity modulated radiation therapy (IMRT) it is now possible to deliver the prescription dose to the bone marrow only, while sparing critical organs, a treatment called Total Marrow Irradiation (TMI). Feasibility studies

have shown that conventional C-arm linear accelerators[23,26,27,44] and Tomotherapy[28,30,31,42,45] can be used to deliver TMI treatments and provide dose reductions of 29%-70% to critical organs relative to conventional TBI treatments. One of the major limitations of TMI is the long treatment time necessary to deliver these modulated fields. Wielkie et al.[23] reported TMI treatment times of nearly 60 minutes. The majority of this time was spent on patient and treatment field setup to deliver the entire plan which consisted of 3 sub-plans. The combined beam-on time for the three sub-plans was only 14 min. Tomotherapy beam-on times for TMI have been reported[28,30,31,42,45,46] with a vast range of 15-50 minutes depending on optimization parameters used.

In this study we used the new Graphics Processing Unit (GPU)-based treatment planning system VoLO (Accuray, Sunnyvale, CA) to create TMI treatment plans for helical delivery on Tomotherapy. The plans were created with a range of clinically acceptable machine optimization parameters. The goal of this study was to develop a TMI planning guide and aid planners with selection of machine optimization parameters to improve the planning results based on desired objectives. A plan quality index (Q) was developed for quantitative analysis of relative plan quality which included mean and maximum doses and beam on time.

4.2 Methods and Materials

In this study we utilized an anthropomorphic Rando phantom (The Phantom Laboratory, Salem, NY) to create TMI treatment plans using the VoLO treatment planning system. The Rando phantom has a human skeleton embedded and is built of a material radiologically similar to soft tissue. It extends from head to mid-femur

and does not have extremities. The phantom was placed in an immobilization device and simulated for treatment using a large bore Somatom Sensation CT scanner (Siemens, Malvern, PA) to acquire a full phantom CT image set with 5mm slice thickness. A planning target volume (PTV) was created by delineating the bony skeleton with the exception of the mandible. An additional margin of 5 mm was added to the ribs and femurs to account for motion. A typical TMI PTV extends from the most superior part of the skull to about mid-femur. It was assumed that since lower extremities don't have critical OARs they would be treated conventionally with 2 sets of abutting AP/PA fields. Evaluated organs at risk (OAR) consisted of lungs, brain, heart, liver, small bowel and kidneys. Since Rando does not have any of these organs other than lungs, the remaining OAR contours were created by a physician to closely approximate their typical size and location.

Optimization objectives were chosen based on previous clinical TMI cases with a goal of reducing the mean dose of OARs to 50% of the prescription dose of 1200 cGy while delivering the prescription dose to 95% of the PTV. The user selectable machine parameters are the field width, pitch and modulation factor. The field width is defined in the superior-inferior (S-I) direction and, since the PTV is extremely large in the S-I direction, only 2.5 and 5cm field widths were evaluated. The pitch is defined as the fraction of the field width that the couch moves per gantry rotation. Pitch values in this study were chosen using the following equation: $p=0.86(1/n)$ where the 0.86 factor is empirical -- caused by beam junctioning --and 'n" is an integer. This pitch equation was originally derived by Kissick et al.[34] to minimize the ripple effect as a result of helical beam junctioning. The pitch values

considered here were obtained for n=1, 2, and 3 corresponding 0.86, 0.43, and 0.287, respectively. The third parameter evaluated was the modulation factor (MF), which is defined as the ratio of the maximum leaf open time to the average leaf open time. Tomotherapy has binary leaves which are either open or closed and the leaf openings are defined through 51 “projections” (approximately 7 degrees) of the gantry rotation and beam modulation is achieved by varying the time that each leaf is open during a projection. Shorter average leaf open times mean greater modulation and result in a larger MF. The modulation factor is set by the planner as a target value for the optimizer (usually 2.0 for clinical cases) and depending on target and OAR constraints, the actual value returned by the optimizer for the plan is within ~20% of the set value. Modulation factors used in this study ranged from 1.25 to 3.0 at 0.25 intervals.

Using one image set and structure set, each TMI plan was optimized for 100 iterations after which the final dose was calculated. The 100 iteration cutoff was chosen based on clinical experience that has demonstrated negligible improvements to dose-volume parameters when allowing further iterations during optimization. Keeping the PTV and OAR objectives the same, the plans were re-optimized with varying field size, MF, and pitch. A summary of all parameter value sets evaluated in this study is presented in table 7.

Field Width (FW)	2.5 and 5.0 cm
Pitch	0.287, 0.43 and 0.86
Modulation Factor (MF)	1.25 - 3.00 @ 0.25 intervals

Table 7. Machine optimization parameters.

Mean and maximum doses for each structure and delivery time for the treatment were compared between plans. In addition, plan quality index (Q) was developed to calculate a relative quality value for each plan. The basic form of equation for Q is shown in Eq. 1:

$$Q = \left(\sum_i^n \ln\left(\frac{D_{ref}}{D_{act}}\right) w_i\right) \quad (1)$$

where, i = PTV and OARs, D_{act} = actual dose achieved, D_{ref} = Reference dose, and w_i = weight as presented in table 8.

i	parameter	D_{ref}	w_i
PTV	Maximum	1320 cGy	2
Lung	Mean	940 cGy	3
Brain	Maximum	1200 cGy	1
Heart	Mean	600 cGy	1
Liver	Mean	600 cGy	1
Small Bowel	Mean	600 cGy	1
Kidneys	Mean	600 cGy	1

Table 8. PTV and OARs constraints.

Mean reference doses were chosen as half of the prescription dose for all OARs other than lung. The dose tolerance limits for all OARs studied here except for lung are well above the prescription dose of 1200 cGy. The weights for these OARs were therefore set at 1 to have the same relative impact on the quality index. Radiation pneumonitis is the most critical morbidity[60] therefore the reference mean lung dose was set at 940 cGy and the relative weight was chosen as 3. This higher weight for lung mean dose was chosen to have higher impact on the quality index and penalize treatment plans that resulted in mean lung dose approaching the limit

of 940 cGy. Maximum PTV reference dose was set at 110% of the prescription or 1320 cGy, based on clinically acceptable dose heterogeneity.

4.3 Results

4.3.1 Field Width.

Plans created with 2.5cm field width had lower PTV mean and maximum doses than plans with 5.0cm field width with the same pitch and MF while maintaining the prescription coverage of 1200 cGy to 95% of the PTV. Figures 6-7 show differences in mean and maximum doses between both field widths for two combinations of pitch and MF. On average the mean and maximum PTV doses were lower for the 2.5cm field width by 0.8% and 4.3%, respectively. Similar results were observed for all the OARs. On average the mean and maximum OAR doses were lower for the 2.5cm field width by 4.1% and 4.3%, respectively.

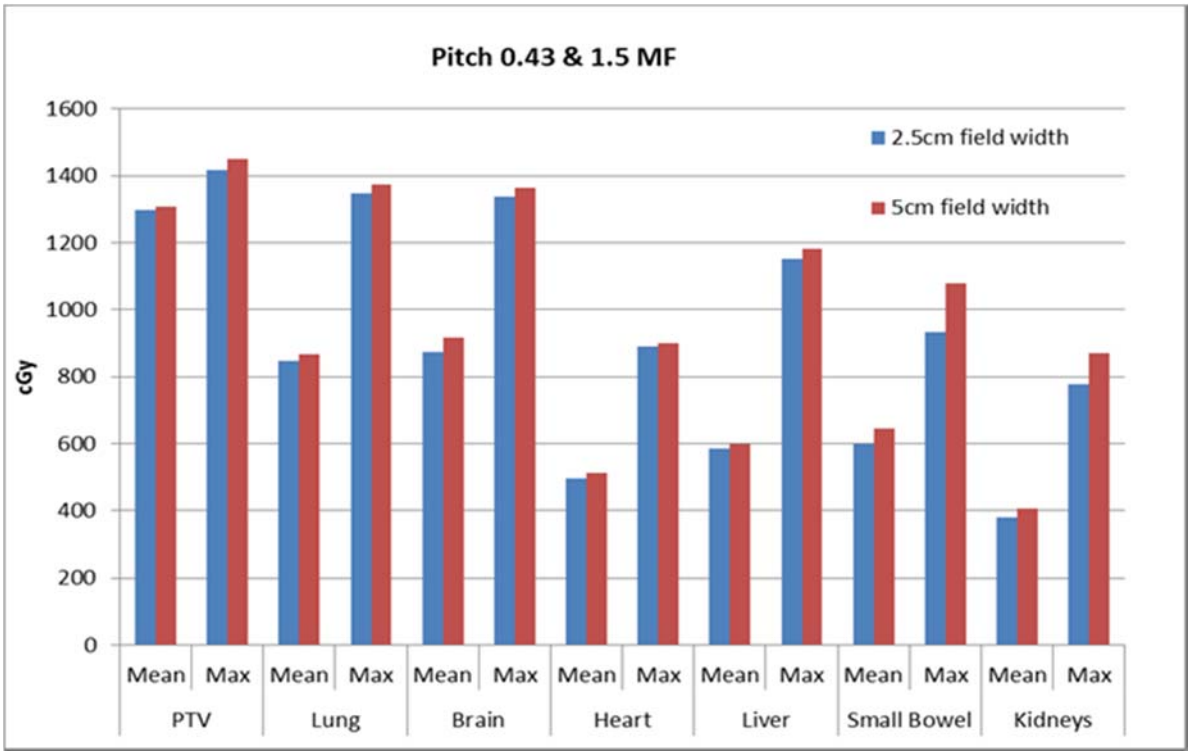

Figure 6. Relative dose difference between FW 2.5 and 5.0cm. Pitch 0.43 & 1.5 MF

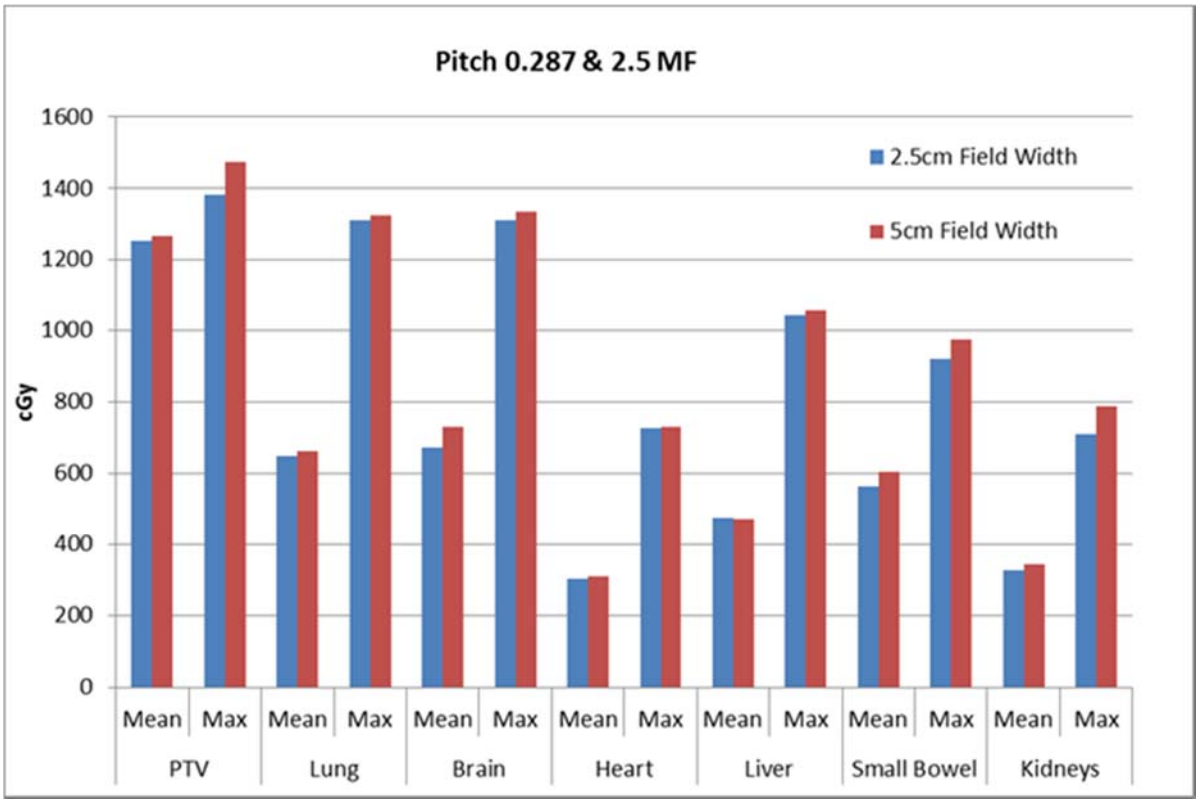

Figure 7. Relative dose difference between FW 2.5 and 5.0cm. Pitch 0.287 &2.5 MF.

4.3.2 Pitch.

In general, the mean and maximum PTV and OAR doses decrease with decreasing pitch with all other parameters constant. For each reduction in pitch the average OAR mean dose was lower by 3.5% and the average maximum dose was lower by 2.0%. The PTV resulted in average mean and maximum dose reductions of 0.8% and 0.7%, respectively, with lower pitch values. Figures 8-9 show two representative examples.

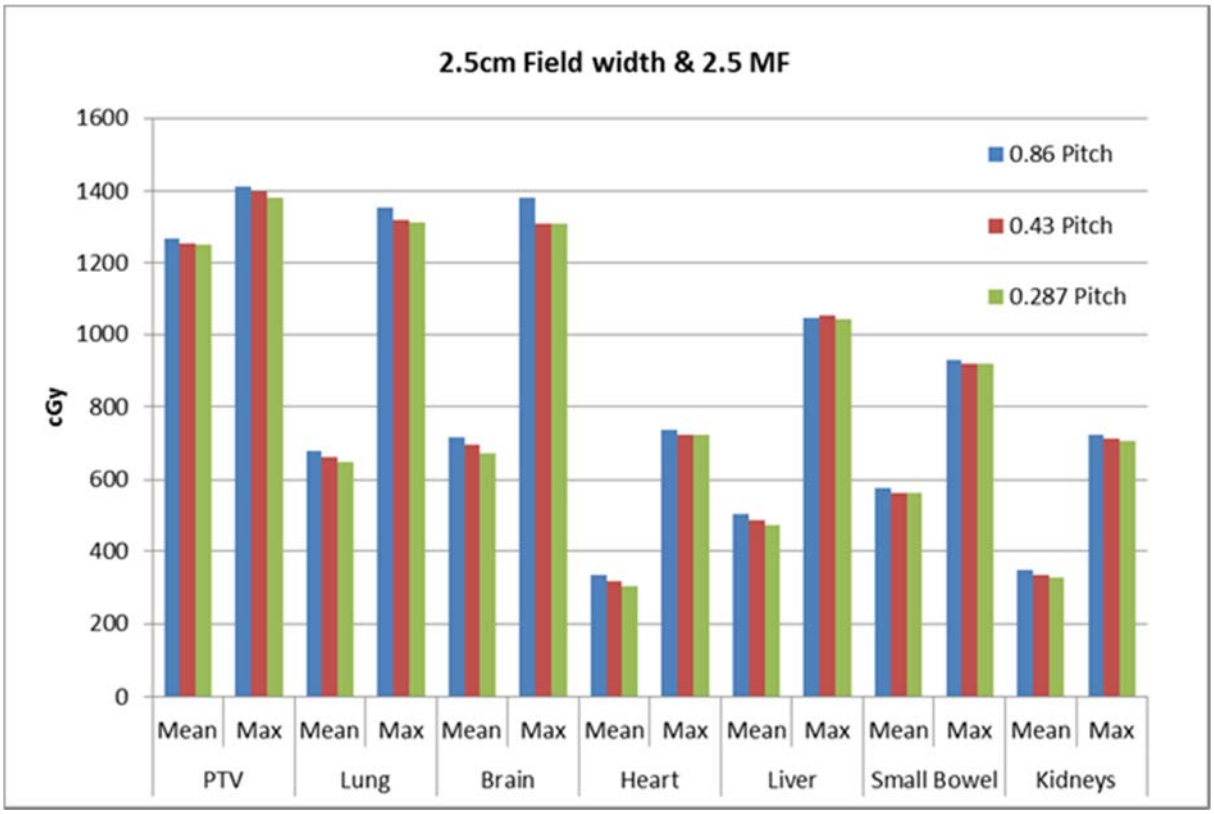

Figure 8. Relative dose difference between pitch 0.287, 0.43 & 0.86. FW 2.5, 2.5MF.

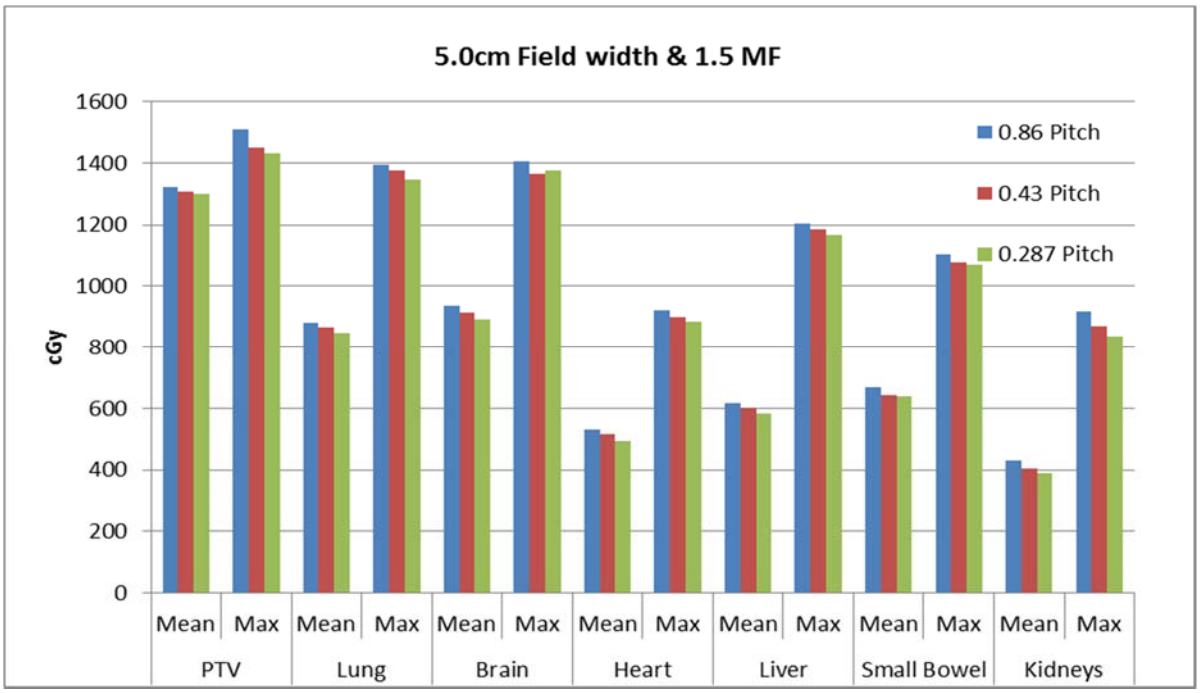

Figure 9. Relative dose difference between pitch 0.287. 0.43 & 0.86. FW 5.0, 1.5MF.

4.3.3 Modulation Factor.

Overall, higher modulation factor resulted in lower mean and maximum doses to the PTV and OARs. The effect of changes in MF on plan quality was larger at lower MF values. The relationship between PTV and OAR doses and modulation factor is illustrated by figures 10 and 11. For plans with a pitch of 0.86, each change in modulation factor of 0.25 changes the beam on time by an average of 10%. The same effect is observed in plans with a pitch of 0.43 and MF >2.0.

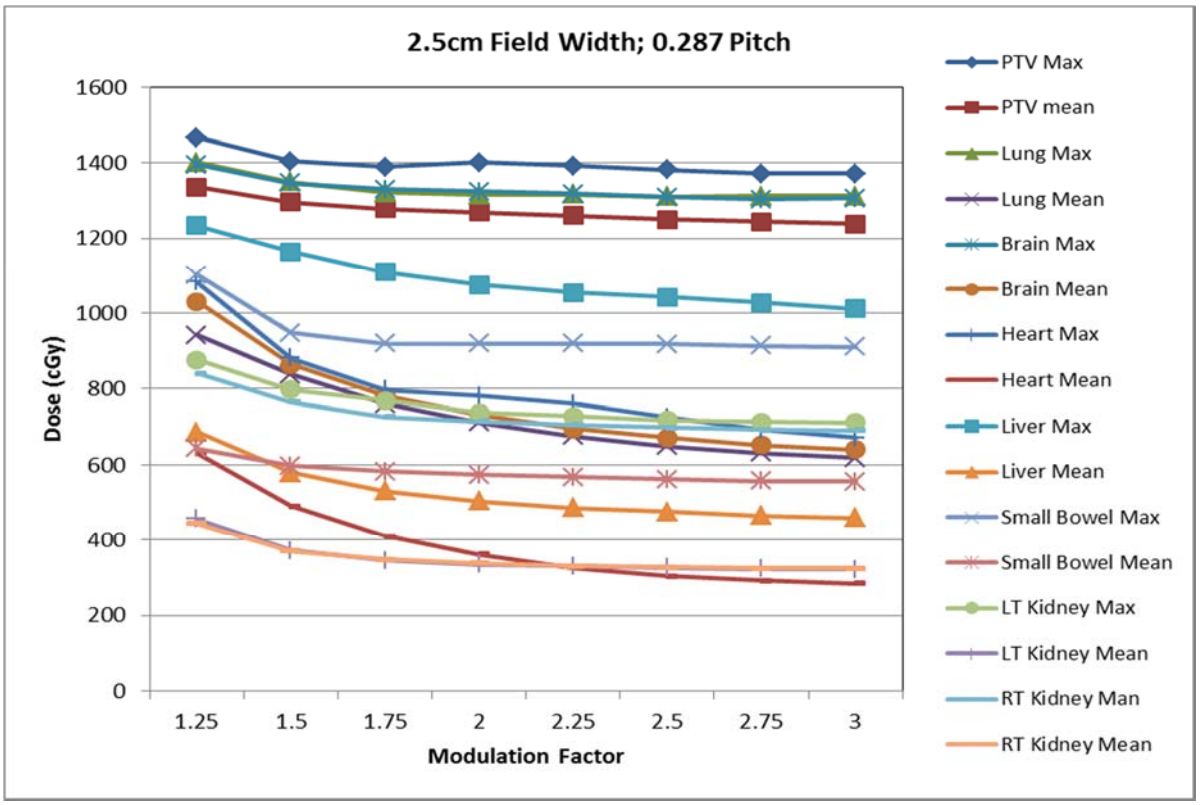

Figure 10. Relative dose difference as a function of MF. FW 2.5, Pitch 0.287.

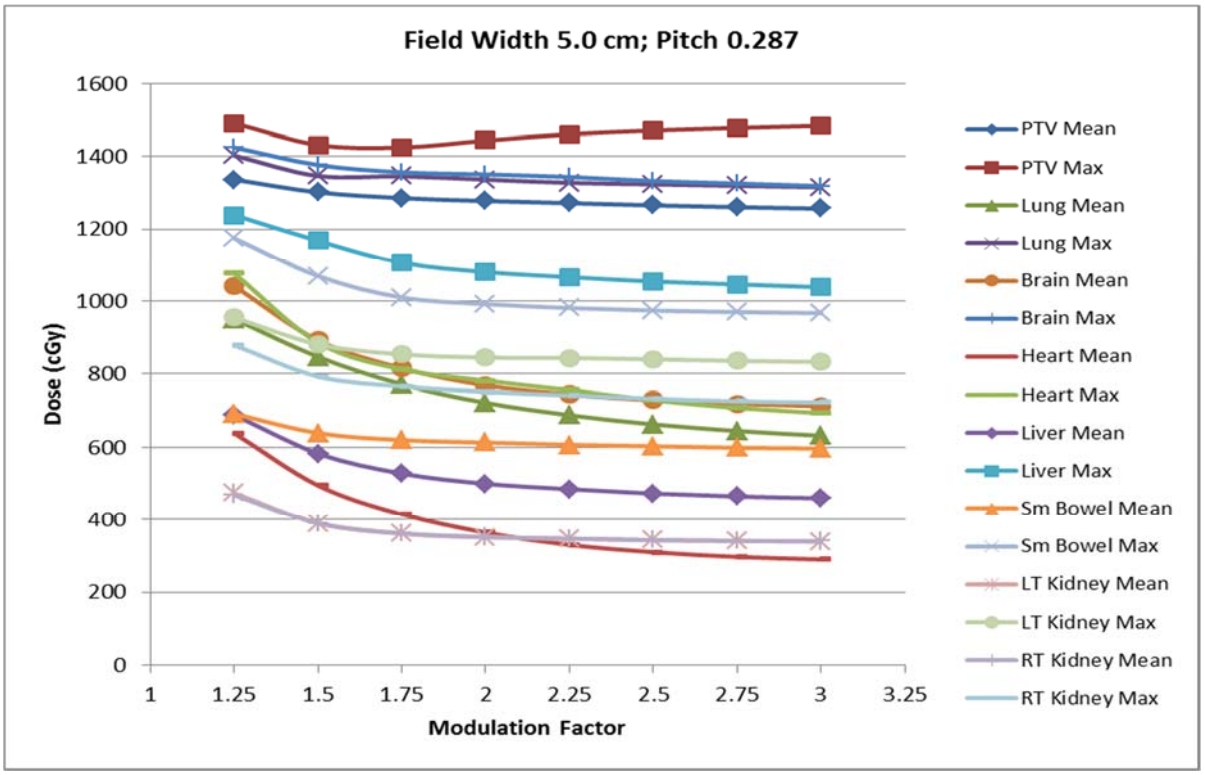

Figure 11. Relative dose difference as a function of MF. FW 5.0, Pitch 0.287.

4.3.4 Beam delivery time.

With one exception, the beam on time increases with increasing MF and/or decreasing pitch for plans with either field size. At the same time, the plan improves with increasing MF and/or decreasing pitch. Figure 12 shows combined effects of the three parameters on beam on time. The beam on time for 2.5cm FW was 85%-99% longer than that for 5.0cm FW for the same pitch and MF.

4.3.5 Plan quality index Q.

Relative plan quality results combining all three optimization parameters is presented in figure 13. Plans with smaller pitch values and smaller field size resulted in higher plan quality index. Plan quality also increases with MF and approaches a plateau at the highest MF studied.

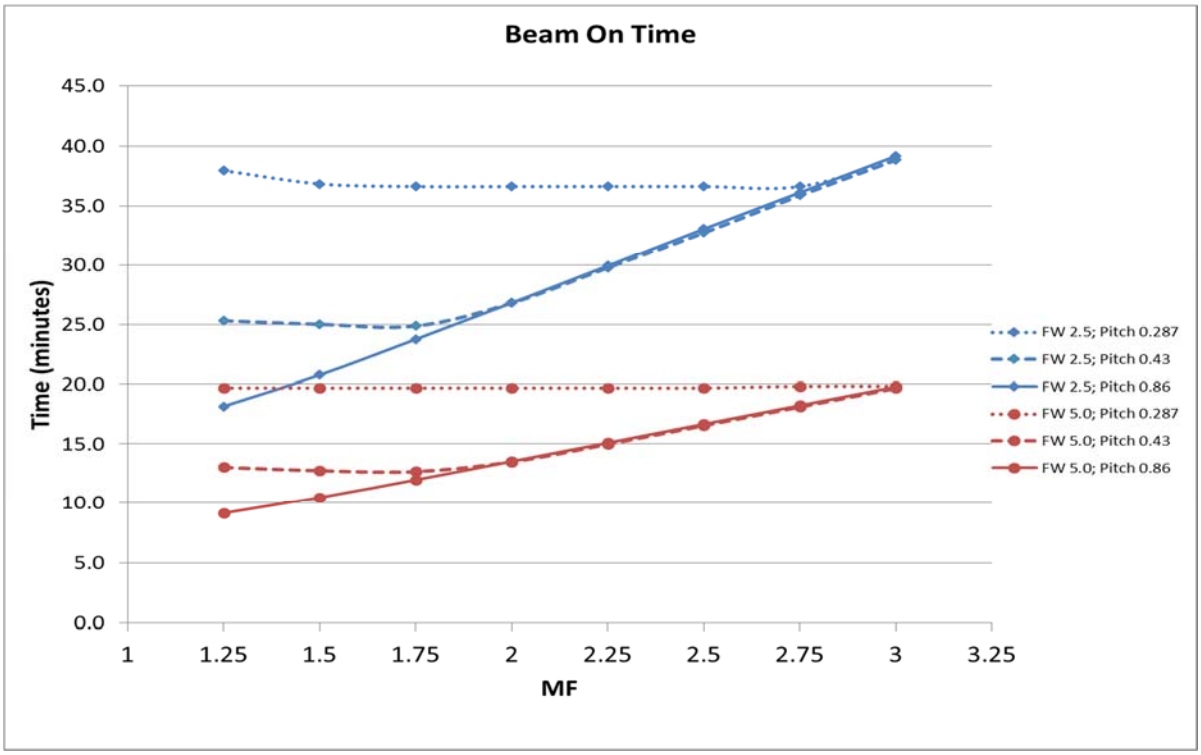

Figure 12. Beam on time as a function of MF.

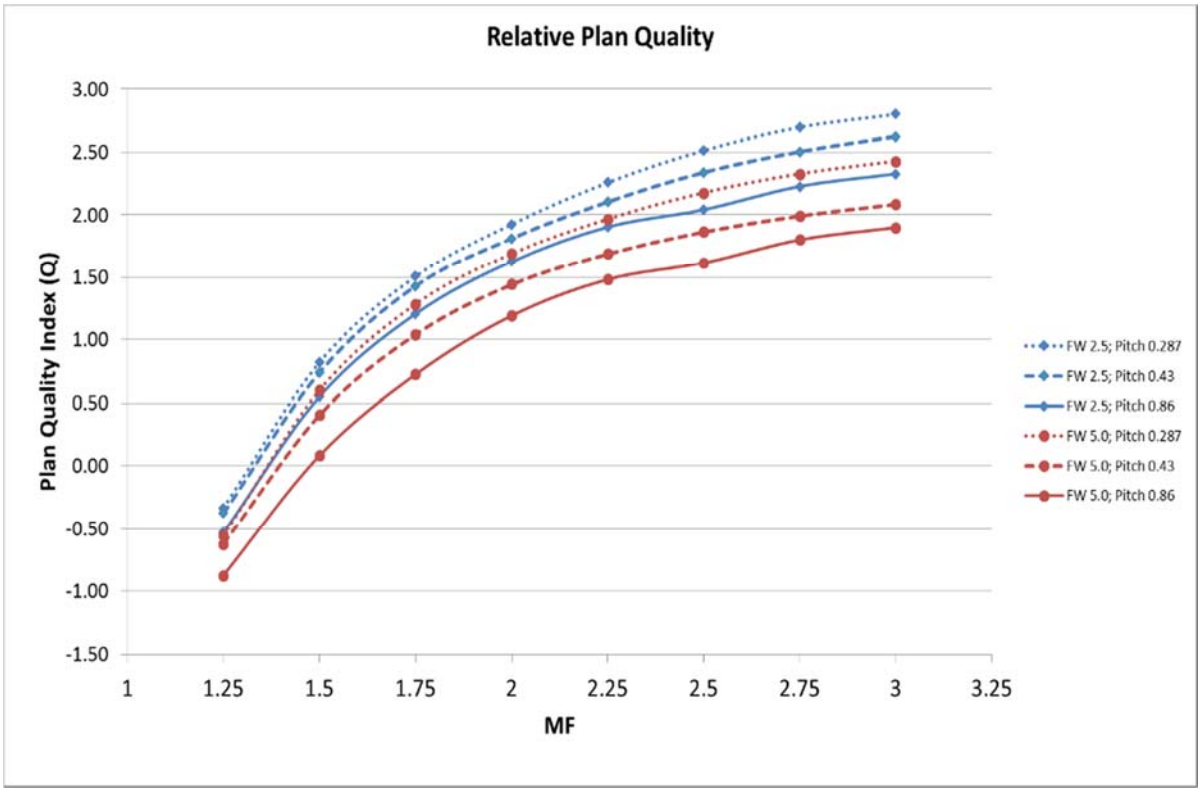

Figure 13. Plan quality summary.

4.4 Discussion.

In this investigation we demonstrate the effects of user selectable parameters (field width, pitch and MF) on relative plan quality keeping all other optimization parameters invariant. As expected, smaller field width provides better control of dose distribution in the cranial-caudal direction resulting in lower OAR doses and better PTV coverage when these volumes are in close proximity. With decreasing pitch the solution space for the optimizer is increased, resulting in better quality plans. In other words, each voxel is covered by a greater number of rotations in the helix when using a smaller pitch, giving the optimizer more choices to find the optimal beam fluence. Increasing the modulation factor will also improve plan quality by allowing a wider range of leaf opening times between projections, which in turn increases the dynamic range of the beam fluence.

By definition, the modulation factor is a ratio and therefore increasing a low MF by 0.25 will have a larger effect on the dose distribution than increasing a high MF by the same amount. The change in beam on time with changing MF is fairly linear for plans with 0.86 pitch. There is no effect on beam on time when changing MF for plans with a pitch of 0.287 and plans with pitch of 0.43 and MF below 2.0. These effects are observed for both field sizes. With low pitch and/or modulation factor the gantry has to rotate faster to deliver the prescribed dose because the radiation output is not variable. With pitch of 0.287 the gantry is approaching the maximum rotational speed therefore having no effect on the beam-on time with changing MF. The same effect is noted for plans with low MF (<2.0) and pitch of 0.43.

Accounting for the ripple effect described by Kissick et al.[34] there are only three clinically usable values for TMI planning: 0.287, 0.43 and 0.86. Values larger than 1.0 would not provide the necessary beam overlap and plan quality would be degraded. The next smaller value would produce plans with excessive beam on time. One could experiment with other values not suggested here and ignore the ripple effect since it may not be clinically significant for the relatively large acceptable tolerance in dose heterogeneity for TMI (±10%). Both the MF and pitch have an incremental effect on plan quality as described in the results section. There is significant variation in beam on time as a function of modulation factor for plans with pitch of 0.86. This effect is also observed in plans with pitch of 0.43 and MF above 2.0. The pitch selection has the largest effect on beam on time, on the order of 40%-50%, for plans with the lowest tested MF of 1.25. The most significant effect on beam on time comes from the selection of the field width. Plans with field size of 2.5cm had marginally (up to 4.3%) lower doses to PTV and OARs as compared to plans with 5cm field width at the expense of significant increases in beam on time. The increase in beam on time for the smaller field size plans varied between 85% and 99%.

The figures and data reported here represent planning results of just one image set and one structure set and are meant to be used for relative comparison between plans with varying parameters. The absolute OAR and PTV doses should not be used for absolute comparison or considered optimal. The PTV coverage and level of OAR sparing will vary from clinic to clinic based on their clinical objectives. The beam on time reported in figure 12 is also only representative for our particular

case. With all parameters invariant, the beam on time will depend on the extent of the PTV in the cranial-caudal direction due to the nature of helical delivery.

4.5 Conclusion

All the optimization parameters have an effect on final plan quality and beam on time. In general as plan quality improves the beam on time increases. Overall, plans with 2.5cm field width will result in better quality but it is possible to achieve comparable if not better plans with 5.0cm field width by decreasing pitch and/or increasing MF. Adjusting the parameters for better plan quality will reach a point of diminishing returns. Very long beam on times will compromise patient comfort, may cause the machine to overheat and could reduce dose delivery efficiency do to highly modulated fluence.

While it would be difficult to recommend specific optimization parameters in general for TMI using Tomotherapy, the results presented here provide a compendium of clinically relevant results that can help the planner understand and anticipate the relative effects of changes in particular parameters. In some cases, for example pediatric patients under anesthesia, faster treatment may be a priority. In cases for which dose escalation is necessary, treatment time might be considered less relevant than OAR sparing. The results presented here not only give results representative of what one might achieve for real clinical cases, but also insight into how to improve the resulting plan characteristics in particular situations without the need for exhaustive planning comparisons varying all of the parameters studied here.

CHAPTER 5 "SINGLE FRACTION RADIOSURGERY/STEREOTACTIC BODY RADIATION THERAPY (SBRT) FOR SPINE METASTASIS: A DOSIMETRIC COMPARISON OF MULTIPLE DELIVERY PLATFORMS".

5.1 Introduction.

Spinal metastases are a common oncologic occurrence that can have a major impact on the cancer patient's quality of life and functional status. It is well known that radiation therapy is an excellent palliative treatment for spine metastases. Currently accepted radiation techniques include a variety of fractionated regimens as well as single fraction treatment, which has historically been delivered at a dose of 8Gy. Multiple studies have shown these techniques to result in a pain response of approximately 60%.[47-48] More recent data supports the use of stereotactic body radiation therapy (SBRT) or radiosurgery for spinal metastases with fewer fractions delivered and greater, more durable responses. Gerszten et al. reported that 86% of patients experienced long-term pain improvement and excellent local control utilizing SBRT.[49] In current practice, an increasing percentage of patients with spine metastases can experience long-term survival. As systemic therapy continues to improve, it becomes even more important to produce durable pain palliation and local control.[50]

SBRT is commonly defined as a treatment that couples a high degree of anatomic targeting accuracy and reproducibility with very high doses of extremely precise, externally generated, ionizing radiation delivered in 5 or fewer fractions to an extracranial target. Treatment consisting of one fraction only is referred to as radiosurgery. The use of radiosurgery/SBRT has increased significantly over the last several years. A recent survey of radiation oncologists practicing in the United

States reported that 63.9% use SBRT for selected patients, the most common treatment locations including lung, spine, and liver.[51] As utilization of this technique increases, so have the number of platforms designed to deliver such treatment. At our own institution, we have multiple treatment planning and delivery systems used for highly conformal SBRT treatments, but no set guidelines for choosing between them. In order to precisely deliver the intended dose and spare adjacent spinal cord, these systems require advanced planning and delivery capabilities. The new GPU based TPS from Accuray has been shown to be accurate and very fast in planning TMI cases and its capabilities will be tested for small and highly conformal targets such as in SRS and SBRT, and compared with other modalities. The systems' new dynamic jaws should further influence plan quality and treatment time.

Previous reports on modality selection for SRS/SBRT have been published for intracranial sites and were either limited to two platforms[52] or compared based on technical specifications.[53] Within this study, we attempt to determine whether there are significant differences in planning and delivery capabilities across these platforms within the context of the current RTOG 0631 radiosurgery/SBRT spine trial. Therefore we designed sample spine metastasis cases within a phantom model and generated radiosurgery treatment plans for five different planning and delivery systems. We hypothesized that, while each modality would be able to meet the constraints of RTOG 0631, there would be differences in dose to critical normal tissue, treatment time, and dose fall off that may assist in the choice of delivery system based on characteristics of the individual case and target shape/volume.

5.2 Methods and Materials

Radiotherapy treatment simulation was performed on an anthropomorphic thorax/abdomen phantom (Integrated Medical Technologies, Troy, NY) using a 40-slice CT scanner with 1.5mm slice thickness. Sample spine radiosurgery plans were created using idealized target volumes created on the phantom. Target volumes were designed using the Eclipse (Varian Medical Systems, Palo Alto, CA) treatment planning system in accordance with parameters in the International Spine Radiosurgery Consortium Consensus Guidelines for Target Volume Definition in Spinal Stereotactic Radiosurgery[54] and the recommendations of RTOG 0631. Four distinct target volumes representing typical case presentations of spine metastases were contoured in both the thoracic and lumbar spine of our anthropomorphic phantom. Target volume "A" included a single vertebral body, target volume "B" included all elements of a single vertebral level completely encircling the spinal cord, target volume "C" included only the spinous process of a single vertebral level, and target volume "D" included two consecutive vertebral bodies (figure 14). The spinal cord was contoured as a structure approximately 7mm in diameter, contained centrally within the bony limits of the spinal canal. The contoured cord was designed to reflect the average cord size of our previous ten radiosurgery spine patients who were planned using fusion of MRI or CT myelogram as well as measurements reported in the literature.[55] To ensure comparability, each contour and image set was communicated unaltered from Eclipse to each of the other treatment planning systems through DICOM-RT.

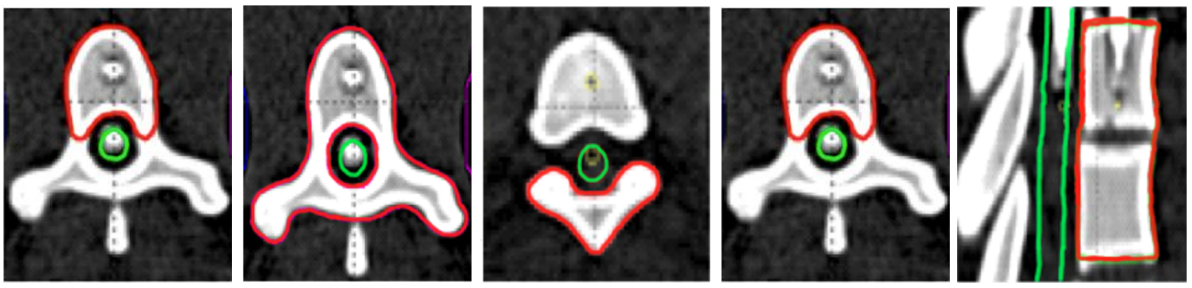

Figure 14. Axial representations of target volumes (Red) and spinal cord (Green) along with sagittal image of target "D" to illustrate its extent across two vertebral levels.

Dose objectives and constraints were designed to meet those required for RTOG 0631 and the target was prescribed 16Gy in a single fraction. Briefly, planning requirements included the following: at least 90% of the target volume receives the prescribed radiosurgery dose; hotspots outside the target were limited to 105% within 1cm of the target volume and 110% anywhere outside the target. Spinal cord constraints included 10Gy to 10% of the partial spinal cord defined as 5-6mm above and below the target, the total volume of spinal cord receiving 10Gy was restricted to below 0.35cc, and the absolute maximum dose to the spinal cord was restricted to 14Gy to a volume of no more than 0.03cc. Additional OAR constraints included cauda equina volume of <0.03cc receiving 16Gy, and <5cc receiving 14Gy. The total lung was limited to a volume of less than 1000 cc receiving 7.4 Gy. A point dose of 110% of the prescribed dose was allowed outside the target volume as long as it was less than 0.03cc, which is an acceptable variation per the protocol.

With these objectives, single fraction radiosurgery plans were designed for each target to be delivered with CyberKnife (CK) with Iris collimator (Accuray, Sunnyvale, CA), Tomotherapy with TomoEDGE™ dynamic jaw (Tomo) (Accuray

Sunnyvale, CA), Vero (BrainLAB, Feldkirchen, Germany and Mitsubishi Heavy Industries, Tokyo, Japan), and Varian TrueBeam (Varian Medical Systems, Palo Alto, CA), the latter utilizing RapidArc (RA) in standard and flattening filter free (FFF) modes. The plans for each system were designed by experienced dosimetrists and physicists responsible for planning clinical cases on these systems. Within the constraints listed, the planner was asked to design the best possible plan with priority on the spinal cord constraints. The planners were blinded to the planning techniques and results of other modalities so as to not influence their results. Each institution chose planning (dose calculation algorithm, grid size, etc.) and machine parameters (number of fields, pitch, gantry angles, etc.) according to their clinical practice.

For the Varian TrueBeam RapidArc with and without flattening filter plans, the Eclipse (v. 10.0.39) treatment planning system was used to create two complete arcs. Dose calculation was performed using the Analytical Anisotropic Algorithm (AAA) using a 2.5mm dose grid. The iPlan (v. 4.1.2) treatment planning system was used to create the Vero treatment plans, utilizing a 2mm dose grid. Thirteen coplanar IMRT beams were uniformly distributed through 360 degrees, and the Monte Carlo dose algorithm was used. For Cyberknife, the MultiPlan (V 5.1) treatment planning system was used with the Monte Carlo Algorithm with high resolution and a 1.0mm x 1.0mm x 1.5mm grid for dose calculation. For the TomoEdge plans, the Tomotherapy VoLO (v. 5.0.0.0) treatment planning system was used with a 2mm grid size used for dose calculations.

We analyzed these plans with priority on the dose to 10% of the partial spinal cord and dose to 0.03 cc of the spinal cord. The Paddick dose gradient index (PGI), defined as the ratio of the volume encompassed by half the prescription dose to the volume encompassed by the prescription dose, was used as a measure of the steepness of the dose gradient around the target.[56] Once we confirmed that each system was able to meet all of the target goals of the protocol, we compared these 2 cord metrics along with their ability to limit the dose to other surrounding tissues using the PGI.

5.3 Results.

A total of 40 plans were generated for the cases listed above (eight for each platform – one for each lumbar and thoracic target). Each system was able to generate plans delivering the prescription dose to 90% of the target volume while meeting all the constraints of RTOG 0631. RA and Tomo achieved the most homogeneous dose distribution within the target. D95 was on average 99.5% and 99.2% of the prescription dose for RA and Tomo, respectively. D95 results for CK and Vero were on average 93.0% and 95.2%, respectively. Target volume C, which was the smallest of the targets, showed the most variability between modalities. For example, the maximum cord dose to 0.03cc was 13.1Gy for RA-FFF versus only 7.7Gy for Vero. Both Vero and CK had lower cord doses and sharper dose falloff than the other modalities for target C. On average, as displayed in figures 15-22, CK was able to achieve the lowest cord doses overall and also generated the sharpest dose falloff as indicated by the Paddick gradient index.

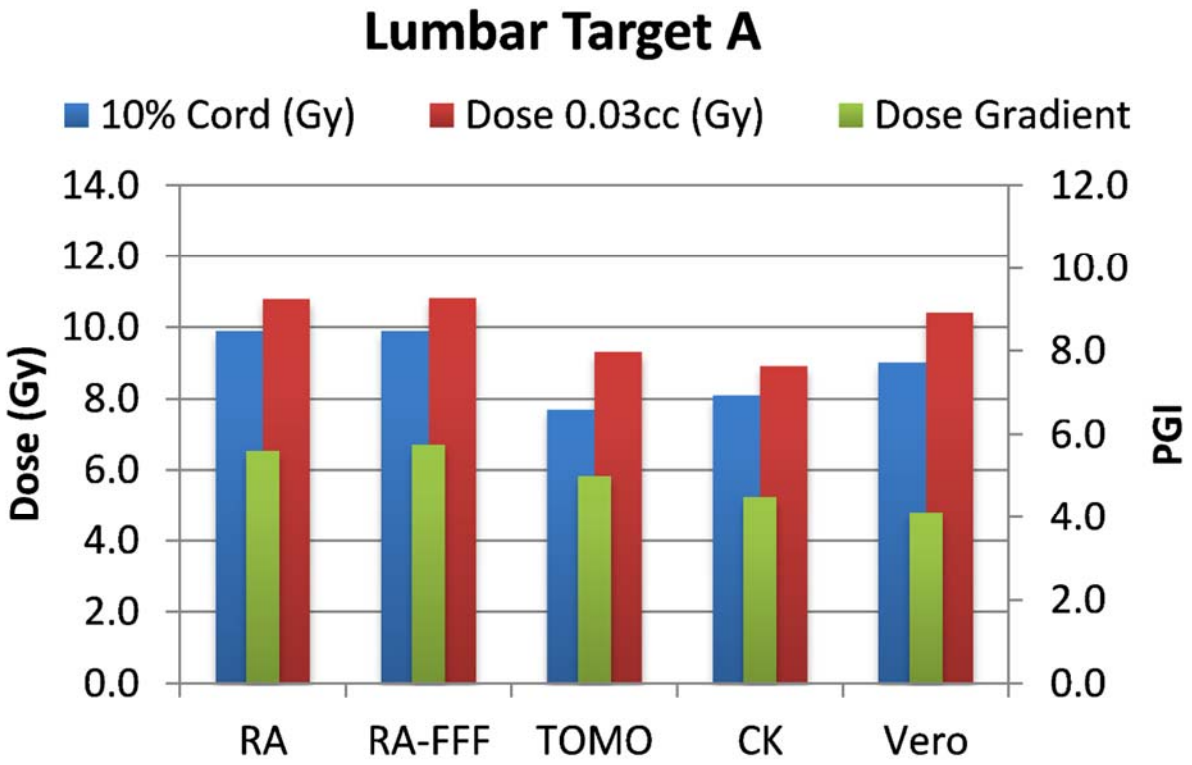

Figure 15. Lumbar Target A.

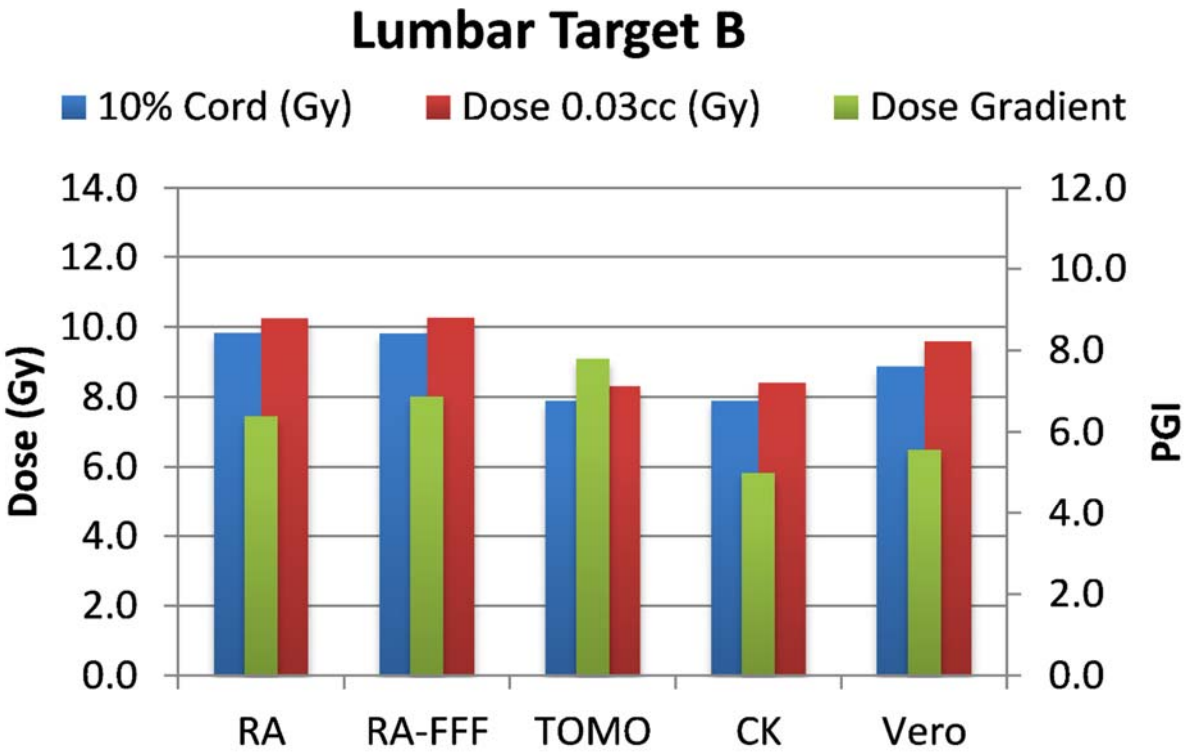

Figure 16. Lumbar Target B.

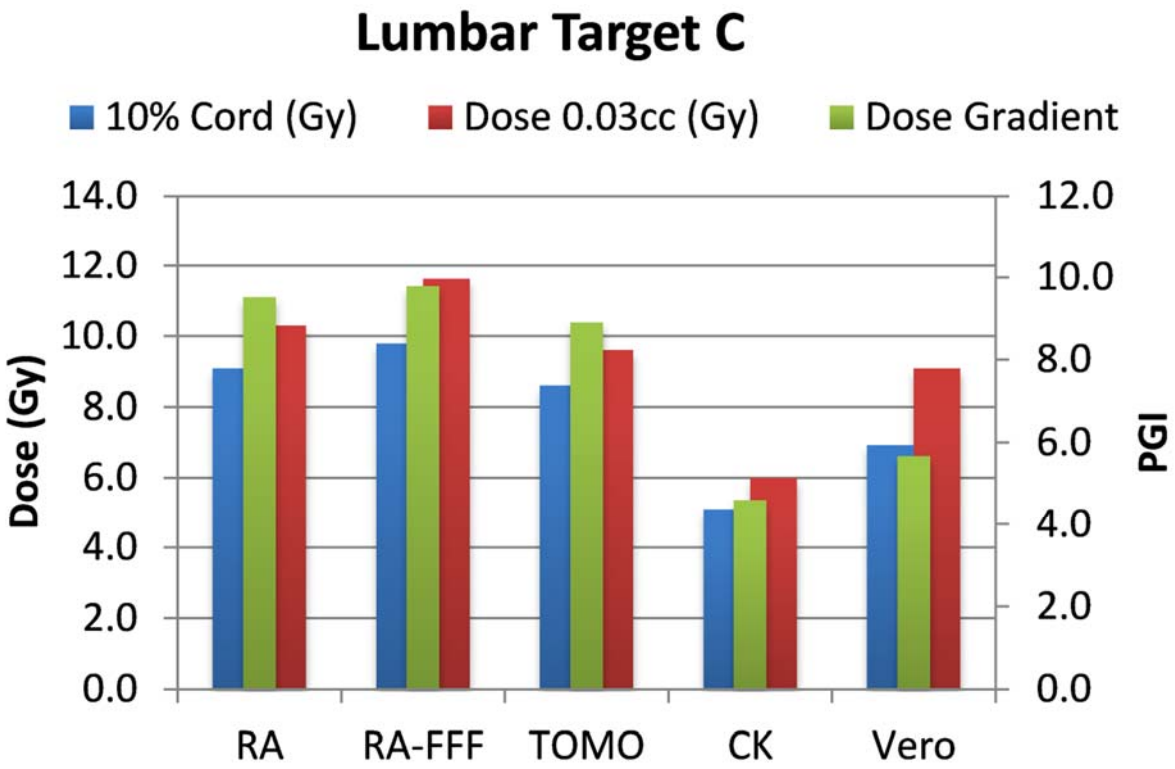

Figure 17. Lumbar Target C.

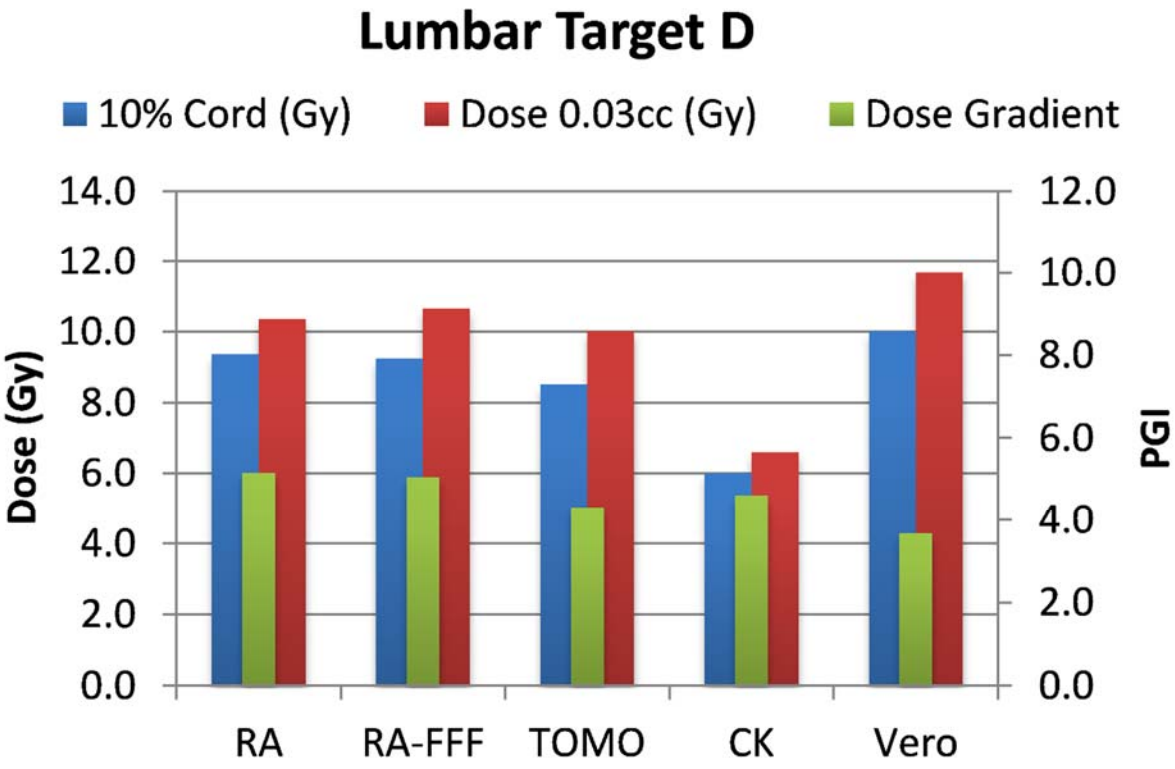

Figure 18. Lumbar Target D.

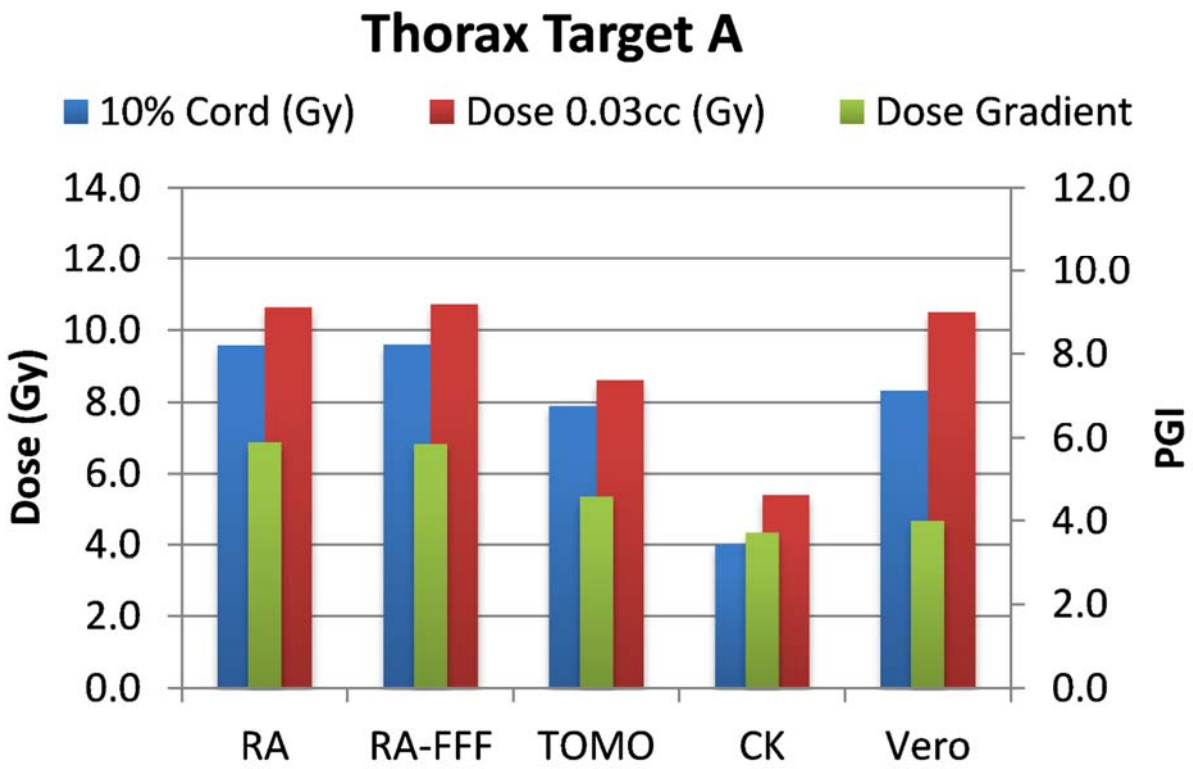

Figure 19. Thorax Target A.

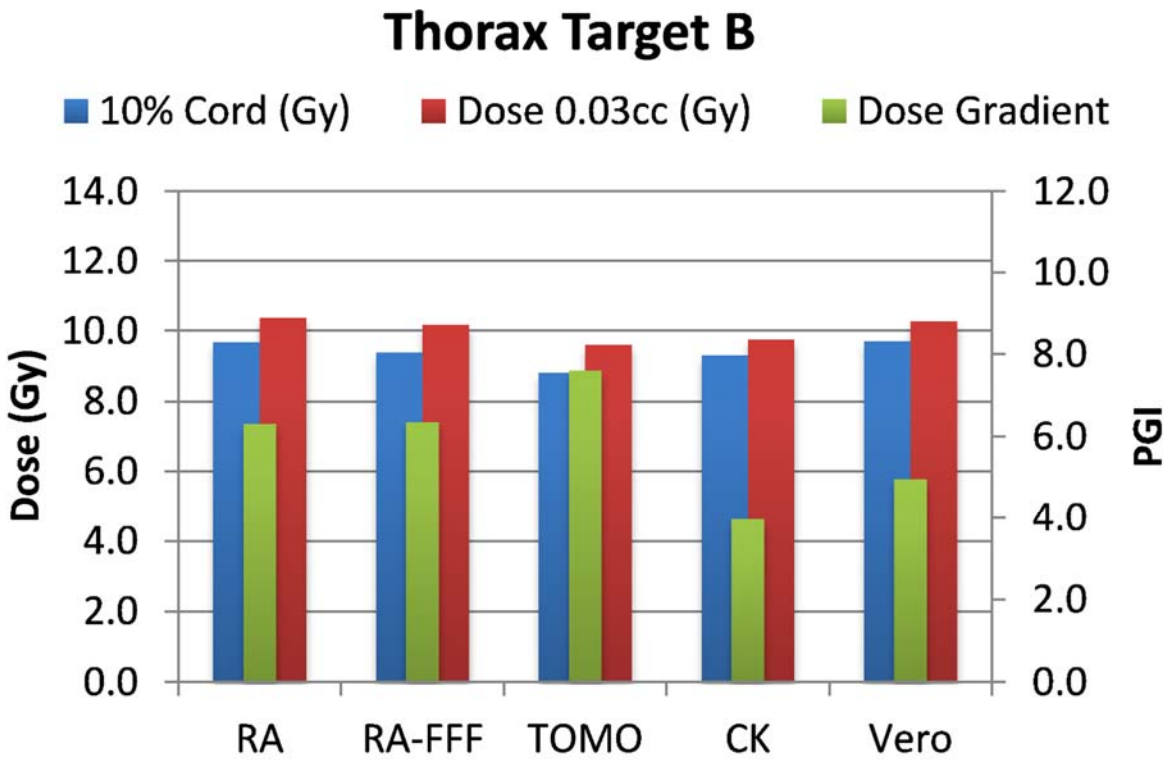

Figure 20. Thorax Target B.

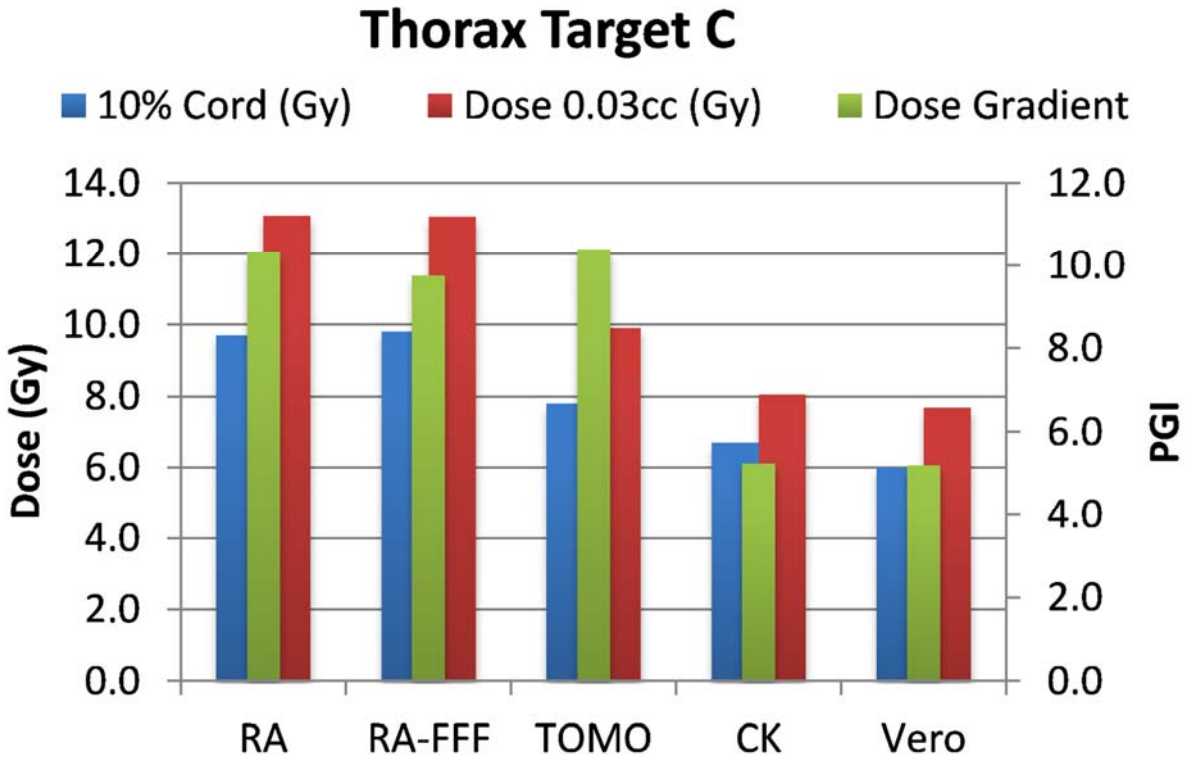

Figure 21. Thorax Target C.

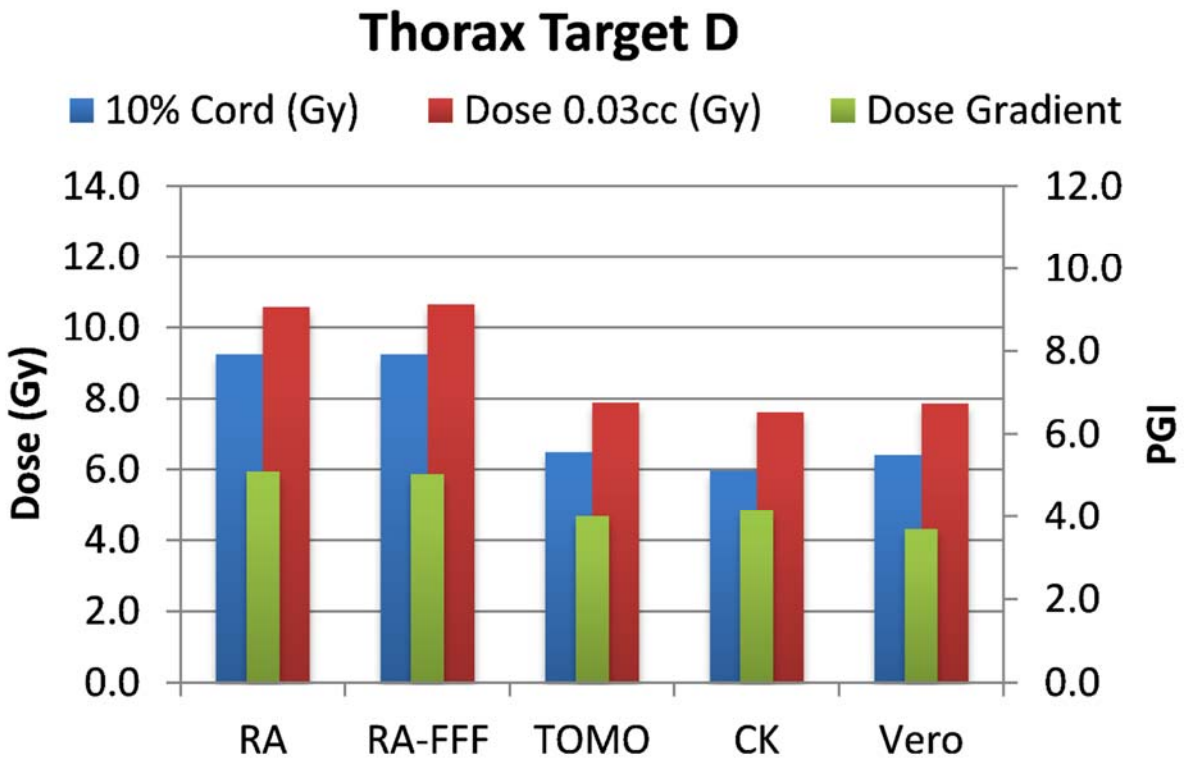

Figure 22. Thorax Target D.

Figure 23 provides a visual representation of the dose distribution created by each modality for the two most complicated cases, B and C. Treatment times varied widely depending on the modality utilized. On average, treatment can be delivered faster with RA-FFF and Tomo, compared to RA, Vero and CK (table 9). It should be noted that we are reporting treatment times for Tomotherapy Edge with dynamic jaws. Treatment times for Tomotherapy with static jaws were 3 to 5 times longer than with Tomo Edge depending on the target.

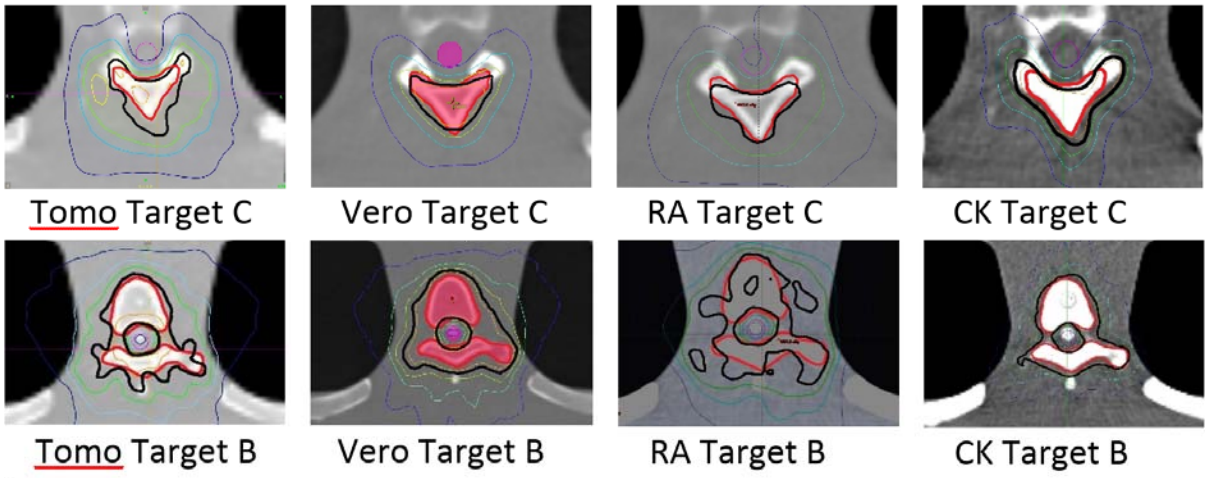

Figure 23. Isodose distribution for Targets B and C (Red) and their relationship with the spinal cord (Purple). Isodose line are as follows: 16.8 Gy – Orange; 16.0 Gy – Black; 14.4 Gy – Green; 12.0 Gy – Light Blue; 8.0 Gy – Dark Blue.

Modality	Average (min)	Range (min)
RA	9.5	7.2-11.2
RA-FFF	4.4	3.5-4.9
Tomo	6.0	5.0-6.8
CK	58.1	32.0-85.0
Vero	19.1	15.0-24.5

Table 9. Average beam on times across all targets for each modality.

5.4 Discussion

With the rapid innovation that is characteristic of the field of radiation oncology, it is important to ensure that adoption of new technology is done with a priority on safety. The delivery of high doses per fraction with radiosurgery/SBRT decreases our margin for error compared with traditional fractionated radiation. Especially in spine radiosurgery/SBRT cases with tumors adjacent to the spinal cord, it is critically important to minimize dose to normal structures while at the same time maintaining the ability to deliver adequate dose to the target. In our study we have shown the dosimetric results of a representative set of cases planned with multiple delivery platforms. These do not by any means encompass the wide variety of cases seen in clinical practice, nor do the 40 plans generated in our study represent the capabilities of other planning teams. Additionally, we recognize that small inaccuracies in patient setup and variability in actual treatment delivery can have serious and significant consequences that could far exceed the differences between modalities that are presented here. Indeed, evaluation of the relative ability of each of these systems to accurately deliver these treatment plans is critical in determining whether there is any real advantage to one over another.

In an associated quality assurance analysis study, [57] both ion chamber and film were used to measure delivered dose for all plans on each modality presented here. The results of these measurements were exceptional, specifically that all ion chamber measurements were within 3.3% of the dose predicted by the respective treatment planning system and all modalities yielded film gamma pass rates better than 96% at 2%/2mm. Finally, while we identified situations in which some systems

provide a dosimetric advantage in treatment plan characteristics for a particular SBRT spine treatment, it is not clear if these differences would translate into a clinical advantage.

We believe that the ability of CK to achieve overall superior dosimetric results comes from use of the smallest aperture and a greater number of possible beam orientations. The CK was the only modality in this study that used non-coplanar beams. The difference between the Vero and TrueBeam results could be attributed to the number of beams since 13 coplanar beams were used for the Vero plans and only 2 arcs were used for the TrueBeam plans. Both machines have an MLC leaf width of 5mm. Also, Burghelea et al.[52] showed that smaller aperture and non-coplanar beams produce plans with better conformity and dose gradient for small targets. Both TrueBeam and Vero could benefit from using non-coplanar beams. In addition, the use of the high definition MLC (HDMLC), which has 2.5mm leaf widths, could be expected to further improve dosimetric results for the TrueBeam plans.

The main objective of this study was to meet or exceed the dose constrains of RTOG 0631 protocol. Each institution was able to choose optimization and machine parameters according to their clinical practice. Although, all institution met all of the constraints of the protocol, there were differences in dose gradient outside the target. These differences can be attributed to different planning techniques. Some institutions adhere to common standards when it comes to hot spots within the target and limit them to 110% of the prescription. This protocol does not have any requirements for dose heterogeneity within the target. Allowing higher hotspots within the target, as it's commonly done in linac based or Gamma Knife SRS

treatments, would result in steeper dose gradients outside of the target. The difference in the dose gradient between the modalities could have been minimized if all the institutions followed the same planning techniques. The results presented here may also be influenced by the difference in dose grid size used by each platform. Other studies suggest that variation in dose calculation for grid sizes used in our study could be around 2-3%.[58-59]

Depending on the goals of treatment, the order of importance of the treatment plan metrics we reported might vary. For example, in the case of a terminal patient with significant difficulty lying in the treatment position, the physician might decide that a short treatment time is more important than a sharp dose gradient or the potential risk of late neurologic complications. However, a patient with a better prognosis might tolerate the treatment well, and in that case lower doses to critical structures would justify a longer treatment time.

5.5 Conclusion.

While all treatment modalities tested were able to create and very accurately deliver treatment plans meeting the dose constraints of RTOG 0631, we observed variations that may impact system selection based on individualized treatment goals. Certain modalities performed better than the others for specific target shapes and locations. Vero and CK excelled in treating small volume targets. CK had the sharpest dose falloff and achieved the lowest overall spinal cord doses at the expense of longest treatment time. Treatment delivery time was fastest for TB-FFF and Tomo. These findings could provide guidance in the process of determining

which of the available modalities would be preferable for the treatment of spine metastases.

CHAPTER 6 "ANALYSIS OF DOSE FRACTIONATION REGIMENS FOR TOTAL BODY IRRADIATION BASED ON INTERSTITIAL PNEUMONITIS RISK FACTORS."

6.1 Introduction

Total body irradiation (TBI) is an important component of the conditioning regimen for patients undergoing bone marrow transplantation (BMT) for a variety of hematological malignancies.[37,38,39,60] While post-transplant relapse rates have improved with radiation dose escalation, overall survival has not improved due to excessive treatment related toxicities.[21,22] These toxicities, therefore, are the most important factors in determining the chemotherapy and radiation treatment regimens. The most common acute toxicities include nausea, vomiting, parotitis, mucositis and xerostomia. These are usually preventable with drugs or the symptoms resolve on their own. One of the most significant complications of TBI conditioning regimen is interstitial pneumonitis (IP) due to its relatively high incidence rate and potential for mortality. The incidence of grades 3/4 IP following BMT which includes a TBI regimen is between 0% and 73% and higher occurrence has been correlated with total lung dose, fractionation scheme and dose rate.[21,22,40,43,45,61-99] It is also known that alkylating chemotherapy agents have a synergistic effect on lung toxicity when combined with radiation.[100]

It is difficult to determine the overall IP risk factors from studies reported by individual institutions because of variation in conditioning regimens as well as inconsistent reporting of methods and materials. Until relatively recently, lung dose statistics in the literature were reported with a large degree of uncertainty due to relatively simple treatment planning methods and the lack of three dimensional dose

information. A literature review by Sampath et al.[100] found IP correlation with Cyclophosphomide (Cy) and lung dose, although the lung dose correlation did not hold for studies that used multiple fraction per day regimens. In this study we plan to use a database of over three thousand patients from 42 published manuscripts presenting data on incidence of IP following TBI for BMT, to quantify a lung dose response for IP, and to relate it to dose fractionation schemes.

6.2 Methods and Materials

Data for this study was obtained from PubMed search engine and included all published manuscripts that had IP, BMT, TBI or TMI as nonabbreviated key words. Only those studies with IP incidence explicitly reported by dose fractionation regimens were included in the analysis. Studies were only included if crude incidence of IP was reported. IP related mortality rates were excluded from this study. There are many factors that contribute to lung toxicities and it's hard to distinguish radiation induced IP from another etiology. The majority of studies analyzed here had TBI/TMI and chemotherapy regimen, therefore all IP etiologies grade 3 and 4 were included in this study. The regimens containing a radiation component only were treated as zero chemotherapy-dose in the database. The follow-up time associated with the reported IP incidence rates was not used as factor in the analysis.

The following variables were obtained from the papers: IP incidence rate, total radiation dose, number of fractions, lung shielding, lung dose, lung dose per fractions, number of fractions per day, interfraction interval, lung dose rate, chemotherapy agent and Cyclophosphamide (Cy) dose. The fractional lung dose

was calculated by dividing reported lung dose by the number of fractions. If lung lose was not reported, it was assumed the lung received 100% of the prescription dose. In some cases, lung dose was estimated from given information about lung blocks either as percent shielding or half value layer (HVL). The lung dose was then converted to EQD2 – biologically equivalent dose in 2 Gy fractions using equation 2, as follows:

$$EQD2 = D * \frac{(d + \alpha/\beta)}{(2 + \alpha/\beta)} \quad (2)$$

where D is total lung dose, d is fractional lung dose and α/β is a term from the linear-quadratic model used to quantify the fractionation sensitivity of tissues. The values of α/β tested in the analysis ranged from 2Gy to 4Gy.[101,102] In order to account for possible incomplete repair of lung tissue in fractionation schemes that required multiple fractions per day, the lung dose was further converted to EQD2_repair using equation 3:

$$EQD2\_repair = D * \frac{(d(1 + Hm) + \alpha/\beta)}{(2 + \alpha/\beta)} \quad (3)$$

H_m in equation 3 is a term used to describe incomplete repair based on time between fractions and repair half time. Lung dose rate was calculated using this simple formula:

$$Lung\ dose\ rate = Nominal\ dose\ rate * \frac{(lung\ dose)}{(total\ dose)}$$

If a range of dose rates was provided, then the mean of the range was used in the analysis. The most prevalent chemotherapy agent was Cy with nearly 80% of studies reporting its use. The use and frequency of Cy and other chemotherapy agents are listed in figure 24. Due to the limited and variable use of the other chemotherapy agents, only Cy was used as a variable in our analysis. In the end, our data set included 42 articles that consisted of 88 patient cohorts and 34 unique fractionation regimens. Figures 25 - 26 show the frequency and distribution of these regimens. The range of all parameters studied here is listed in table10.

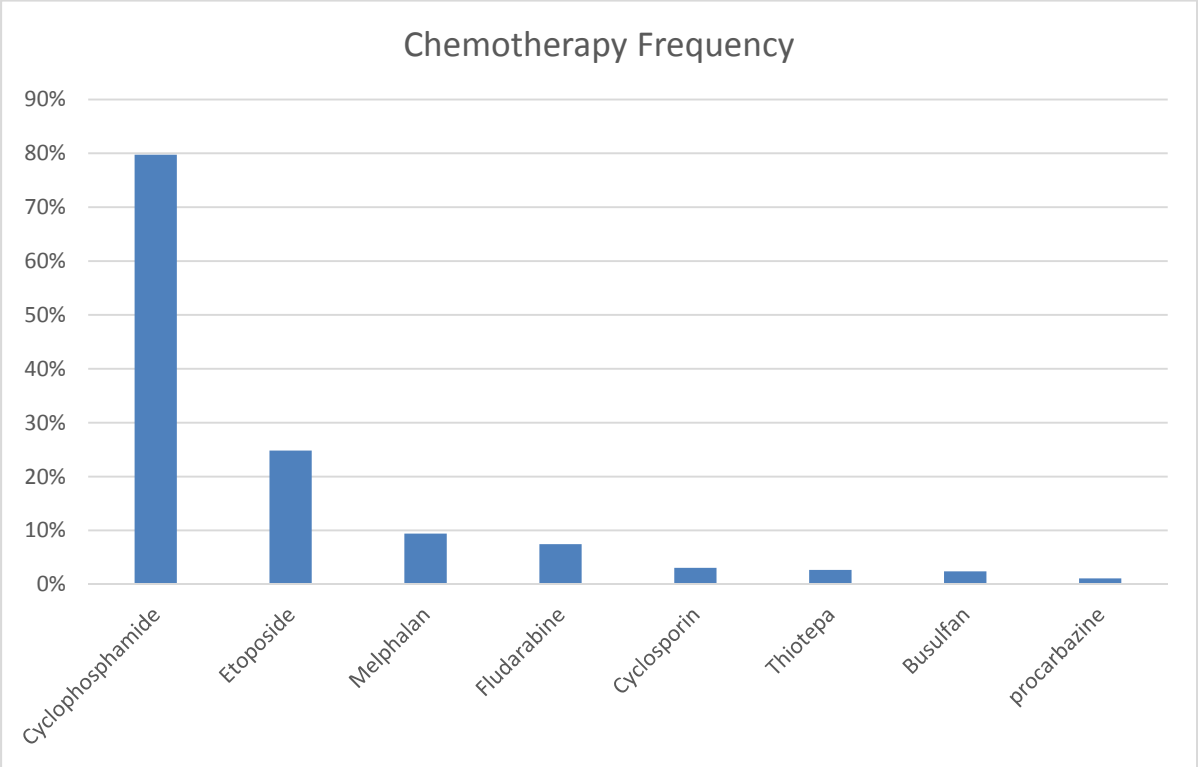

Figure 24. Frequency and type of chemotherapy used.

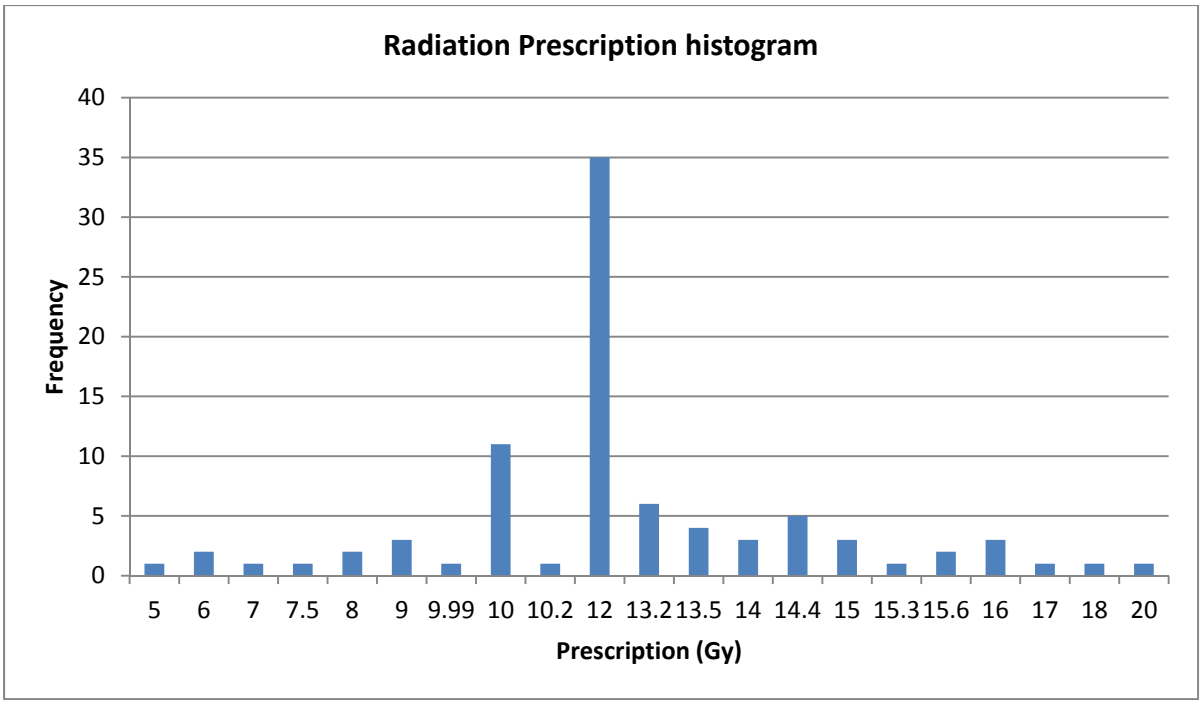

Figure 25. Radiation prescription histogram.

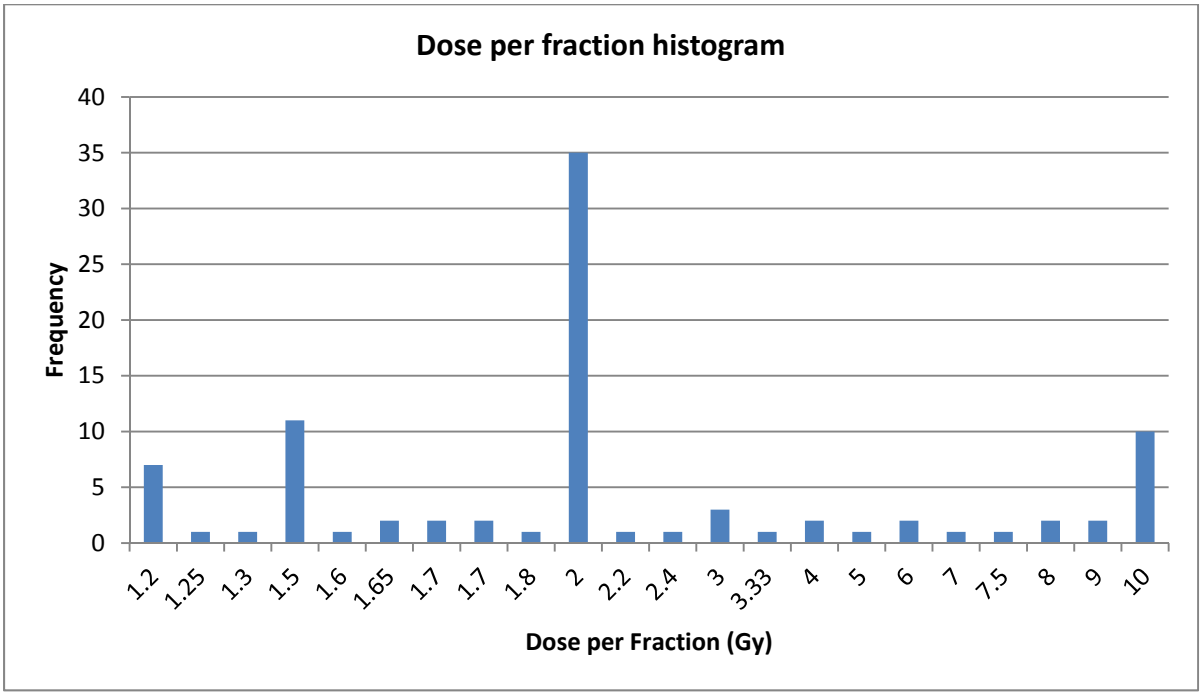

Figure 26. Dose per fraction histogram.

Parameter	Range
Lung EQD2 (Gy)	3.9-26
Lung EQD2_repair (Gy)	4.2-26
Number of fractions	1-13
Dose per fraction (Gy)	1.2-10
Fractions per day	1-3
Lung dose rate (cGy/min)	2.2-425
Cy dose (mg/kg)	0-200

Table 10. Range of parameters used in the analysis.

The first goal of this study was to determine whether the following variables are statistically significant predictors of IP – (i) lung EQD2, (ii) EQD2_repair, (iii) dose rate and (iv) Cy dose. Using SPSS statistical software package, version 20.0 (SPSS, Chicago, IL) we performed a multivariate analysis (MVA) of the data by the step-wise Cox logistic regression. In logistic regression analyses, logarithm of the odds of the event (incidence of IP) is taken as the response variable and is regressed on selected predictor variables as defined by the conceptual framework of the model. The form of the regression model is as follows:

Log $(p / (1-p)) = \beta_0 + \beta_1 X_1 + \beta_2 X_2 + \ldots\ldots\ldots\ldots\ldots + \beta_k X_k + \varepsilon$, where β_0 is the intercept and β_i is the slope of logit coefficient corresponding to the predictor variable X_i. Overall significance of the fitted model is done using Wald's Chi-square test. Significance of the logit coefficient or equivalently, odds ratio (OR) estimates are also calculated using Wald's Chi square test. Here we test the null hypothesis Ho : $\beta_i = 0$ (Odds ratio = 1) against the alternative hypothesis H1: $\beta_i \neq 0$ (Odds ratio = ≠ 1). Predicted probability of incidence of IP is computed using the expression,

Estimated $p = e^{\beta 0 + \beta 1 X1 + \ldots\ldots\ldots + \beta k Xk} / (1 + e^{\beta 0 + \beta 1 X1 + \ldots\ldots\ldots + \beta k Xk})$

Cox regression analyses were performed using two different models. These models differ in terms of predictor variables included and also the data set (subset) used to fit and validate the model. Model I is formed using selected predictor variables (i) LungEQD2_repair, (ii) dose rate, and (iii) Cy dose. Model II is built using the predictor variables - (i) LungEQD2, (ii) dose rate, and (iii) Cy dose.

Model 1: $\text{Log}\ (p / (1-p)) = \beta_0 + \beta_1$ LungEQD2_repair $+ \beta_2$ dose rate $+ \beta_3$ Cy dose $+ \varepsilon_1$

Model 2: $\text{Log}\ (p / (1-p)) = \beta_0 + \beta_1$ LungEQD2$+ \beta_2$ dose rate $+ \beta_3$ Cy dose $+ \varepsilon_1$

Using the models, dose response curves were generated for different fractionation schemes.

6.3 RESULTS

Table 11 below reports a summary of Cox logistic regression results for model I. This model has all the patients irrespective of chemotherapy agents used and the treatment (radiation or radiation & chemo). Hosmer Lemeshow test which assesses whether or not the observed event rates match expected event rates indicate that the overall model fit is good ($p = .065$). Calculated probability values of $p > 0.05$ indicate that model's observed and predicted events do not differ significantly. Table 3 reports logit coefficient estimates and the associated odds ratio for the selected predictor variables Cy dose, Lung EQD2_repair and dose rate. Cy dose taken as a continuous predictor variable in the model reports significant association with incidence of IP. Estimated associated OR = 1.006 (95% CI (1.003, 1.009)). This indicates that an increase of one unit in the Cy dose reports an average increase of 0.6% in the odds of incidence of IP adjusting for the effect of other predictors. EQD2_repair taken as a continuous predictor variable in the model

reports significant association with incidence of IP. The estimated associated OR = 1.024 (95% CI (1.002, 1.046)). This indicates that an increase of one unit in the LungEQD2_repair results in an average increase of 2.4% in the odds of incidence of IP adjusting for the effect of other predictors. Lung dose rate taken as a continuous predictor variable in the model reports no significant association with incidence of IP.

	B	S.E.	P	OR	95% CI for OR	
LungEQD2_repair	.024	.011	.029	1.024	1.002	1.046
Dose Rate	.001	.001	.485	1.001	.999	1.003
Cy dose	.006	.002	<.001	1.006	1.003	1.009
Constant	-2.759	.278	.000	.063		

Table 11. Cox logistic regression results for model I. OR=odds ratio, S.E. = standard error

Results from model II are very similar to model I and are presented in table 12 below.

	B	S.E.	P	OR	95% CI for OR	
EQD2	.030	.011	.004	1.031	1.010	1.052
Dose Rate	.001	.001	.437	1.001	.999	1.003
Cy dose	.006	.002	<.001	1.006	1.003	1.010
Constant	-2.865	.279	<.001	.057		

Table 12. Cox logistic regression results for model II. *OR=odds ratio, S.E. = standard error*

Figures 27-28 respectively show EQD2_repair response functions for all fractionation regimens and multi-fraction per day regimens along with discrete data points. The model of predicted lung pneumonitis as a function of mean lung dose (MLD) obtained from QUANTEC[103] is included in the figures for comparative purposes (orange line). QUANTEC's data reports MLD for radiotherapy treatments with a typical prescription of 60 Gy in 2Gy fractions. Therefore, MLD of 30Gy would suggest lung receiving 1Gy per fraction. The reported MLD was converted to EQD2 using equation (2) and the resulting predictive model is represented as "QUANTEC EQD2" in color blue on the graph. The size of the data points (green) represents relative size of number of patients in the study.

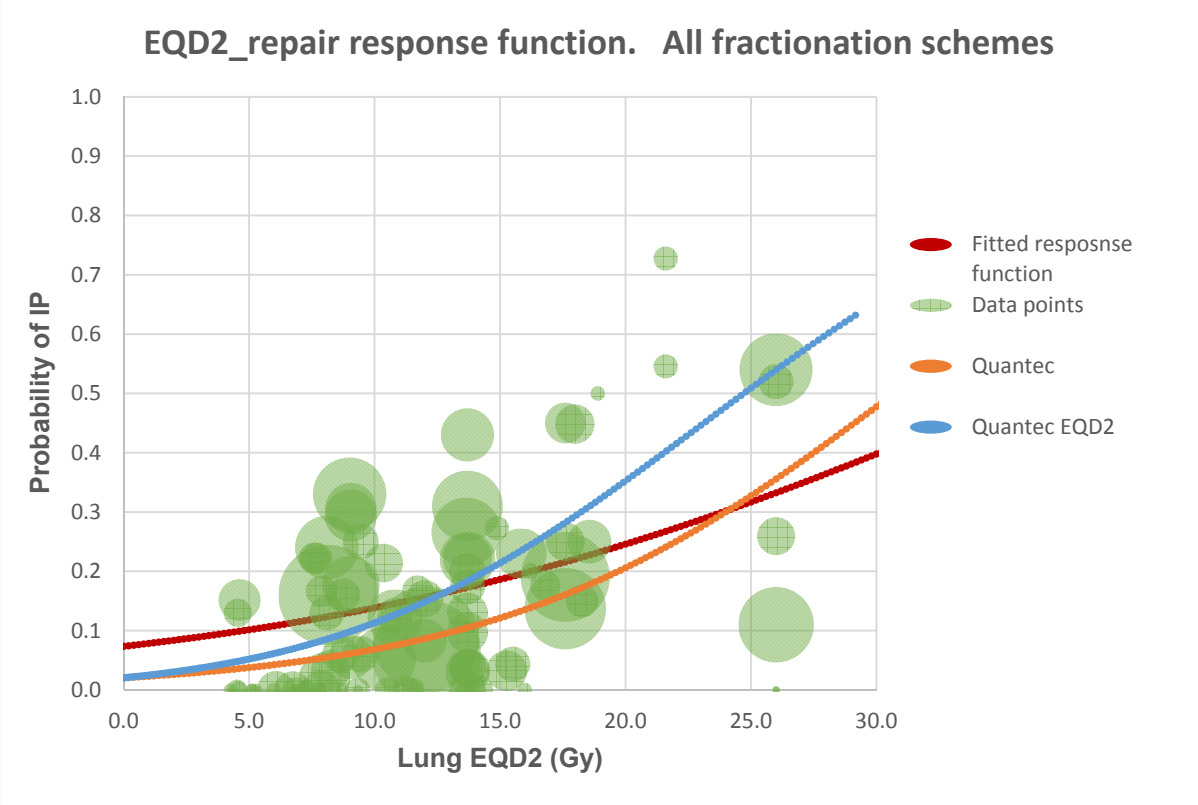

Figure 27. Lung EQD2_repair response function for all fractionation schemes.

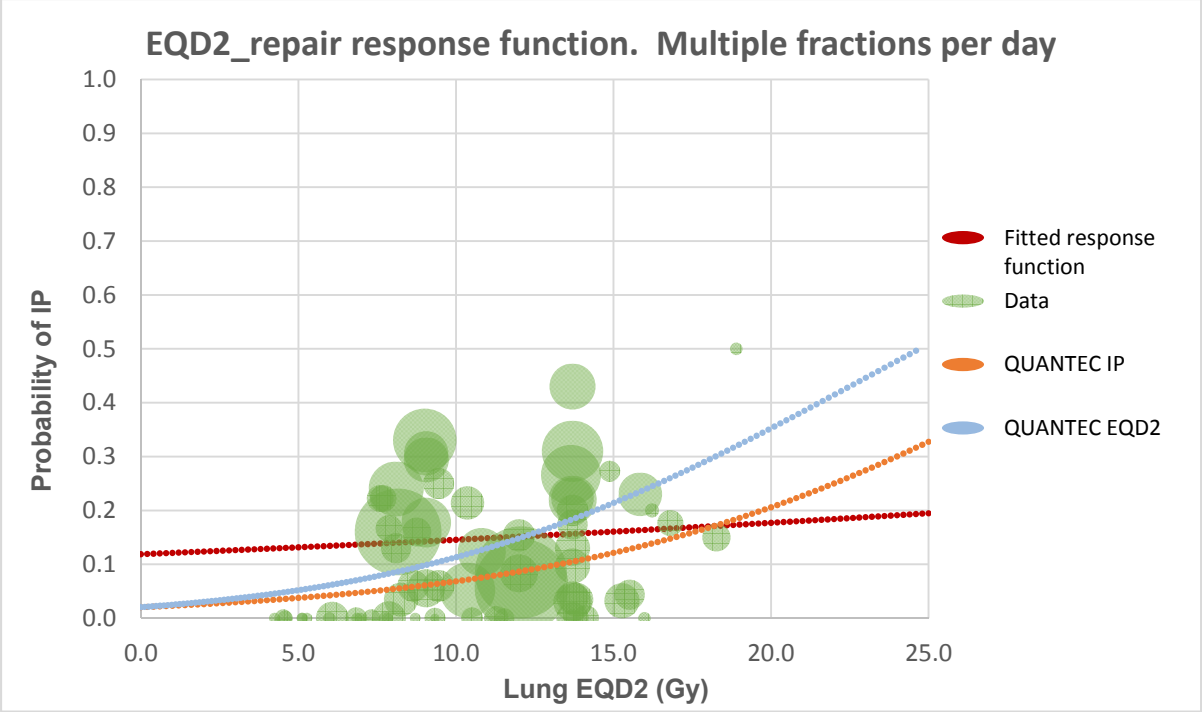

Figure 28. Lung EQD2_repair response function for multiple fraction per day schemes.

6.4 DISCUSSION

The goal of this study was to quantify lung dose response for IP based on retrospective analysis of published results. Although both models found EQD2, EQD2_repair and Cy to be statistically significant predictors of IP incidence, the magnitude of the effect was very small. The significance of the results may also be misleading due to the large sample size of our data. Although the models correctly predict the expected increase of IP with lung dose and Cy the dose response function doesn't show a good fit with the discrete data points (figures 27-28). Similar to QUANTEC's logistic fit of pneumonitis rates vs MLD data, our curve only shows gradual increase of IP probability with dose without defined dose levels below which there is no risk of IP. The y-axis intercept and the slope of the curve also suggest

poor prediction of actual IP rates. In the case of the logistic fit to multi fraction regimen data, the curve predicts 11% and 30% chance of IP for zero dose and 50Gy EQD2, respectively. This prediction does not correlate well with clinical data analyzed in this study. We removed the data from single large fraction regimens as these regimens are not common anymore. Modeling the resulting data was proven to be even more difficult as the remaining data points were clustered together with even less points at end of the spectrum of dose or IP rates.

We did not find dose rate to be an independent risk factor for IP. We investigated this predictor as a continuous as well as categorical variable and we did not find correlation between dose rate and IP. We also looked at a number of subsets of the data including fractionated and single fraction regimens. Some studies found lung dose rate being a risk factor for IP for single fraction myeloablative (>8Gy) dose of TBI.[64,104] Reports by Peters et al.[105,106] state that the dose rate is of little importance for fractionated (2Gy) treatments since cell death results predominantly from non-repairable single hit killing. Our analysis agrees with other studies that have found no effect of dose rate on IP for dose rates up to 8.9cGy/min and doses up to 12Gy.[70,107] In contrast, studies by Crruthers et al.[86] and Corvo et al.[108] reported correlation of dose rates >7.5cGy/min and >6cGy/min to IP for fractionated treatments, respectively. There seems to be a threshold lung dose for fractionated treatments below which dose rate has no effect on IP rates. Girinsky et al. suggested that the dose rate only relates to IP when total lung dose exceeds 8-9Gy. This statement could be supported by the data from City of Hope

Comprehensive Cancer Center[45,98] that show no IP rates for doses of up to 7.9Gy and instantaneous dose rates of 850 cGy/min.

The majority of the fractionation regimens consisted of 2 or 3 fractions per day. We have separately analyzed all patients in the database as well as the subset of these patients receiving multiple fractions per day. Historical TBI treatments of a single large fraction are not common anymore and we did not analyze them separately. Sampath et al.[100] was able to find a lung dose response for treatments delivered in a single fraction only but the results may not be applicable to multi-fraction per day treatments frequently used now.

The large dispersion of the data points as seen in figures 27 and 28 is potentially the main cause of the dose response prediction failure. Inconsistent institutional reporting and limited data for high IP incidence rates or low lung doses most likely contributed to the failed probability model. Our data did not contain any studies with patients receiving lung dose below 4.2Gy and the IP rate of 34% or more was observed in only 57 out of 2384 patients. In addition, most of the lung dose reported is estimated from surface measurements due to lack of three dimensional dose information. Some of the data was reported as an average with a wide range which could have negatively affected the prediction model. Variability of lung shielding methods and frequency may also contribute to inaccurate reporting of lung dose. The use of chemotherapy agents within conditioning regimens was evaluated for total reported dose only regardless of its concurrent or sequential use with TBI. Another cause of data spread may be due to differences in reported IP diagnostic criteria.

Analysis of the discrete data points shows a lung dose threshold of 7.6Gy (EQD2_repair, a/b=3Gy, repair half-life = 4hr) that clearly separates studies with no IP toxicities within multiple fractions per day regimens (figure 28). This dose threshold was validated using statistical method of recursive partitioning with essentially the same results. This dose threshold corresponds to EQD2_repair doses of 7.2Gy and 7.7Gy for α/β values of 2Gy and 4Gy respectively. The studies that define that threshold report the use of cyclophosphamide of at least 100mg/kg. Accounting for the synergistic effect of Cy with radiation and the resulting dose modifying factor of 1.2 (for 120mg/kg) calculated by Sampath et al.[100] the 7.6Gy threshold observed in our study is equivalent to 9.1Gy (EQD2_repair) for regimens that do not use Cy or similar alkylating agent.

From our analysis we estimate that a lung EQD2_repair of 7.6Gy delivered in 2Gy fractions twice a day with at least 6 hours separation between the fractions and Cy of 120 mg/kg should result in negligible probability of IP. Using the most prevalent fractionation regimen of 12Gy delivered in 2Gy fractions BID and 120mg/kg of Cy as an example, one can achieve the threshold lung dose by reducing the lung dose by 33% or more either through blocking or intensity modulation. It is also possible to increase fractional dose and reduce the number of fractions and achieve the same EQD2 for marrow while keeping the lung dose under the 7.6Gy threshold by delivering fractions once a day and allowing full repair of lung tissue between fractions. Using an α/β value of 3Gy, lung tissue repair half-life of 4 hours and 33% lung block for all fractions, one can change the fractionation regimen to only 3 daily fractions of 3.54Gy without sacrificing marrow dose or lung toxicity. A

similar fractionation scheme of 3 x 3.33Gy has been proposed by Della Volpe et al.[40] In their study they found a lethal pulmonary complication (LPC) rate of 3.8% for patients that receive a MLD of less than 9.4Gy. They suggest keeping the MLD below 9Gy which is equivalent to 10.8Gy EQD2 in order to keep LPC rate below 5%. Based on our research, the threshold value of 7.6Gy should prevent IP grade 3 or 4 and it's easily achievable with lung block or intensity modulation.

6.5 CONCLUSION

Our analysis of 3194 patients that underwent a BMT conditioning regimen that included many different radiation and chemo regimens, indicates that lung dose and Cy dose are statistically significant predictors of development of IP. The prediction model does not accurately reflect the IP rates of published data, especially in the high and low range of lung doses. Inconsistent and incomplete institutional reporting required a lot of assumptions which resulted in vast dispersion of the data points and resulted in inaccurate prediction model. We were, however, able to identify a lung dose threshold of 7.6Gy (EQD2) and 120mg/kg of Cy that should result in negligible IP toxicities of grade 3 or higher. We did not find any evidence that increase in dose rate would increase IP incidence.

As with all retrospective analyses, these findings may provide guidance in lung dose constraints or fractionation selection, but they must be validated with prospective studies. The fractionation schemes greatly depend on the accurate knowledge of the α/β ratios and lung tissue repair half-life. Our predicted lung threshold dose is based on lung α/β value of 3Gy. This threshold will change if more current and accurate α/β value for lung becomes available. The calculations

presented here also assume incomplete repair model for BID treatments with fractionations separated by 6 hours and lung tissue repair half time of 4 hours. Care should be exercised when applying the threshold dose to compute alternative fractionation regimes.

CHAPTER 7 "CONCLUSION"

7.1 Summary of findings.

The series of studies presented here represent evaluations of novel treatment planning optimization and dose calculation algorithms and their applications for complex sites such as TMI and SBRT. In addition to validating GPU algorithms and developing structured planning processes for TMI, we evaluated fractionation schemes and lung toxicity based on historical published data and current radiobiological models.

The first objective of this research focused on validating the new GPU based TomoTherapy treatment planning system and its feasibility in extremely large target volumes. Using three different target volumes for TMI treatments and several combinations of machine optimization parameters, we created plans on both CPU and GPU based systems, keeping the optimization constraints and number of iterations the same. We demonstrated that despite the algorithms being fundamentally different, the difference in plan quality between the systems was very small. The differences were most likely the result of the gradient descent nature of the optimization algorithms and fixed number of iterations that may stop the process at a slightly different solution each time. Our results are consistent with other studies[36] that validated the GPU based system for smaller target volumes. It was also shown that the new algorithm is about 20 times faster than the old planning system. This is a significant improvement since it previously took about 9 – 10 hours to optimize and calculate TMI plan creating a bottle neck and impeding clinical work flow.

In the second aim of this study, discussed in chapter 3, we focused on comparing the dosimetric and computational results of TomoTherapy's GPU planning system with another rotational modality, specifically Eclipse's VMAT. The first clear advantage of Tomotherapy's helical mode of delivery for treatment of TMI was the ability to create one plan for the entire target volume (target volume being from head to mid femur). VMAT plan had to be split up into four isocenters and each sub-plan had to be optimized separately adding complexity and affecting the overall plan quality. Thanks to the larger aperture, the VMAT plans resulted in much shorter beam on time, however that benefit was reduced when overall treatment time was considered due to the need to set up each of the four VMAT sub-plans individually. We also demonstrated superior plan quality using the GPU system in terms of PTV hot spots and OAR sparing. However, the inferior plan quality for VMAT plans was attributed to the software limitations, which precluded the sum of all VMAT arc degrees from exceeding 1500. With this limitation, most of the voxels in the target volume were "exposed" to only one arc limiting the solution space available to the optimizer. With improvements in TPS computing power, this limitation will not be a factor in the future. While VMAT plans with additional arcs should in theory be able to achieve plans comparable to those from TomoTherapy's GPU based system, the additional arcs will increase overall beam on time, minimizing the advantage of VMAT's faster treatment time. We have also reported overall optimization and calculation times of 0.9 hours and 3.9 hours for TomoTherapy and Eclipse, respectively. The difference in the computational speed comes mainly from TomoTherapy's parallel nature of the GPU system.

The work that followed chapters 2 and 3 represented an attempt to provide planning and optimization standards aimed at designing a comprehensive planning guide for TMI. We have demonstrated the effects of field width, pitch and modulation factor on relative plan quality. In general, the plan quality improves with smaller field size, lower pitch or higher modulation factor. However, the gain in relative plan quality is offset by an increase in beam on time. The most significant effect on beam on time comes from the selection of the field width. We have also shown that there is no change in beam on time with change in MF for plans with a pitch of 0.287 and plans with pitch of 0.43 and MF below 2.0. We developed a plan quality index "Q" to quantify the relative differences between the plans. This quality index shows that the relative improvement in plan quality starts to plateau for all plans reaching a MF of 3 or higher. In other words, increasing MF past 3 will add to beam on time without much benefit to plan quality improvement. The development of this planning guide clearly illustrates the limitations of machine optimization parameters for planning of TMI. This reference is a useful guide for TomoTherapy users that are currently planning or intend to start TMI treatments. It describes the effects of user selectable parameters on the treatment plan and can eliminate the need for exhaustive planning trials in order to improve the plan quality or shorten the beam on time.

In the next aim of this study we investigated the capability of TomoTherapy's GPU based planning system for small and complicated SBRT target volumes. We planned cases based on the RTOG 0631 protocol and compared the dosimetric results against other modalities and their respective planning systems. We

demonstrated that the GPU based system was able to create plans that met the dose constraints of RTOG 0631. However, plans created on Cyber Knife and Vero were able to further reduce dose to OARs in some cases. For CK, this may have been a result of the use of non-coplanar beams. We have also shown that beam on time for TomoTherapy equipped with dynamic jaws was on average 6 minutes which was much faster than all the other modalities except RA FFF. The results in this chapter show that the new GPU based planning system along with TomoTherapy equipped with dynamic jaw can create high quality SBRT treatment plans comparable to or better than other systems and deliver the treatment faster than most other modalities.

Finally, the last aim evaluated the possibility of utilizing different fractionation schemes for TMI/TBI treatments without increasing lung toxicities and maintaining bone marrow target dose. We have demonstrated that lung EQD2 and Cy are predictors of IP. The reported data was inconsistent and in some cases incomplete between the institutions and contributed to dispersion of the data. There was also limited information on IP rates for high and low range of the lung doses. These factors, we believe, contributed to the resulting dose response prediction that does not accurately represent clinical data. However, we were able to identify a dose threshold from the discrete data points below which no IP cases were reported. This dose threshold of 7.6Gy (EQD2_repair) was obtained from multi fraction per day regimens and was based on α/β value of 3Gy and lung tissue repair half-life of 4 hours. Alternative fractionation schemes that may be clinically or logistically more desirable can be derived from this threshold dose by using EQD2 equation and

appropriate values of lung tissue fractionation sensitivity and half-life repair time. This study did not find the dose rate to be related to the development of IP at any dose levels.

REFERENCES

1. Siegel, R. L., Miller, K. D. and Jemal, A. (2017), Cancer Statistics, 2017. CA: A Cancer Journal for Clinicians, 67: 7–30. doi:10.3322/caac.21387.
2. Brahme A, inventor; Instrument AB Scanditronax, assignee. (1987).Multi leaf collimator. United States patent US 4,672,212.
3. Carol, M., Grant, W. H., Bleier, A. R., Kania, A. A., Targovnik, H. S., Butler, E. B., & Woo, S. W. (1996). The field-matching problem as it applies to the Peacock three dimensional conformal system for intensity modulation. *International Journal of Radiation Oncology* Biology* Physics*, *34*(1), 183-187.
4. Low, D. A., & Mutic, S. (1997). Abutment region dosimetry for sequential arc IMRT delivery. *Physics in medicine and biology*, *42*(7), 1465.
5. Mackie, T. R., Holmes, T., Swerdloff, S., Reckwerdt, P., Deasy, J. O., Yang, J., ... & Kinsella, T. (1993). Tomotherapy: a new concept for the delivery of dynamic conformal radiotherapy. *Medical physics*, *20*(6), 1709-1719.
6. Mackie TR. Tomotherapy. Proceedings of the XII International Conference on the Use of Computers in Radiation Therapy, Salt Lake City, Utah. 1997.
7. Chen, Y., Chen, Q., Chen, M., & Lu, W. (2011). Dynamic tomotherapy delivery. *Medical physics*, *38*(6), 3013-3024.
8. Yu, C. X. (1995). Intensity-modulated arc therapy with dynamic multileaf collimation: an alternative to tomotherapy. *Physics in medicine and biology*, *40*(9), 1435.

9. Yu, C. X., Symons, M. J., Du, M. N., Martinez, A. A., & Wong, J. W. (1995). A method for implementing dynamic photon beam intensity modulation using independent jaws and a multileaf collimator. *Physics in medicine and biology*, *40*(5), 769.

10. Yu, C. X. (1997). Intensity modulated arc therapy: a new method for delivering conformal radiation therapy. *The Theory and Practice of Intensity Modulated Radiotherapy. Madison, WI: Advanced Medical Publishing*, 107-120.

11. Otto, K. (2008). Volumetric modulated arc therapy: IMRT in a single gantry arc. *Medical physics*, *35*(1), 310-317.

12. Webb, S. (1999). Conformal intensity-modulated radiotherapy (IMRT) delivered by robotic linac-testing IMRT to the limit?. *Physics in medicine and biology*, *44*(7), 1639.

13. Webb, S. (2000). Conformal intensity-modulated radiotherapy (IMRT) delivered by robotic linac-conformality versus efficiency of dose delivery. *Physics in medicine and biology*, *45*(7), 1715.

14. Mackie, T. R., Reckwerdt, P., McNutt, T., Gehring, M., & Sanders, C. (1996). Photon beam dose computations. *Teletherapy: Present and future*, 103-135.

15. Ahnesjö, A., & Aspradakis, M. M. (1999). Dose calculations for external photon beams in radiotherapy. *Physics in medicine and biology*, *44*(11), R99.

16. Chen, Q., Chen, M., & Lu, W. (2011). Ultrafast convolution/superposition using tabulated and exponential kernels on GPU. *Medical physics*, *38*(3), 1150-1161.

17. Aristei, C., Latini, P., Terenzi, A., Felicini, R., & Aversa, F. (2001). Total body irradiation-based regimen in the conditioning of patients submitted to

haploidentical stem cell transplantation. *Radiotherapy and Oncology*, *58*(3), 247-249.

18. Bunin, N., Aplenc, R., Kamani, N., Shaw, K., Cnaan, A., & Simms, S. (2003). Randomized trial of busulfan vs total body irradiation containing conditioning regimens for children with acute lymphoblastic leukemia: a Pediatric Blood and Marrow Transplant Consortium study. *Bone marrow transplantation*, *32*(6), 543-548.
19. Blaise, D., Maraninchi, D., Michallet, M., Reiffers, J., Jouet, J. P., Milpied, N., ... & Ifrah, N. (2001). Long-term follow-up of a randomized trial comparing the combination of cyclophosphamide with total body irradiation or busulfan as conditioning regimen for patients receiving HLA-identical marrow grafts for acute myeloblastic leukemia in first complete remission. *Blood*, *97*(11), 3669-3671.
20. Dusenbery, K. E., Daniels, K. A., McClure, J. S., McGlaver, P. B., Ramsay, N. K., Blazar, B. R., ... & Woods, W. G. (1995). Randomized comparison of cyclophosphamide-total body irradiation versus busulfan-cyclophosphamide conditioning in autologous bone marrow transplantation for acute myeloid leukemia. *International Journal of Radiation Oncology* Biology* Physics*, *31*(1), 119-128.
21. Clift, R. A., Buckner, C. D., Appelbaum, F. R., Bryant, E., Bearman, S. I., Petersen, F. B., ... & Bensinger, W. I. (1991). Allogeneic marrow transplantation in patients with chronic myeloid leukemia in the chronic phase: a randomized trial of two irradiation regimens. *Blood*, *77*(8), 1660-1665.

22. Clift, R. A., Buckner, C. D., Appelbaum, F. R., Sullivan, K. M., Storb, R., & Thomas, E. D. (1998). Long-term follow-up of a randomized trial of two irradiation regimens for patients receiving allogeneic marrow transplants during first remission of acute myeloid leukemia. *Blood*, *92*(4), 1455-1456.

23. Wilkie, J. R., Tiryaki, H., Smith, B. D., Roeske, J. C., Radosevich, J. A., & Aydogan, B. (2008). Feasibility study for linac-based intensity modulated total marrow irradiation. *Medical physics*, *35*(12), 5609-5618.

24. Surucu, M., Yeginer, M., Kavak, G. O., Fan, J., Radosevich, J. A., & Aydogan, B. (2012). Verification of dose distribution for volumetric modulated arc therapy total marrow irradiation in a humanlike phantom. *Medical physics*, *39*(1), 281-288.

25. Aydogan, B., Yeginer, M., Kavak, G. O., Fan, J., Radosevich, J. A., & Gwe-Ya, K. (2011). Total marrow irradiation with RapidArc volumetric arc therapy. *International Journal of Radiation Oncology* Biology* Physics*, *81*(2), 592-599.

26. Fogliata, A., Cozzi, L., Clivio, A., Ibatici, A., Mancosu, P., Navarria, P., ... & Scorsetti, M. (2011). Preclinical assessment of volumetric modulated arc therapy for total marrow irradiation. *International Journal of Radiation Oncology* Biology* Physics*, *80*(2), 628-636.

27. Han, C., Schultheisss, T. E., & Wong, J. Y. (2012). Dosimetric study of volumetric modulated arc therapy fields for total marrow irradiation. *Radiotherapy and Oncology*, *102*(2), 315-320.

28. Schultheiss, T. E., Wong, J., Liu, A., Olivera, G., & Somlo, G. (2007). Image-guided total marrow and total lymphatic irradiation using helical tomotherapy. *International Journal of Radiation Oncology* Biology* Physics*, *67*(4), 1259-1267.

29. Schultheiss, T., Liu, A., Wong, J., Olivera, G., & Kapatoes, J. (2004). Total marrow and total lymphatic irradiation with helical tomotherapy. *Medical Physics*, *31*(6), 1845.

30. Wong, J. Y., Liu, A., Schultheiss, T., Popplewell, L., Stein, A., Rosenthal, J., ... & Somlo, G. (2006). Targeted total marrow irradiation using three-dimensional image-guided tomographic intensity-modulated radiation therapy: an alternative to standard total body irradiation. *Biology of Blood and Marrow Transplantation*, *12*(3), 306-315.

31. Hui, S. K., Kapatoes, J., Fowler, J., Henderson, D., Olivera, G., Manon, R. R., ... & Welsh, J. S. (2005). Feasibility study of helical tomotherapy for total body or total marrow irradiationa). *Medical physics*, *32*(10), 3214-3224.

32. Lu, W. (2010). A non-voxel-based broad-beam (NVBB) framework for IMRT treatment planning. *Physics in medicine and biology*, *55*(23), 7175.

33. Somlo, G., Spielberger, R., Frankel, P., Karanes, C., Krishnan, A., Parker, P. M., ... & Liu, A. (2008). Total Marrow Irradiation (TMI): A New Ablative Regimen as Part of Tandem (T) Autologous Peripheral Blood Progenitor Cell Transplant (AT) for Patients (pts) with Multiple Myeloma (MM). *Blood*, *112*(11), 3326-3326.

34. Kissick, M. W., Fenwick, J., James, J. A., Jeraj, R., Kapatoes, J. M., Keller, H., ... & Soisson, E. T. (2005). The helical tomotherapy thread effect. *Medical physics*, *32*(5), 1414-1423.

35. Low, D. A., Harms, W. B., Mutic, S., & Purdy, J. A. (1998). A technique for the quantitative evaluation of dose distributions. *Medical physics*, *25*(5), 656-661.

36. Chen, Q., Lu, W., Chen, Y., Chen, M., Henderson, D., & Sterpin, E. (2012). Validation of GPU based TomoTherapy dose calculation engine. *Medical physics*, *39*(4), 1877-1886.

37. Khan, F. M., & Gibbons, J. P. (2014). *Khan's the physics of radiation therapy*. Lippincott Williams & Wilkins.

38. Van Dyk, J., Galvin, J. M., Glasgow, G. P., & Podgorsak, E. B. (1986). The physical aspects of total and half body photon irradiation. *Task Group*, *29*, 3-4.

39. Washington, C. M., & Leaver, D. T. (2015). *Principles and practice of radiation therapy*. Elsevier Health Sciences.

40. Della Volpe, A., Ferreri, A. J. M., Annaloro, C., Mangili, P., Rosso, A., Calandrino, R., ... & Fiorino, C. (2002). Lethal pulmonary complications significantly correlate with individually assessed mean lung dose in patients with hematologic malignancies treated with total body irradiation. *International Journal of Radiation Oncology* Biology* Physics*, *52*(2), 483-488.

41. Takahashi, Y., & Hui, S. K. (2013). Impact of very long time output variation in the treatment of total marrow irradiation with helical tomotherapy. *Radiation Oncology*, *8*(1), 1.

42. Nalichowski, A., & Burmeister, J. (2013). Dosimetric comparison of helical tomotherapy treatment plans for total marrow irradiation created using GPU and CPU dose calculation engines. *Medical physics*, *40*(7), 071716.

43. Corvò, R., Zeverino, M., Vagge, S., Agostinelli, S., Barra, S., Taccini, G., ... & Bacigalupo, A. (2011). Helical tomotherapy targeting total bone marrow after total body irradiation for patients with relapsed acute leukemia undergoing an allogeneic stem cell transplant. *Radiotherapy and oncology*, *98*(3), 382-386.

44. Aydogan, B., Mundt, A. J., & Roeske, J. C. (2006). Linac-based intensity modulated total marrow irradiation (IM-TMI). *Technology in cancer research & treatment*, *5*(5), 513-519.

45. Wong, J. Y., Rosenthal, J., Liu, A., Schultheiss, T., Forman, S., & Somlo, G. (2009). Image-guided total-marrow irradiation using helical tomotherapy in patients with multiple myeloma and acute leukemia undergoing hematopoietic cell transplantation. *International Journal of Radiation Oncology* Biology* Physics*, *73*(1), 273-279.

46. Shueng, P. W., Lin, S. C., Chong, N. S., Lee, H. Y., Tien, H. J., Wu, L. J., ... & Hsieh, C. H. (2009). Total marrow irradiation with helical tomotherapy for bone marrow transplantation of multiple myeloma: first experience in Asia. *Technology in cancer research & treatment*, *8*(1), 29-37.

47. Chow, E., Zeng, L., Salvo, N., Dennis, K., Tsao, M., & Lutz, S. (2012). Update on the systematic review of palliative radiotherapy trials for bone metastases. *Clinical Oncology*, *24*(2), 112-124.

48. Hartsell, W. F., Scott, C. B., Bruner, D. W., Scarantino, C. W., Ivker, R. A., Roach, M., ... & Konski, A. A. (2005). Randomized trial of short-versus long-course radiotherapy for palliation of painful bone metastases. *Journal of the National Cancer Institute*, *97*(11), 798-804.

49. Gerszten, P. C., Burton, S. A., Ozhasoglu, C., & Welch, W. C. (2007). Radiosurgery for spinal metastases: clinical experience in 500 cases from a single institution. *Spine*, *32*(2), 193-199.

50. Hellman, S., & Weichselbaum, R. R. (1995). Oligometastases. *Journal of Clinical Oncology*, *13*(1), 8-10.

51. Pan, H., Simpson, D. R., Mell, L. K., Mundt, A. J., & Lawson, J. D. (2011). A survey of stereotactic body radiotherapy use in the United States. *Cancer*, *117*(19), 4566-4572.

52. Burghelea, M., Verellen, D., Gevaert, T., Depuydt, T., Poels, K., Simon, V., & De Ridder, M. (2014). Feasibility of using the Vero SBRT system for intracranial SRS. *Journal of Applied Clinical Medical Physics*, *15*(1).

53. Nguyen, T., Hsu, W., Lim, M., & Naff, N. (2011). Delivery of stereotactic radiosurgery: a cross-platform comparison. *Neurological research*, *33*(8), 787-791.

54. Cox, B. W., Spratt, D. E., Lovelock, M., Bilsky, M. H., Lis, E., Ryu, S., ... & Soltys, S. (2012). International Spine Radiosurgery Consortium consensus guidelines for target volume definition in spinal stereotactic radiosurgery. *International Journal of Radiation Oncology* Biology* Physics*, *83*(5), e597-e605.

55. Ko, H. Y., Park, J. H., Shin, Y. B., & Baek, S. Y. (2004). Gross quantitative measurements of spinal cord segments in human. *Spinal Cord*, *42*(1), 35-40.

56. Paddick, I., & Lippitz, B. (2006). A simple dose gradient measurement tool to complement the conformity index. *Special Supplements*, *105*(7), 194-201.

57. Gallo, J. J., Kaufman, I., Powell, R., Pandya, S., Somnay, A., Bossenberger, T., ... & Burmeister, J. (2015). Single-fraction spine SBRT end-to-end testing on TomoTherapy, Vero, TrueBeam, and CyberKnife treatment platforms using a novel anthropomorphic phantom. *Journal of Applied Clinical Medical Physics*, *16*(1).

58. Chung, H., Jin, H., Palta, J., Suh, T. S., & Kim, S. (2006). Dose variations with varying calculation grid size in head and neck IMRT. *Physics in medicine and biology*, *51*(19), 4841.

59. Dempsey, J. F., Romeijn, H. E., Li, J. G., Low, D. A., & Palta, J. R. (2005). A Fourier analysis of the dose grid resolution required for accurate IMRT fluence map optimization. *Medical physics*, *32*(2), 380-388.

60. Zilli, T., Miralbell, R., & Ozsahin, M. (2009). [Total body irradiation: present and future]. *Cancer radiotherapie: journal de la Societe francaise de radiotherapie oncologique*, *13*(5), 428-433.

61. Thomas, E. D., Buckner, C. D., Banaji, M., Clift, R. A., Fefer, A., Flournoy, N., ... & Sale, G. E. (1977). One hundred patients with acute leukemia treated by chemotherapy, total body irradiation, and allogeneic marrow transplantation. *Blood*, *49*(4), 511-533.

62. Fryer, C. J. H., Fitzpatrick, P. J., Rider, W. D., & Pooh, P. (1978). Radiation pneumonitis: experience following a large single dose of radiation. *International Journal of Radiation Oncology* Biology* Physics*, *4*(11-12), 931-936.

63. Thomas, E. D., Clift, R. A., Hersman, J., Sanders, J. E., Stewart, P., Buckner, C. D., ... & Storb, R. (1982). Marrow transplantation for acute nonlymphoblastic leukemia in first remission using fractionated or single-dose irradiation. *International Journal of Radiation Oncology* Biology* Physics*, *8*(5), 817-821.

64. Barrett, A., Depledge, M. H., & Powles, R. L. (1983). Interstitial pneumonitis following bone marrow transplantation after low dose rate total body irradiation. *International Journal of Radiation Oncology* Biology* Physics*, *9*(7), 1029-1033.

65. Shank, B., Chu, F. C., Dinsmore, R., Kapoor, N., Kirkpatrick, D., Teitelbaum, H., ... & O'Reilly, R. T. (1983). Hyperfractionated total body irradiation for bone marrow transplantation. Results in seventy leukemia patients with allogeneic transplants. *International Journal of Radiation Oncology* Biology* Physics*, *9*(11), 1607-1611.

66. Kim, T. H., Rybka, W. B., Lehnert, S., Podgorsak, E. B., & Freeman, C. R. (1985). Interstitial pneumonitis following total body irradiation for bone marrow transplantation using two different dose rates. *International Journal of Radiation Oncology* Biology* Physics*, *11*(7), 1285-1291.

67. Cosset, J. M., Baume, D., Pico, J. L., Shank, B., Girinski, T., Benhamou, E., ... & Dutreix, J. (1989). Single dose versus hyperfractionated total body irradiation

before allogeneic bone marrow transplantation: a non-randomized comparative study of 54 patients at the Institut Gustave-Roussy. *Radiotherapy and Oncology*, *15*(2), 151-160.

68. Kim, T. H., McGlave, P. B., Ramsay, N., Woods, W., Bostrom, B., Vercellotti, G., ... & Khan, F. (1990). Comparison of two total body irradiation regimens in allogeneic bone marrow transplantation for acute non-lymphoblastic leukemia in first remission. *International Journal of Radiation Oncology* Biology* Physics*, *19*(4), 889-897.
69. Latini, P., Aristei, C., Aversa, F., Checcaglini, F., Maranzano, E., Panizza, B. M., ... & Martelli, M. F. (1992). Interstitial pneumonitis after hyperfractionated total body irradiation in HLA-matched T-depleted bone marrow transplantation. *International Journal of Radiation Oncology* Biology* Physics*, *23*(2), 401-405.
70. Ozsahin, M., Pene, F., Touboul, E., Gindrey-Vie, B., Dominique, C., Lefkopoulos, D., ... & Rio, B. (1992). Total-body irradiation before bone marrow transplantation. Results of two randomized instantaneous dose rates in 157 patients. *Cancer*, *69*(11), 2853-2865.
71. Petersen, F. B., Deeg, H. J., Buckner, C. D., Appelbaum, F. R., Storb, R., Clift, R. A., ... & Doney, K. (1992). Marrow transplantation following escalating doses of fractionated total body irradiation and cyclophosphamide—a phase I trial. *International Journal of Radiation Oncology* Biology* Physics*, *23*(5), 1027-1032.

72. Sibley, G. S., Mundt, A. J., Goldman, S., Nachman, J., Reft, C., Weichselbaum, R. R., ... & Johnson, L. (1995). Patterns of failure following total body irradiation and bone marrow transplantation with or without a radiotherapy boost for advanced neuroblastoma. *International Journal of Radiation Oncology* Biology* Physics*, *32*(4), 1127-1135.

73. Chou, R. H., Wong, G. B., Kramer, J. H., Wara, D. W., Matthay, K. K., Crittenden, M. R., ... & Wara, W. M. (1996). Toxicities of total-body irradiation for pediatric bone marrow transplantation. *International Journal of Radiation Oncology* Biology* Physics*, *34*(4), 843-851.

74. Dusenbery, K. E., Steinbuch, M., McGlave, P. B., Ramsay, N. K., Blazar, B. R., Neglia, J. P., ... & Woods, W. G. (1996). Autologous bone marrow transplantation in acute myeloid leukemia: the University of Minnesota experience. *International Journal of Radiation Oncology* Biology* Physics*, *36*(2), 335-343.

75. Morgan, T. L., Falk, P. M., Kogut, N., Shah, K. H., Tome, M., & Kagan, A. R. (1996). A comparison of single-dose and fractionted total-body irradiation on the development of pneumonitis following bone marrow transplantation. *International Journal of Radiation Oncology* Biology* Physics*, *36*(1), 61-66.

76. Ozsahin, M., Belkacémi, Y., Laporte, J. P., Rio, B., Leblond, V., Korbas, D., ... & Laugier, A. (1996). Interstitial pneumonitis following autologous bone-marrow transplantation conditioned with cyclophosphamide and total-body

irradiation. *International Journal of Radiation Oncology* Biology* Physics*, *34*(1), 71-77.

77. Bradley, J., Reft, C., Goldman, S., Rubin, C., Nachman, J., Larson, R., & Hallahan, D. E. (1998). High-energy total body irradiation as preparation for bone marrow transplantation in leukemia patients: treatment technique and related complications. *International Journal of Radiation Oncology* Biology* Physics*, *40*(2), 391-396.
78. Gerrard, G. E., Vail, A., Taylor, R. E., Pitchford, W. G., Gilson, D., Povall, J. M., & Morgan, A. M. (1998). Toxicity and dosimetry of fractionated total body irradiation prior to allogeneic bone marrow transplantation using a straightforward radiotherapy technique. *Clinical Oncology*, *10*(6), 379-383.
79. Lohr, F., Wenz, F., Schraube, P., Flentje, M., Haas, R., Zierhut, D., ... & Wannenmacher, M. (1998). Lethal pulmonary toxicity after autologous bone marrow transplantation/peripheral blood stem cell transplantation for hematological malignancies. *Radiotherapy and oncology*, *48*(1), 45-51.
80. Sobecks, R. M., Daugherty, C. K., Hallahan, D. E., Laport, G. F., Wagner, N. D., & Larson, R. A. (2000). A dose escalation study of total body irradiation followed by high-dose etoposide and allogeneic blood stem cell transplantation for the treatment of advanced hematologic malignancies. *Bone marrow transplantation*, *25*(8).
81. Gopal, R., Ha, C. S., Tucker, S. L., Khouri, I. F., Giralt, S. A., Gajewski, J. L., ... & Champlin, R. E. (2001). Comparison of two total body irradiation fractionation

regimens with respect to acute and late pulmonary toxicity. *Cancer*, *92*(7), 1949-1958.

82. Chen, C. I., Abraham, R., Tsang, R., Crump, M., Keating, A., & Stewart, A. K. (2001). Radiation-associated pneumonitis following autologous stem cell transplantation: predictive factors, disease characteristics and treatment outcomes. *Bone marrow transplantation*, *27*(2).
83. Gutierrez-Delgado, F., Maloney, D. G., Press, O. W., Golden, J., Holmberg, L. A., Maziarz, R. T., ... & Bensinger, W. I. (2001). NON-HODGKIN'S LYMPHOMA-Autologous stem cell transplantation for non-Hodgkin's lymphoma: Comparison of radiation-based and chemotherapy-only preparative regimens. *Bone marrow transplantation*, *28*(5), 455-462.
84. McAfee, S. L., Powell, S. N., Colby, C., & Spitzer, T. R. (2002). Dose-escalated total body irradiation and autologous stem cell transplantation for refractory hematologic malignancy. *International Journal of Radiation Oncology* Biology* Physics*, *53*(1), 151-156.
85. Beyzadeoglu, M., Oysul, K., Dirican, B., Arpaci, F., Balkan, A., Surenkok, S., & Pak, Y. (2004). Effect of dose-rate and lung dose in total body irradiation on interstitial pneumonitis after bone marrow transplantation. *The Tohoku journal of experimental medicine*, *202*(4), 255-263.
86. Carruthers, S. A., & Wallington, M. M. (2004). Total body irradiation and pneumonitis risk: a review of outcomes. *British journal of cancer*, *90*(11), 2080-2084.

87. Zaucha, R. E., Buckner, D. C., Barnett, T., Holmberg, L. A., Gooley, T., Hooper, H. A., ... & Bensinger, W. I. (2006). Modified total body irradiation as a planned second high-dose therapy with stem cell infusion for patients with bone-based malignancies. *International Journal of Radiation Oncology* Biology* Physics*, *64*(1), 227-234.

88. Petropoulos, D., Worth, L. L., Mullen, C. A., Madden, R., Mahajan, A., Choroszy, M., ... & Chan, K. W. (2006). Total body irradiation, fludarabine, melphalan, and allogeneic hematopoietic stem cell transplantation for advanced pediatric hematologic malignancies. *Bone marrow transplantation*, *37*(5), 463-467.

89. Nagata, Y., Tachiiri, S., Okada, T., Yano, S., Hiraoka, M., Ishikawa, T., ... & Sasai, K. (2006). Influence of radiation dose rate and lung dose on interstitial pneumonitis after fractionated total body irradiation: acute parotitis may predict interstitial pneumonitis. *International journal of hematology*, *83*(1), 86-91.

90. Soejima, T., Hirota, S., Tsujino, K., Yoden, E., Fujii, O., Ichimiya, Y., & Mizuno, I. (2007). Total body irradiation followed by bone marrow transplantation: comparison of once-daily and twice-daily fractionation regimens. *Radiation medicine*, *25*(8), 402-406.

91. Schneider, R. A., Schultze, J., Jensen, J. M., Hebbinghaus, D., & Galalae, R. M. (2008). Long-term outcome after static intensity-modulated total body radiotherapy using compensators stratified by pediatric and adult cohorts. *International Journal of Radiation Oncology* Biology* Physics*, *70*(1), 194-202.

92. Shigematsu, A., Kondo, T., Yamamoto, S., Sugita, J., Onozawa, M., Kahata, K., ... & Wakasa, K. (2008). Excellent outcome of allogeneic hematopoietic stem cell transplantation using a conditioning regimen with medium-dose VP-16, cyclophosphamide and total-body irradiation for adult patients with acute lymphoblastic leukemia. *Biology of blood and marrow transplantation*, *14*(5), 568-575.

93. Linsenmeier, C., Thoennessen, D., Negretti, L., Bourquin, J. P., Streller, T., Lütolf, U. M., & Oertel, S. (2010). Total body irradiation (TBI) in pediatric patients. *Strahlentherapie und Onkologie*, *186*(11), 614-620.

94. Liu, H. W., Seftel, M. D., Rubinger, M., Szwajcer, D., Demers, A., Nugent, Z., ... & Cooke, A. (2010). Total body irradiation compared with BEAM: long-term outcomes of peripheral blood autologous stem cell transplantation for non-Hodgkin's lymphoma. *International Journal of Radiation Oncology* Biology* Physics*, *78*(2), 513-520.

95. Pica, G., Vagge, S., Beltrami, G., Nati, S., Catania, G., Corvò, R., & Carella, A. M. (2011). A Phase I Study of Hypofractionated Tailored Total Marrow or Total Lymphoid Irradiation with Helical Tomotherapy Plus Chemotherapy As a Conditioning Regimen for Autologous Stem Cell Transplantation. *Blood*, *118*(21), 4523-4523.

96. Kelsey, C. R., Horwitz, M. E., Chino, J. P., Craciunescu, O., Steffey, B., Folz, R. J., ... & Marks, L. B. (2011). Severe pulmonary toxicity after myeloablative conditioning using total body irradiation: an assessment of risk

factors. *International Journal of Radiation Oncology* Biology* Physics*, *81*(3), 812-818.

97. Rosenthal, J., Wong, J., Stein, A., Qian, D., Hitt, D., Naeem, H., ... & Forman, S. (2011). Phase 1/2 trial of total marrow and lymph node irradiation to augment reduced-intensity transplantation for advanced hematologic malignancies. *Blood*, *117*(1), 309-315.
98. Wong, J. Y., Forman, S., Somlo, G., Rosenthal, J., Liu, A., Schultheiss, T., ... & Stein, A. (2013). Dose escalation of total marrow irradiation with concurrent chemotherapy in patients with advanced acute leukemia undergoing allogeneic hematopoietic cell transplantation. *International Journal of Radiation Oncology* Biology* Physics*, *85*(1), 148-156.
99. Aristei, C., Carotti, A., Palazzari, E., Amico, L., Ruggeri, L., Perrucci, E., ... & Aversa, F. (2016). The Total Body Irradiation Schedule Affects Acute Leukemia Relapse After Matched T Cell–Depleted Hematopoietic Stem Cell Transplantation. *International Journal of Radiation Oncology* Biology* Physics*, *96*(4), 832-839.
100. Sampath, S., Schultheiss, T. E., & Wong, J. (2005). Dose response and factors related to interstitial pneumonitis after bone marrow transplant. *International Journal of Radiation Oncology* Biology* Physics*, *63*(3), 876-884.
101. M. Bentzen, JZ Skoczylas, J. Bernier, S. (2000). Quantitative clinical radiobiology of early and late lung reactions. *International journal of radiation biology*, *76*(4), 453-462.

102. Dubray, B., Henry-Amar, M., Meerwaldt, J. H., Noordijk, E. M., Dixon, D. O., Cosset, J. M., & Thames, H. D. (1995). Radiation-induced lung damage after thoracic irradiation for Hodgkin's disease: the role of fractionation. *Radiotherapy and Oncology*, *36*(3), 211-217.

103. Marks, L. B., Bentzen, S. M., Deasy, J. O., Bradley, J. D., Vogelius, I. S., El Naqa, I., ... & Jackson, A. (2010). Radiation dose–volume effects in the lung. *International Journal of Radiation Oncology* Biology* Physics*, *76*(3), S70-S76.

104. Bortin, M., Kay, H. M., Gale, R. P., & Rimm, A. (1982). Factors associated with interstitial pneumonitis after bone-marrow transplantation for acute leukaemia. *The Lancet*, *319*(8269), 437-439.

105. Peters, L. (1980). Discussion: The radiobiological bases of TBI. *International Journal of Radiation Oncology* Biology* Physics*, *6*(6), 785-787.

106. Peters, L. J., Withers, H. R., Cundiff, J. H., & Dicke, K. A. (1979). Radiobiological Considerations in the Use of Total-Body Irradiation for Bone-Marrow Transplantation 1. *Radiology*, *131*(1), 243-247.

107. Gogna, N. K., Morgan, G., Downs, K., Atkinson, K., & Biggs, J. (1992). Lung dose rate and interstitial pneumonitis in total body irradiation for bone marrow transplantation. *Australasian radiology*, *36*(4), 317-320.

108. Corvò, R., Paoli, G., Barra, S., Bacigalupo, A., Van Lint, M. T., Franzone, P., ... & Vitale, V. (1999). Total body irradiation correlates with chronic graft versus host disease and affects prognosis of patients with acute lymphoblastic leukemia receiving an HLA identical allogeneic bone marrow

transplant. *International Journal of Radiation Oncology* Biology* Physics*, *43*(3), 497-503.

109. Girinsky, T., Benhamou, E., Bourhis, J. H., Dhermain, F., Guillot-Valls, D., Ganansia, V., ... & Baume, D. (2000). Prospective randomized comparison of single-dose versus hyperfractionated total-body irradiation in patients with hematologic malignancies. *Journal of Clinical Oncology*, *18*(5), 981-981.
110. Hasenbalg, F., Neuenschwander, H., Mini, R., & Born, E. J. (2007). Collapsed cone convolution and analytical anisotropic algorithm dose calculations compared to VMC++ Monte Carlo simulations in clinical cases. *Physics in medicine and biology*, *52*(13), 3679.

ABSTRACT

CLINICAL APPLICATIONS OF ADVANCED ROTATIONAL RADIATION THERAPY

by

ADRIAN NALICHOWSKI

May 2017

Advisor: Dr. Jacob Burmeister

Major: Medical Physics

Degree: Doctor of Philosophy

Purpose: With a fast adoption of emerging technologies, it is critical to fully test and understand its limits and capabilities. In this work we investigate new graphic processing unit (GPU) based treatment planning algorithm and its applications in helical tomotherapy dose delivery. We explore the limits of the system by applying it to challenging clinical cases of total marrow irradiation (TMI) and stereotactic radiosurgery (SRS). We also analyze the feasibility of alternative fractionation schemes for total body irradiation (TBI) and TMI based on reported historical data on lung dose and interstitial pneumonitis (IP) incidence rates.

Methods and Materials: An anthropomorphic phantom was used to create TMI plans using the new GPU based treatment planning system and the existing CPU cluster based system. Optimization parameters were selected based on clinically used values for field width, modulation factor and pitch. Treatment plans were also created on Eclipse treatment planning system (Varian Medical Systems Inc, Palo Alto, CA) using volumetric modulated arc therapy (VMAT) for dose delivery on IX treatment unit. The constraints ware selected to ensure that at least 95% of

the PTV received the prescription dose while minimizing the doses to OARs which consisted of lungs, heart, liver, kidneys, brain, and small bowel. Resulting plans were evaluated based on plan quality, optimization and dose calculation times, and beam on times. Gamma indices (Γ) were also used to compare planar dose distributions between the planning systems. In addition a plan quality index (Q) was developed for quantitative analysis of relative plan quality which included mean and maximum doses. The GPU planning systems was also evaluated for single fraction radiosurgery/SBRT capabilities. Treatment plans were created for spine metastases based on national protocol RTOG 0631 and the dosimetric results were compared to four other modalities.

A retrospective review was performed of 42 publications that reported IP rates along with lung dose, fractionation regimen, dose rate and chemotherapy. The analysis consisted of nearly thirty two hundred patients and 34 unique radiation regimens. Multivariate logistic regression was performed to determine parameters associated with IP and establish does response function.

Results: The results showed very good dosimetric agreement between the GPU and CPU calculated plans. A gamma analysis Γ(3%, 3 mm) < 1 of the GPU plan resulted in average of 97% of calculated voxels satisfying Γ < 1 criterion as compared to baseline CPU plans. The optimization/dose calculation time with the new GPU system is about 20 times faster than with the CPU system. Is was also about 4 times faster than Eclipse treatment planning system while achieving superior OAR dose sparing ranging from 3% to 52%. Analysis of optimization parameters showed increase in plan quality index (Q) with lower pitch, smaller field size and

higher modulation factor. The beam on time increases with increasing plan quality index and associated optimization parameters with the highest effect observed with field size.

The results from SBRT study show that GPU planning system can maintain 90% target coverage while meeting all the constraints of RTOG 0631 protocol. Beam on time for Tomotherapy and flattening filter free RapidArc was much faster than for Vero or Cyberknife.

Retrospective data analysis showed that lung dose and Cyclophosphomide (Cy) are both predictors of IP in TBI/TMI treatments. The dose rate was not found to be an independent risk factor for IP. The model failed to establish accurate dose response function, but the discrete data indicated a radiation dose threshold of 7.6Gy (EQD2_repair) and 120 mg/kg of Cy below which no IP cases were reported.

Conclusion: The TomoTherapy GPU based dose engine is capable of calculating TMI treatment plans with plan quality nearly identical to plans calculated using the traditional CPU/cluster based system, while significantly reducing the time required for optimization and dose calculation. The new system was able to achieve more uniform dose distribution throughout the target volume and steeper dose fall off, resulting in superior OAR sparing when compared to Eclipse treatment planning system for VMAT delivery. The machine optimization parameters tested for TMI cases provide a comprehensive overview of the capabilities of the treatment planning station and associated helical delivery system. The new system also proved to be dosimetrically compatible with other leading modalities for treatments of small and complicated target volumes and was even superior when treatment

delivery times were compared. These finding demonstrate that the advanced treatment planning and delivery system from TomoTherapy is well suitable for treatments of complicated cases such as TMI and SRS and it's often dosimetrically and/or logistically superior to other modalities. The new planning system can easily meet the constraint of threshold lung dose established in this study. The results presented here on the capabilities of Tomotherapy and on the identified lung dose threshold provide an opportunity to explore alternative fractionation schemes without sacrificing target coverage or lung toxicity.

AUTOBIOGRAPHICAL STATEMENT
ADRIAN NALICHOWSKI

EDUCATION

2012-2017 Ph.D. Medical Physics, Wayne State University, Detroit, MI
2003-2004 M.S. Radiological Physics, Wayne State University, Detroit, MI
1997-2001 B.S. Mechanical Engineering, Kettering University, Flint, MI

CERTIFICATION

2008 American Board of Radiology

PROFESSIONAL APPOINTMENTS

2008- Adjunct Instructor, Radiation Oncology, Wayne State University School of Medicine

ACADEMIC AND PROFESSIONAL MEMBERSHIPS

2013- European Society for Radiotherapy & Oncology)
2011- American Brachytherapy Society
2005- American Society for Therapeutic Radiology and Oncology
2005- American Association of Physicists in Medicine
2009- Great Lakes Chapter of American Association of Physicists in Medicine
1997-2003 Automotive Society of Mechanical Engineers Member

COMMITTEE APPOINTMENTS

2015- Member, ASTRO Physics Core Curriculum Subcommittee
2015- Member, AAPM portal dosimetry task group

PUBLICATIONS

1. **Nalichowski, A**., Kaufman, I., Gallo, J., Bossenberger, T., Solberg, T., Ramirez, E., ... & Burmeister, J. (2017). Single fraction radiosurgery/stereotactic body radiation therapy (SBRT) for spine metastasis: A dosimetric comparison of multiple delivery platforms. *Journal of Applied Clinical Medical Physics*, *18*(1), 164-169.
2. **Nalichowski, A**., Eagle, D. G., & Burmeister, J. (2016). Dosimetric evaluation of total marrow irradiation using 2 different planning systems. *Medical Dosimetry*, *41*(3), 230-235.
3. Meerschaert, R., **Nalichowski, A**., Burmeister, J., Paul, A., Miller, S., Hu, Z., & Zhuang, L. (2016). A comprehensive evaluation of adaptive daily planning for cervical cancer HDR brachytherapy. *Journal of Applied Clinical Medical Physics*, *17*(6).
4. Dominello, M. M., **Nalichowski, A**., Paximadis, P., Kaufman, I., McSpadden, E., Joiner, M., ... & Konski, A. (2014). Limitations of the bowel bag contouring technique in the definitive treatment of cervical cancer. *PRO*, *4*(1), e15-e20.
5. **Nalichowski, A**., & Burmeister, J. (2013). Dosimetric comparison of helical tomotherapy treatment plans for total marrow irradiation created using GPU and CPU dose calculation engines. *Medical physics*, *40*(7).
6. Weyh, A., Konski, **A., Nalichowski**, A., Maier, J., & Lack, D. (2013). Lung SBRT: dosimetric and delivery comparison of RapidArc, TomoTherapy, and IMR. *Journal of Applied Clinical Medical Physics*, *14*(4).